Anderson, Robert Stewart

SEDIMENT TRANSPORT BY WIND: SALTATION, SUSPENSION, EROSION AND RIPPLES

University of Washington PH.D. 1986

PLEASE NOTE:

In all cases this material has been filmed in the best possible way from the available copy. Problems encountered with this document have been identified here with a check mark __✓__.

1. Glossy photographs or pages _____
2. Colored illustrations, paper or print _____
3. Photographs with dark background __✓__
4. Illustrations are poor copy _____
5. Pages with black marks, not original copy _____
6. Print shows through as there is text on both sides of page _____
7. Indistinct, broken or small print on several pages __✓__
8. Print exceeds margin requirements _____
9. Tightly bound copy with print lost in spine _____
10. Computer printout pages with indistinct print _____
11. Page(s) _____ lacking when material received, and not available from school or author.
12. Page(s) _____ seem to be missing in numbering only as text follows.
13. Two pages numbered _____. Text follows.
14. Curling and wrinkled pages _____
15. Dissertation contains pages with print at a slant, filmed as received __✓__
16. Other _____

_____

_____

University
Microfilms
International

SEDIMENT TRANSPORT BY WIND: SALTATION, SUSPENSION, EROSION AND RIPPLES

by

Robert Stewart Anderson

A dissertation submitted in partial fulfillment
of the requirements for the degree of

Doctor of Philosophy

University of Washington

1986

Approved by _____
(Chairperson of Supervisory Committee)

_____

_____

Program Authorized
to Offer Degree Department of Geological Sciences

Date June 13, 1986

Doctoral Dissertation

In presenting this dissertation in partial fulfillment of the requirements for the Doctoral degree at the University of Washington, I agree that the Library shall make its copies freely available for inspection. I further agree that extensive copying of this dissertation is allowable only for scholarly purposes, consistent with "fair use" as prescribed in the U.S. Copyright Law. Requests for copying or reproduction of this dissertation may be referred to University Microfilms, 300 North Zeeb Road, Ann Arbor, Michigan 48106, to whom the author has granted "the right to reproduce and sell (a) copies of the manuscript in microform and/or (b) printed copies of the manuscript made from microform."

Signature 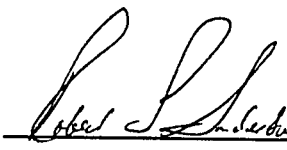

Date June 13, 1986

University of Washington

Abstract

SEDIMENT TRANSPORT BY WIND: SALTATION, SUSPENSION, EROSION AND RIPPLES

by Robert Stewart Anderson

Chairperson of the Supervisory Committee: Professor Bernard Hallet
Deptartment of Geological Sciences

A general model for sediment transport by wind is developed and tested against available data sets on the vertical variation of sediment concentration, mass flux, wind velocity and erosion by windblown particles. The full spectrum of particle behavior, from saltation through suspension is addressed.

Saltation is treated through calculation of single trajectories that are fully determined by the initial conditions of liftoff speed, angle and spin. By specifying the ejection rate of grains from the bed and the broad distribution of liftoff velocities that arise from the stochastic nature of grain impacts with a granular bed, vertical profiles of mass flux can be calculated and are in accord with measurements.

An existing diffusion model of suspension is calibrated with available blowing snow and dust profiles using reference level concentrations. The suspension phenomenon is further explored to define more explicitly the coupling of the saltation and suspension processes at the bed. Individual suspension trajectories are calculated by incorporating turbulent fluctuations using a modified Langevin equation. Ensembles of trajectories are summed to yield concentration profiles that agree well with expected power law behavior.

The horizontal force on the wind due to the downwind acceleration of particles acts to decrease wind velocity gradients near the ground. Force profiles are calculated using ejection rates and initial velocity distributions calibrated with empirical mass flux data. The resulting reduction in stress available to shear the air, when coupled with an eddy viscosity closure hypothesis, yields modified wind velocity profiles that capture well the near-bed reduction in velocity gradients.

Erosion by wind-blown particles is shown to result from the flux of kinetic energy to an obstacle surface by grains entrained by the wind. Kinetic energy fluxes

due to both saltating and suspended grains peak well above the ground in strong winds, in accord with observed abrasion profiles for vertical cylindrical obstacles and for ventifacts. Abrasion due to suspended particles should dominate well above the ground, and should sensitively record the deflection of air flow around the obstacle.

New insights into the grain-bed impact process arising from experiments involving single grain impacts lead to a simple model of eolian impact ripples. A stability analysis demonstrates that a flat bed is unstable, and that the fastest-growing undulations have a wavelength an order of magnitude greater than the mean hop length of the numerous grains mobilized by energetic saltation impacts.

TABLE OF CONTENTS

LIST OF FIGURES

PREFACE

Parts of the work presented in this thesis have already been submitted for publication in professional journals. The material in Chapter 1 was published as Anderson and Hallet (1986); the material in Chapter 4 has been accepted for publication in late 1986 as Anderson (1986). Other chapters, all of which have been written to stand alone as publishable pieces, will soon be submitted for publication.

ACKNOWLEDGMENTS

I wish to thank Bernard Hallet for his consistent encouragement throughout the five years represented by this dissertation. His enthusiasm for science is contagious; I am happily infected. Bernard balanced well my needs for both guidance and independence.

The excellent teaching of Jim Smith provided the foundation for my work in sediment transport theory, for which I am very grateful. Tom Dunne, through both his teaching and his willingness to promote scholarly discussion among graduate students interested in geomorphology, has been a consistent inspiration. I would also like to thank Marcia Baker for encouraging me to treat formally the stochastic portions of the problem, and for pointing me toward the extensive body of research on the topic in atmospheric science. Ed Waddington has been extremely helpful and patient in tutoring me through several mathematical aspects of the work.

The independence of the research both allowed and necessitated correspondence with researchers in other institutions both in the U.S. and abroad. Foremost among these has been Peter Haff, whose enthusiasm for eolian science has greatly enhanced the quality and enjoyment of my research. I also appreciate particularly the communications with Dale Gillette, Ron Greeley, Julian Hunt, Robert Sharp, R.A. Schmidt, and Bruce White.

I would like to express my gratitude to Michael Sorenson and Ole Barndorff-Nielson for their hospitality while on a brief visit to the Aarhus campus in Denmark in November 1985. The free exchange of ideas there, and the encouragement both then and since has been particularly timely.

Grateful acknowledgment is made to the donors of the Petroleum Research Fund of the American Chemical Society, for the support of the research. In addition, I thank the members of the Achievement Rewards for College Scientists foundation, whose support through an ARCS fellowship in 1985 has made this final year considerably more tolerable.

University of Washington students, both present and former, to whom I owe particular intellectual debts include Bill Dietrich, Neil Humphrey, Leslie Reid, and Chris Stubbs. I thank them and I thank many other friends in the Seattle area who have made my stay in the Pacific Northwest a time to cherish.

To the memories of my grandfathers,

WILLIAM E. ANDERSON (June 5th 1889 - March 26th 1985), a chemist,

and

KARL S. VAN DYKE (December 8th 1892 - October 5th 1966), a physicist,

both scholars, both gentlemen.

INTRODUCTION

Sediment transport by wind -- or eolian sediment transport -- is the result of the interaction of the turbulent atmospheric boundary layer with a substrate comprised of loose grains of various sizes. Many practical and scientific problems require quantitative assessment of sediment transport by wind. For example, the ability to predict the total sediment flux and its spatial variation would provide qualitative insight into the process of desertification through soil loss. Calculations of vertical profiles of sediment concentration are central to the interpretation of the remote sensing data from which major eolian events both on Earth and on other planets are inferred. On the other hand, a means of predicting the kinetic energy flux to an obstacle surface by particles of all sizes entrained by the wind is necessary to elucidate their relative importance in forming ventifacts.

Although many field and wind tunnel experiments have been performed to describe these quantities and their spatial variations under various conditions, there exists no rigorous, quantitative theoretical framework to allow the necessary predictions, or to interpret insightfully the available empirical data. It is toward the development of such a theory that this dissertation is aimed.

The eolian sediment transport system may be subdivided into three principal interactions: (1) the wind-grain interaction that entrains and accelerates particles, (2) the grain-wind interaction that modifies the wind velocity profile, and (3) the grain-bed interaction, representing the response of the granular bed to energetic impacts of grains. Aerodynamic drag and lift forces both initiate grain transport and determine the subsequent particle trajectories. Particle accelerations give rise to the two additional interactions. First, Newton's third law requires an equal and opposite force be applied to the wind by the grains, thereby reducing both the near-bed wind velocities and the attendant aerodynamic initation of particle trajectories. Second, grains attain high velocities, resulting in energetic impacts with the bed that generally produce not only new ejected grains, but a net rearrangement of grains within the bed, which may collectively be termed "creep." The grain-wind interaction is a negative feedback, the grain-bed a positive feedback. The steady state transport of sediment must therefore result from a balance of these system components; without proper

models of each of these, no complete model of the transport system may be contemplated.

The philosophy adopted in the present work was to utilize the extensive existing data bases to calibrate and to test physical models of the wind-grain and grain-wind interactions. This dissertation concentrates upon the nature of these two interactions, the complexity of which arises from the wide spectrum of possible particle behaviors in the system, ranging from "saltation" to "suspension". Saltation in this sense refers to the trajectories of particles large enough to follow essentially *deterministic* paths insensitive to the turbulent fluctuations of the air; i.e., once the initial conditions of particle speed and liftoff angle are specified, the trajectory is completely determined. Suspension represents the other end-member of the spectrum, wherein the particles are small enough to respond significantly to the turbulent fluctuations of the wind, and hence travel erratic paths. As the instantaneous velocities of suspended particles may be defined only in some statistical sense, the suspension trajectory process is a *stochastic* one. Ensembles of such trajectories lead to the diffusive nature of the suspension process.

Although in essence the grain-bed interaction is simple, in that it involves normal and shear forces at grain-grain contacts, the problem is difficult because of the large number of grains that may participate in any single impact. As the packing of non-uniform, non-spherical grains is by no means regular, the problem is entirely stochastic, and requires special experimental and numerical techniques being developed elsewhere. At present, we rely upon empirical data on distributions of initial velocities, and total mass flux to circumvent the need to know the physical details of the grain-bed interaction. The numerical models developed can, however, be readily modified to incorporate alternate initial velocity distributions as they become available.

In Chapter 1, a saltation trajectory model is presented in which trajectories are purely deterministic. Testing with existing empirical mass flux profiles demonstrates the need to incorporate a realistic distribution of initial velocities that ultimately results from the grain-bed interaction. The velocity distribution and the total number of grains in transport are calibrated using existing empirical data sets.

Suspension is first treated as a simple continuum diffusion problem relying heavily upon the analogy between transport of momentum and mass. The resulting concentration profiles require calibration using a reference level concentration set by use of data sets on both blowing snow and blowing dust.

In Chapter 2 the assumption of a deterministic trajectory is relaxed. Turbulent fluctuations of the wind are introduced, and are parameterized to represent both the atmospheric boundary layer and the nature of the particle slip relative to the air. The full spectrum of particle behavior, from saltation through suspension may therefore be treated. The use of the reference level concentration in the suspension case is replaced by the ejection rate and distribution of initial velocities found to be important in the saltation case, thereby making explicit the coupling of all trajectory processes through the grain-bed interaction.

Chapter 3 is devoted to a detailed analysis of the modification of the wind profile by the acceleration of transported grains: the grain-wind interaction. Given an ejection rate and a particular set of particle trajectories, a body force on the wind may be evaluated. The resulting reduction in the turbulent stress available to shear the air reduces the near-bed velocity gradient. These calculations are tested against available wind velocity data collected during sediment transport.

In the last two chapters the transport model is used to shed light on two geomorphic phenomena. The vertical variation in the flux of kinetic energy, which dictates erosion by windblown particles, is calculated in Chapter 4. Comparison with measured erosion profiles provides another exacting test of the general transport model. In addition, the relevant physics involved in creating ventifacts is clarified, producing a quantitative framework within which the relative importance of various grain sizes in the process may be assessed. In Chapter 5 an analysis of eolian impact ripples is presented that relies heavily upon insights gained from recent single-grain impact experiments conducted at the California Institute of Technology, where the grain-bed interaction is being actively studied by P.K. Haff and coworkers. A simple stability analysis demonstrates that a flat bed is unstable to small perturbations; a fastest-growing wavelength emerges naturally that is scaled not by the mean saltation length, but by the hop lengths of those grains splashed from the granular surface by high energy impacts.

In summary, the dissertation provides a useful conceptual framework for addressing the general class of problems related to the transport of sediment by wind. The initial calibration of the wind-grain and grain-wind components of the general model is shown to capture the essence of the available empirical data on particle concentration, mass flux, wind velocity, and abrasion profiles. Importantly, the development of quantitative, physical models of the grain-bed interaction emerges as the most pressing research need. The general model presented here is shown to provide new insights into the formation of ventifacts and ripples. Moreover, it has great promise in providing the basis for numerous other geomorphic applications.

CHAPTER 1

SEDIMENT TRANSPORT BY WIND: TOWARD A GENERAL MODEL

In his pioneering studies of eolian sediment transport, Bagnold (1941) described the basic mechanics of saltation and suspension, and presented a comprehensive framework of theoretical, experimental, and field work. This seminal work provided considerable guidance for subsequent studies. However, to this day there is no general quantitative model of eolian sediment transport capable of analyzing each transport mode and their mutual interactions.

Such a general model is desirable for several reasons, both practical and scientific. An understanding of environmental problems plaguing the arid regions of the modern world, especially sub-Saharan Africa, requires the ability to predict rates of dune migration, of soil losses from croplands, and of deflation rates in arid basins (Hassan,1984). The environmental consequences of dust storms, and their role in both continental and marine deposition is a topic of increasing concern and scientific interest (Morales,1979; Schutz,1980; Pewe,1981; Goudie,1983; Rea et.al.,1985; Blank et.al.,1985). On a larger scale, the flux of windblown snow off the Antarctic continent may well influence global climate and sea level through its effect on the water balance of that continent. The importance of eolian deposition and erosion on Mars and Venus has become evident in analyses of both lander and orbiter imagery (Sharp and Malin,1984; Ward et.al.,1985; Greeley and Marshall,1985). Large eolian transport events both on Earth and on Mars are now detectable using remote sensing of surface albedos (Gierasch,1974; Veverka et.al.,1974; Greeley et.al.,1982). Quantitative interpretation of these events requires a theory to calculate particulate concentrations in the entire atmospheric column.

Many geomorphic questions still surround the formation of ripples, ventifacts and yardangs. Geologists have long been intrigued by the characteristic regularity of ripple spacing. The most common explanation calls for a rhythmic bombardment of the surface by saltating grains, the spacing reflecting a "mean" or "characteristic" saltation trajectory length. Yet, no adequate assessment of the details of the distribution of saltation lengths, nor of the creep induced by saltation impacts exists. The

relative importance of saltating and suspended grains in sandblasting ventifacts and yardangs is strongly debated (Whitney,1973,1983; McCauley et.al.1977). This issue can be settled through calculations of the flux of kinetic energy to surfaces exposed to the flow, which will include contributions from each grain size available, whether transported in suspension or in saltation.

The identification of small scale eolian features in the rock record has spurred much recent geologic work in eolian sandstones (Brookfield,1977; Hunter,1977; Koceruk and Dott,1981; Rubin and Hunter,1982). Yet the process by which these features are formed, and particularly the sorting that allows the otherwise homogeneous sandstone records to be "read", is not fully understood, and necessarily requires a knowledge of the behaviour of each grain size.

In this paper, after a review of the literature on both eolian saltation and suspension, we present a general model of eolian sediment transport in order to 1) clarify the processes involved, 2) determine the degree to which existing data may be explained with this simple model, and 3) point to the most fruitful directions for subsequent refinements of the model. Subsequent papers will present some of the proposed refinements, and their applications to the formation of ventifacts, and to the prediction of blowing snow profiles.

1.1 LITERATURE REVIEW

1.1a Saltation

Following the comprehensive studies of Bagnold (1941), the single most important contribution to the theoretical framework of eolian saltation was made by Owen (1964), who developed solutions for the wind velocity profiles both in and outside the saltation layer, and for the fluxes of saltating grains, taken to travel identical trajectories. Ungar and Haff (1985) have recently presented a model relaxing this and other assumptions; the stochastics of particle-bed interactions are treated explicitly, and the steady state profiles of mass flux and wind velocity are found numerically.

A major thrust of eolian saltation research has been the analysis of individual saltation trajectories. White and Schulz(1977) present both theoretical analyses and experimental data on eolian saltation trajectories; they argue strongly for the importance of including the lift force due to particle spin in fitting observed eolian saltation trajectories. White(1982) reports further experimental evidence of high spin rates (100-500 rps) in air, as well as the first good documentation of particle velocity distributions as a function of height.

An analysis of successive saltation hops leading to "stationary saltation" was made by Tsuchiya (1969a), a theme taken up more rigorously by Reizes (1978). Ellwood et.al.(1975) incorporated the results of a set of simple grain bounce experiments in a numerical solution for "steady state saltation".

Wind tunnel studies of saltation include the pioneering work of Bagnold(1941), Chepil(1945), and Chepil and Woodruff(1963), the extensive experiments of Kawamura(1951), Zingg(1953), and Williams(1964), and the more recent work of White and Schulz(1977), White(1982), Gerety and Slingerland(1983), and Willetts(1983). In an extensive research program on Martian and Venusian eolian processes, studies of saltation under reduced and enhanced atmospheric pressures have been conducted by Greeley and coworkers (e.g. Iversen et.al.,1976; White,1982; Greeley et.al.1982; Greeley et.al.1984).

1.1b SUSPENSION

Theoretical and field studies of both blowing dust and snow have contributed to a growing body of literature on eolian suspension. The experimental and field data on the suspension of small sediment grains by wind is relatively scanty. Gillette et.al.(1972,1974), Gillette and Goodwin (1974), and Gillette and Walker (1977), performed field studies of dust production over agricultural sites in Oklahoma, Kansas and Texas, showing that the concentration profiles of the power law form proposed by Rouse(1937) provided good fits to the data. No reliable expression emerged for the concentration at the base of the profile, however. Nickling (1978,1983) reported vertical profiles of mass flux and sediment size associated with dust storms over Yukon Territory's Slim River Valley. The profiles are derived from wind conditions

integrated over one hour periods.

Extensive theory and field data exist for eolian suspension of blowing snow. The same transport modes apply, though the reduced density of snow makes it more likely to be suspended. Moreover, wind conditions at the most frequently studied sites, in Antarctica, are probably the most intense on Earth, again favoring the suspended mode of transport. The cold conditions make snow particles there behave rather elastically, minimizing complications related to the surface water layer existing at temperatures close to the melting point. Early theoretical work on blowing snow (e.g. Mellor and Radok,1960) followed closely that on suspension in aqueous systems, developed primarily by Rouse (1937), and Vanoni(1946). The proposed simple balance between gravitational settling and turbulent diffusion led to power law solutions for concentration above a reference height. As a result of the extensive Byrd Snow Drift Project, Budd (1966) proposed a model including a variable settling velocity with height to explain the departure of mass flux and concentration profiles from the power law. Further work of Mellor(1965), Radok(1968), Kind(1976), Tabler(1980), Male(1980), the extensive work of Schmidt(1977, 1982a, 1982b, personal communication 1983, 1984) and the research of Oura(1967), Kobayashi(1972), Kikuchi(1981), and Takeuchi(1980) in Japan make the data base on blowing snow an impressive one.

Considerable insight into eolian suspension can be gained from recent theoretical analyses of aqueous suspension by Smith(1977), and coworkers (Smith and McLean,1977; Long,1981; Guelphenbaum and Smith,1985). They make several important corrections to the simple diffusion model, allowing a remarkable fit to the flume data sets of Vanoni(1946) and Einstein and Chien(1955). These refinements include the treatment of 1) each size class of particles independently, 2) stratification effects on the turbulent structure caused by the total concentration gradient, and 3) the displacement of fluid by settling grains. These effects are considerably more important than that due to thermal stratification, recently analyzed by Berg(1983).

Despite these treatments of suspension and saltation, as well as those based upon mixture theory (Drew,1975; McTigue,1983; Decker and Brown,1983), there still exists considerable uncertainty about 1) the relative importance of saltation and suspension, 2) the importance of stratification effects on the sediment concentration and wind velocity profiles in suspension, 3) the role of the saltation process in setting

the lower boundary conditions (concentration and wind velocity) for the upper, diffusive region, and 4) the interaction of impacting particles with a granular bed.

1.2 GENERAL DESCRIPTION OF EOLIAN SEDIMENT TRANSPORT

A general model of eolian sediment transport must be able to address a range of sediment sizes subjected to a variety of wind regimes. It must include all modes of sediment transport, including saltation, suspension, and creep, and must address their interactions. The model must treat not only the action of the wind on the sediment, but also the action of the sediment on the wind, both through the extraction of momentum by saltating grains, and by the modification of the turbulence field by the stratification imposed by sediment concentration gradients.

Given a range of grain sizes subjected to a known local shear velocity of the wind, u_*, we expect very large grains to be immobile or to creep along the ground surface, for large grains to move along smooth saltation trajectories, and for small grains to follow complicated suspension trajectories, reflecting fluctuations of the air velocity.

Impacts of saltating grains accelerated by the wind transfer energy to the bed, causing pervasive granular rearrangements, and ejection of one or more particles, one of which may or may not be the original impacting grain. This interaction of incident grains with a bed of high roughness at the granular scale is a stochastic process, in which different grain sizes will display different characteristic ranges of ejection speeds and angles for a given intensity of bombardment. This process will govern the concentration and mass flux profiles for each grain size.

Suspension is inherently stochastic as well. Much as momentum is transferred from one level to another by wind velocity fluctuations, grains suspended in air are transported from one level to another. This transport is diffusive, and may be characterized by an effective diffusion coefficient for sediment that is highly dependent on grain size, yielding different concentration profiles for different grain sizes in

suspension. A full solution of the diffusion profile for the sediment requires a knowledge of the rate at which small particles are introduced into the flow from the bed, which depends upon (1) the frequency, energy and efficiency of saltation impacts, and (2) the aerodynamic force available for lifting small grains off the bed, which itself is modified by the presence of saltating grains in the flow.

It is clear that the general model is a complex one with its manifold couplings. We believe it most appropriate to address first the saltation process, as a knowledge of both the strength of the suspension source and the character of the bed rearrangements we choose to call creep depend on saltation.

We start with the simplest problem in which all grains are assumed to travel identical trajectories, prescribed by a single set of initial conditions. We then show how more realistic initial conditions that reflect the stochastic nature of the particle-bed interactions lead to favorable comparison with concentration and mass flux profiles measured over single grain size beds in wind tunnels. In a more realistic mixed grain size bed, a simple kinetic energy argument leads to a plausible model for the variation in the initial liftoff conditions for the different grain sizes. We then present a first order suspension model and show that this is consistent with reported concentration and mass flux profiles in both dust and snow transport. Existing data sets are used to set a free coefficient in a simple, semi-empirical formula for the reference level concentrations.

Combination of the saltation and suspension models allows calculation of total concentration and mass flux profiles expected for given grain size distribution and shear velocity. As the solutions overlap, the "saltation layer" naturally emerges as that in which the saltation fluxes dominate, and the "suspension region" that in which suspension fluxes dominate. At present eolian creep, the integrated effect of granular rearrangements of the bed, is not treated.

1.3 SALTATION TRAJECTORIES

A numerical model was developed to study eolian saltation, through calculations of trajectories given any wind velocity profile, grain size and density, and set of initial liftoff angles, speeds, and spins. The analysis is restricted to two-dimensional trajectories and to spherical particles. Desired model outputs include vertical profiles of concentration and mass flux, for comparison with published profiles.

Forces acting on the particle are 1) downward body force due to gravity, $\underline{F_g}$, 2) aerodynamic drag, $\underline{F_d}$, 3) aerodynamic lift, $\underline{F_l}$, and 4) Magnus lift due to particle spin, $\underline{F_m}$. (Here and throughout the text vector quantities are underlined.)

As the density of both sand and windblown snow grains are roughly three orders of magnitude greater than that of air, buoyancy can be neglected and $\underline{F_g}$ becomes simply the weight of the particle. Aerodynamic drag is a function of the velocity of the particle relative to the air, $\underline{U_{rel}}$, for both ascending and descending portions of a trajectory (figure 1.1). $\underline{U_{rel}}=\underline{U}-\underline{U_p}$, where $\underline{U}$ is the mean velocity of the wind, assumed parallel to the ground and steady in both speed and direction, and $\underline{U_p}$ is the particle velocity. The drag force on the particle acts in the direction of the relative velocity, and may be expressed as

$$\underline{F_d}=\frac{1}{2}C_d A \rho_a U_{rel} \underline{U_{rel}} \tag{1.1}$$

where A is the cross sectional area of the particle perpendicular to the force vector ($=\pi D^2/4$ for a sphere of diameter D), ρ_a is the density of air, and C_d is the drag coefficient. For spheres, C_d is a well known function of the Instantaneous particle Reynolds number, $\mathrm{Re}=\frac{U_{rel} D}{\nu}$, where ν is the kinematic viscosity of air. Following White and Schulz(1977), we used the curve-fitting formulas for $C_d=C_d(Re)$ presented in Morsi and Alexander(1972).

Aerodynamic lift arises from shear in the flow that gives rise to a pressure gradient normal to the shear in the direction of increasing velocity. The magnitude of the resulting lift force may be expressed as

$$F_l=\frac{1}{2}\rho_a C_l A (U_{top}^2-U_{bott}^2) \tag{1.2}$$

where U_{top} and U_{bott} are the air speeds at a height corresponding to the top and bottom of the grain, and C_l is the lift coefficient, taken to be $0.85C_d$ (Chepil,1958). In

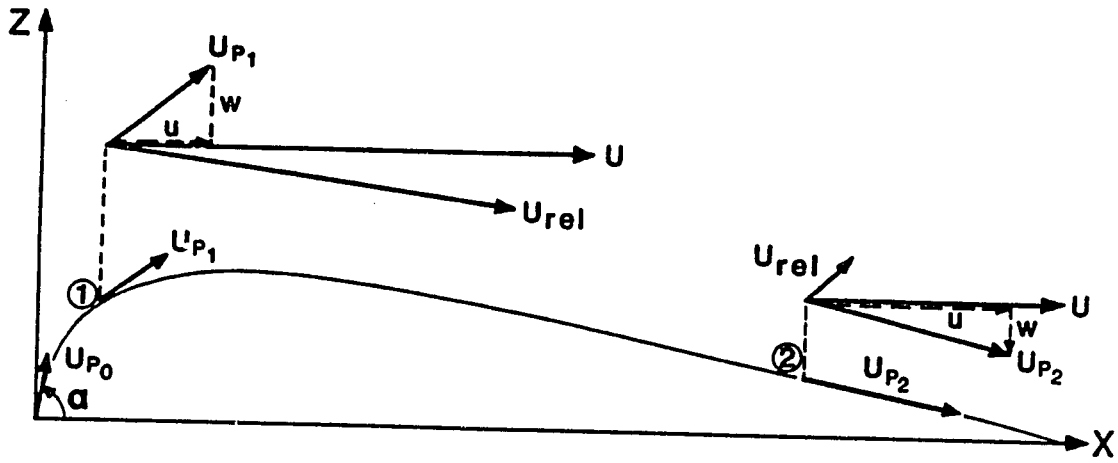

Figure 1.1. Coordinate system, and relation of relative velocity , $\underline{U}_{rel}$, between wind velocity, $\underline{U}$, and particle velocities, $\underline{U}_{p1}$ and $\underline{U}_{p2}$, at two positions in a typical particle trajectory. Particle velocity components, u and w, initial particle velocity $\underline{U}_{po}$, and liftoff angle α are shown as well.

general, aerodynamic lift in air will only be important very near the bed, where the velocity gradients are greatest. However, Owen (1964) showed that shear throughout the saltation layer is greatly reduced by the grain motion, leading subsequent researchers (e.g. Tsuchiya(1969a,b)) to assume a uniform air velocity within the saltation layer, and to ignore aerodynamic lift in calculations of saltation trajectories. Although to first order lift forces can be neglected for trajectories resulting from energetic impacts, they may be important for those trajectories that never get far from the bed. Aerodynamic lift also contributes to the initiation of saltation, which in general requires a complicated mixture of both fluid drag and lift.

The Magnus lift force on a rotating grain is

$$E_m = \pi \rho_a \frac{D^3}{8} (\Omega \, X \, \underline{U}_{rel}) \tag{1.3}$$

where Ω is the angular velocity of the particle (White and Schulz,1977; Rubinow and Keller,1961), taken to be positive for topspin. The angular acceleration of the particle is

$$\frac{d\Omega}{dt} = \pi \mu \frac{D^3}{I} \left(\frac{1}{2} \frac{\partial \underline{U}}{\partial z} - \Omega \right) \tag{1.4}$$

where I is the moment of inertia ($I = 0.1MD^2$ for a spherical grain of mass M), and μ is the dynamic viscosity of the air (Rubinow and Keller, 1961). The first term on the right hand side expresses the acceleration of the spin due to the difference of the air velocity on opposite sides of the grain, while the second term reflects decelleration due to the viscosity of the air.

Though our calculations involve only ideal spheres, we note that the drag, shear lift, and Magnus forces will be modified due to the departure of natural grains from spherical shapes. In an extensive analysis of the dependence of settling velocity on particle shape and roundness, Dietrich (1982) presents results that may be used to assess the departure of the $C_d(Re)$ function from that for ideal spheres. For a reasonable range of natural grain shapes and Reynolds numbers, the drag coefficient may be enhanced by approximately 10-25%. The lift forces will be altered in both magnitude and direction as different cross-sections become perpendicular to the shear. These effects are probably minor in the eolian transport of relatively well-rounded sands, though they may play an important role in the aqueous transport of

ellipsoidal particles (see Wiberg and Smith,1985).

The four forces acting on a grain may be decomposed into x and z components to yield the following respective equations of motion for a saltating particle through a two-dimensional trajectory.

$$M\frac{\partial u}{\partial t}=\frac{1}{2}\rho_a C_d A U_{rel}(U-u)+\frac{\pi\rho_a D^3}{8}w\Omega \tag{1.5}$$

$$M\frac{\partial w}{\partial t}=-Mg-\frac{1}{2}\rho_a C_d A U_{rel} w+\frac{\pi\rho_a D^3}{8}(U-u)\Omega+\frac{1}{2}\rho_a(.85C_d)A(U_{top}^2-U_{bott}^2) \tag{1.6}$$

where u and w are the x and z components of the particle velocity, respectively, Ω is the component of angular velocity perpendicular to the x-z plane, and g is the acceleration due to gravity. For grains with topspin ($\Omega>0$), the Magnus force will accelerate the grain upward as long as the horizontal velocity of the grain is less than that of the wind; in the horizontal the Magnus force will accelerate the grain downwind on the upward limb ($w<0$) of the trajectory, and decellerate it on the descent.

Solving (4) for angular velocity, we also have

$$\Omega(t)=\Omega_o\, exp\left(\frac{-60\mu t}{\rho_p D^2}\right)+\frac{30\mu}{\rho_p D^2}\int_0^t exp\left(\frac{60\mu(t'-t)}{\rho_p D^2}\right)\frac{\partial U}{\partial z}dt' \tag{1.7}$$

where Ω_o is the initial angular velocity perpendicular to the x-z plane.

Dividing through by the mass of the particle yields equations for the accelerations. We first specify D, ρ_p, and the wind profile $U(z)$. Then given a liftoff angle, α, speed of liftoff, U_{po}, and initial particle spin in revolutions per second, S_o, the initial conditions become:

$$u_o=U_{po}\cos\alpha \tag{1.8a}$$

$$w_o=U_{po}\sin\alpha \tag{1.8b}$$

$$\text{and}\qquad \Omega_o=2\pi S_o \tag{1.8c}$$

The numerical calculations of trajectories involve time iterations. At each time step the instantaneous Reynolds number is calculated, a drag coefficient is found, and

the spin rate and local shear are calculated to allow tabulation of an updated set of accelerations, velocities, and displacements.

Motion in the cross-wind direction is not accounted for in these two-dimensional equations. Though the effects of the variability in the wind direction, non-zero vertical components of the angular velocity, and non-zero cross-wind components of the initial particle velocity are therefore not treated, the goal of the present analysis is the vertical distribution of concentration and mass flux, which should be relatively unaltered by these omissions. These effects, however, obviously play important roles in the horizontal dispersion of saltating grains.

As our aim is to calculate the vertical profiles of concentration and mass flux that can be checked against measured profiles, we subdivide the trajectory height into equal increments, dz (taken to be the grain diameter D), and record average horizontal and vertical velocities of the particle as it traverses each increment on both ascending and descending limbs of the trajectory. The likelihood of finding that particle in any height increment, dz, of its trajectory is inversely related to its vertical velocity. Considering first the contribution from a set of trajectories characterized by a single particle ejected per unit area of bed per unit time, all with identical initial conditions, the effective "single trajectory volumetric concentration" is:

$$c_1(z) = N_1 V\left(\frac{1}{|w|_+} + \frac{1}{|w|_-}\right) \tag{1.9}$$

where V is the volume of the particle, N is the number of grains ejected per unit area of bed per unit time (we take N_1=1 for the single trajectory case), and the + and - depict upward and downward limbs of the trajectory, respectively, making explicit the summation over all appearances of the particle in the slice $(z-dz, z)$. Similarly, the "single trajectory mass flux" is:

$$q_{m\,1}(z) = N_1 M\left(\frac{u}{|w|_+} + \frac{u}{|w|_-}\right) \tag{1.10}$$

Once the concentration and mass flux have been calculated for any particular trajectory, these quantities must be summed for each trajectory comprising a representative population. To do this properly, we must know the number of particles ejected per unit area of bed per unit time, N, and the proportion of these

particles travelling along each of many possible trajectories, which can be expressed as a probability density of liftoff conditions, including spin, speed, and angle. Because the most important of these is the vertical component of the liftoff velocity, w_o, we may simplify this facet of the problem to defining the probability density of vertical liftoff velocity, $P(w_o)$. The expressions for concentration, $c(z)$, and mass flux, $q_m(z)$, then become:

$$c(z)=\frac{N}{N_1}\int_0^\infty P(w_o)c_1(z)dw_o \tag{1.11}$$

$$q_m(z)=\frac{N}{N_1}\int_0^\infty P(w_o)q_{m\,1}(z)dw_o \tag{1.12}$$

where the "1" subscripts on N, c and q_m again denote single trajectory quantities.

The simplest possible form for the probability density of liftoff velocities is a delta function: all particles travel identical trajectories. In this case, the integral equations reduce simply to the product of the ejection rate, N, with the single trajectory quantities. For a chosen representative trajectory characterized by an initial vertical velocity, w_o, the ejection rate is set by calculating the integral of the single trajectory mass flux, $q_{m\,1}$, over the height of the trajectory, and by comparing it with the total mass flux expected from an empirical relation between the shear velocity, u_* ($=\sqrt{\tau_b/\rho_a}$, where τ_b is the shear stress at the bed), particle size, and mass flux. We have used two such relations in our calculations: (1) Bagnold's (1941,p.67,eq.9) simple relation,

$$Q=.18\left(\frac{\rho_a}{g}\right)\left(\frac{.00025}{D}\right)^{\frac{1}{2}}u_*^{\,3} \tag{1.13a}$$

and (2) White's (1979) relation,

$$Q=.261\left(\frac{\rho_a}{g}\right)(u_*+u_{*cf})^2(u_*-u_{*cf}) \tag{1.13b}$$

where u_{*cf} is the fluid threshold shear velocity needed to initiate saltation (see figure 1.15). Both relations are expressed in units of $\frac{kg}{m\ s}$. For typical conditions, White's empirical equation yields mass fluxes roughly twice those predicted by Bagnold's equation.

1.4 RESULTS OF NUMERICAL SALTATION MODEL

Typical trajectories are presented in figure 1.2 for a range of liftoff angles. The calculated trajectories and related profile quantities were found to be relatively insensitive to the detailed structure of the wind within the saltation layer. Three wind profiles were explored (see figure 1.3): 1) matched logarithmic profiles, the lower with a slope of $\frac{u_{*cf}}{k}$ and a roughness height of D/30 (Nikuradse roughness, appropriate for hydraulically rough flows), the upper with slope $\frac{u_*}{k}$ and a roughness height described by Owen's $z_o = 0.0207 u_*^2/2g$; 2) Owen's analytic form of the velocity structure (Owen, 1964, eqn.42); and 3) uniform wind of $8.5u_*$. The first structure was used by White and Schulz(1977), and the third by Tsuchiya(1969a,b) in his numerical work on trajectories. We prefer the first structure because the wind velocity 1) goes to zero at a reasonable height, avoiding unrealistic lift forces on particles in the bed; and 2) extends smoothly to levels well above the saltation layer. The choice of velocity structure is not as critical as may be anticipated; resulting trajectory heights and lengths typically vary only 10 % when particles with identical initial conditions are subjected to the three wind structures.

Our calculated trajectories agree with White and Schulz's(1977), allowing similar conclusions regarding the importance of the various forces on the particle. In the no-spin cases, the maximum trajectory height is consistently 20 to 60 % below that estimated assuming all the initial kinetic energy has been converted to potential energy (i.e. assuming no drag and no lift in the vertical): $z_{max} = \frac{w_o^2}{2g}$, where w_o is the vertical component of the liftoff velocity. As drag in the vertical is roughly proportional to the square of the vertical component of the liftoff velocity, particles ejected at high angles and at high speeds will fall shorter of this "no-drag height" than others (figure 1.4).

For spherical particles, aerodynamic lift forces enhance trajectory heights by 4 to 15 %, depending upon the proportion of the trajectory spent in the zone of highest shear near the bed. For medium sand (D=.25mm), at a height of only 10

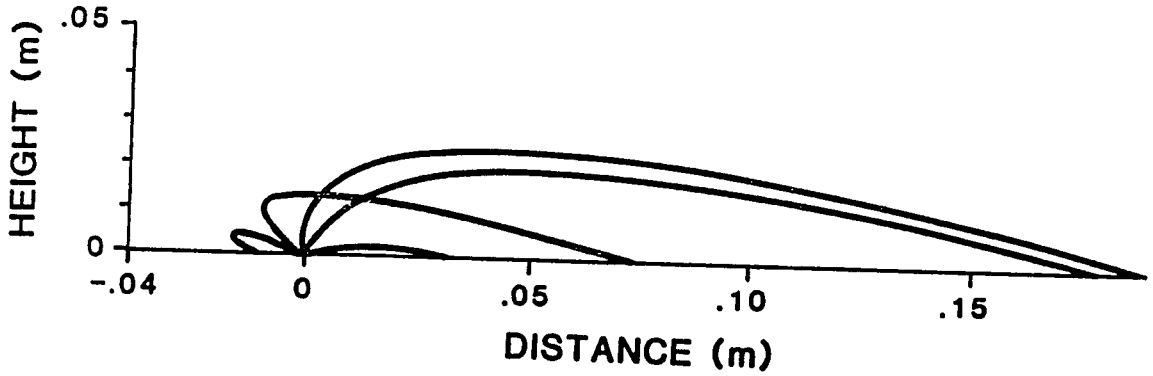

Figure 1.2. Particle trajectories for quartz particles of diameter D=.3mm (u_{*cf} =.25m/s), u_*=.6m/s, liftoff speed U_{p0} =.84m/s, and liftoff angles α=160,140,90,60,10 degrees. Wind velocity profile used is the "matched log" profile in figure 1.3.

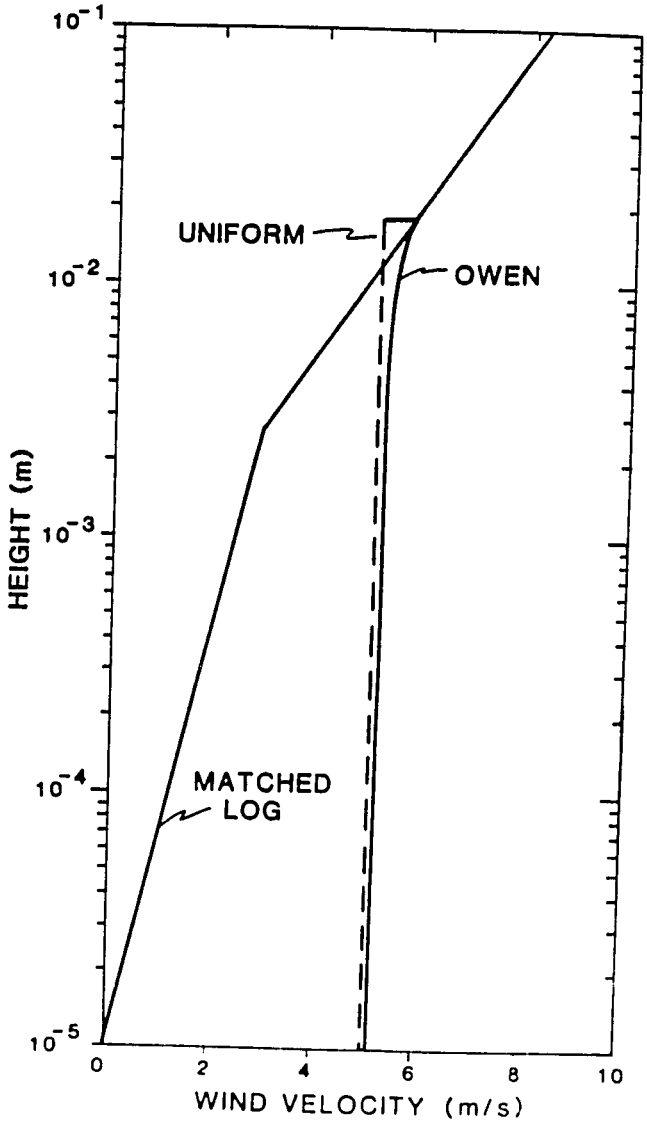

Figure 1.3. Three wind velocity profiles, all for $u_* = .6$m/s, D=.25mm ($u_{*t} = .19$m/s). The profiles coincide above the height $\frac{u_*^2}{2g}$. "Matched log" profile was used in White and Schulz (1977), and is used in our calculations. "Uniform profile" is that used by Tsuchiya (1969a), as an approximation to the solution suggested by the analytical work of Owen (1964), also shown.

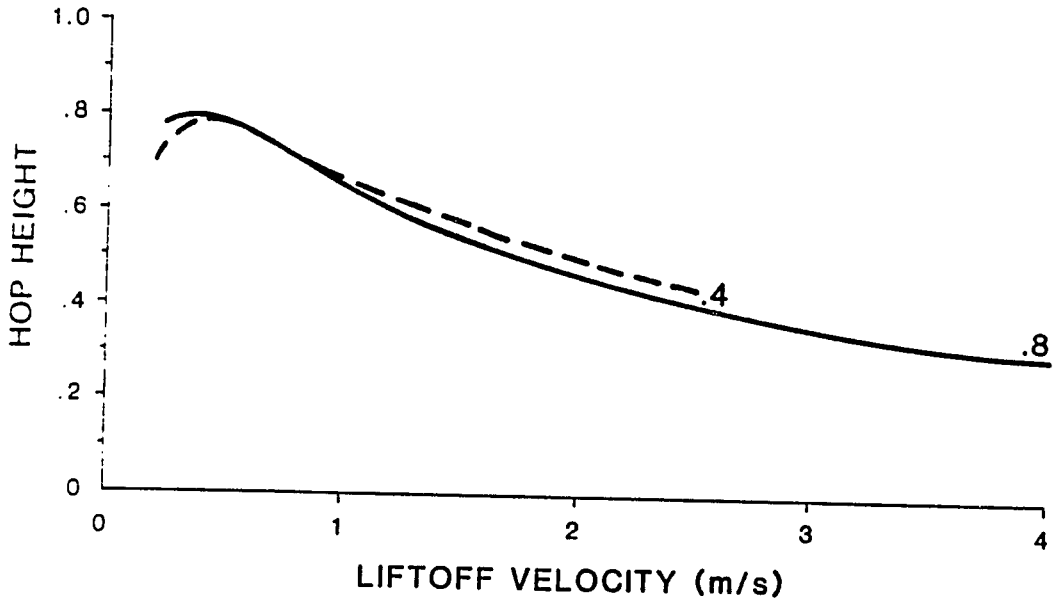

Figure 1.4. Hop height relative to $\frac{w_o^2}{2g}$, the height a particle would reach in the absence of non-gravitational forces, plotted as a function of liftoff velocity, w_o. D=.25mm; liftoff angle is vertical. Labels refer to shear velocities, u_*, in m/s.

grain diameters above the bed the lift on the particle has decreased by more than tenfold from its take-off value. Lift forces have greatest effects on trajectories with low liftoff angles and speeds. For the maximum spin rates of hundreds of revolutions per second, reported for both saltating sand (White and Schulz,1977), and saltating snow (Kobayashi, 1972), trajectories may exceed the no-drag height by up to 25%. We may therefore expect that averaging over the range of realistic spin rates and orientations may yield a mean trajectory height close to the no-drag and no-spin height.

Typical trajectory durations are on the order of .1-.2s, and are consistently within 10% of $2\frac{w_o}{g}$, the duration expected in the absence of non-gravitational forces. According to equation 7, particle spins at impact may still be half those at liftoff for typical saltating grains of diameter .25 mm. Particles half and twice this diameter will impact with about 10 and 85% of their liftoff spins, respectively.

The trajectory length is strongly influenced by the vertical component of the liftoff velocity, for a given wind strength (figure 1.5). Therefore, a large range of hop lengths can be expected to result from a realistic range of vertical liftoff speeds, such as that measured by White and Schulz(1977). Hop lengths are remarkably similar for different grain sizes between .15 and .35 mm, experiencing identical liftoff conditions. Because drag is inversely related to grain size, smaller grains do not travel as high, but undergo greater horizontal acceleration than larger grains. Despite the resulting variation in aspect ratios of trajectories with particle size, the impact angles are nearly independent of grain size. Similarly, the impact angles are only weakly dependent on liftoff velocity (see figure 1.6), in accord with Bagnold's (1941) original observations, and with more detailed measurements of impact angle made by White and Schulz(1977).

Particles ejected with a wide range of vertical velocities will impact the surface with three to five times their initial velocities (figure 1.7), or roughly 10 to 20 times their initial kinetic energy. This additional energy will be partitioned between the subsequent, or "successive" saltation of the same grain, the ejection of one or more additional grains from the bed, and absorbtion by friction between grains in the bed. This calculation provides some constraint upon the energy available to fracture

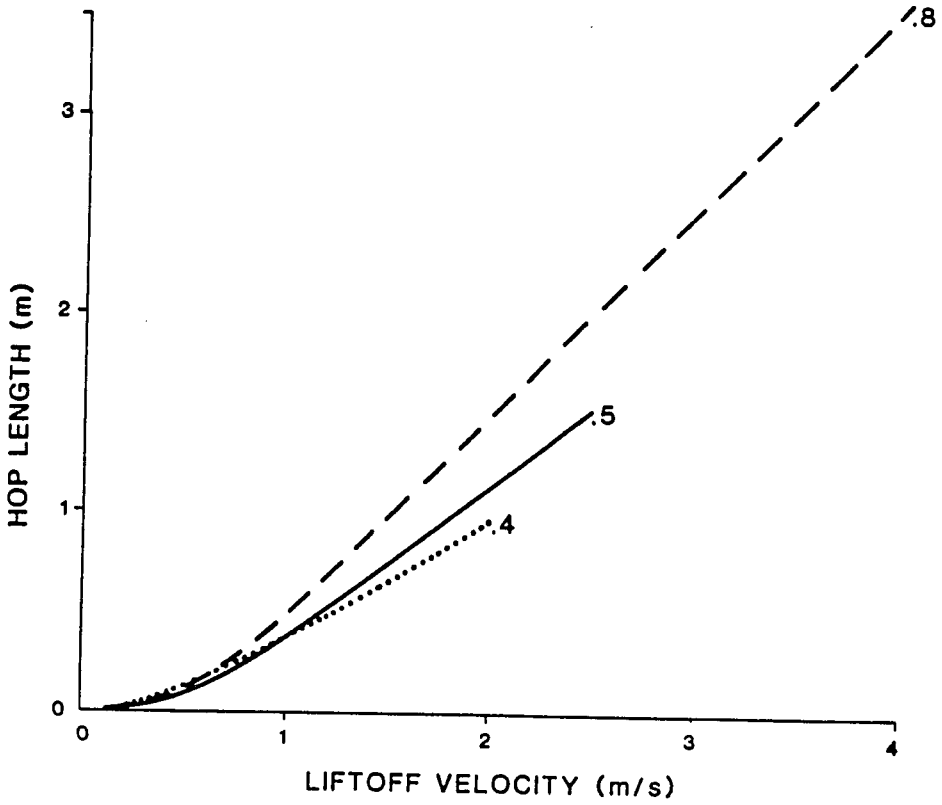

Figure 1.5. Hop length as a function of liftoff velocity for $u_* = .4, .5$, and .8 m/s. D=.25mm, α=90.

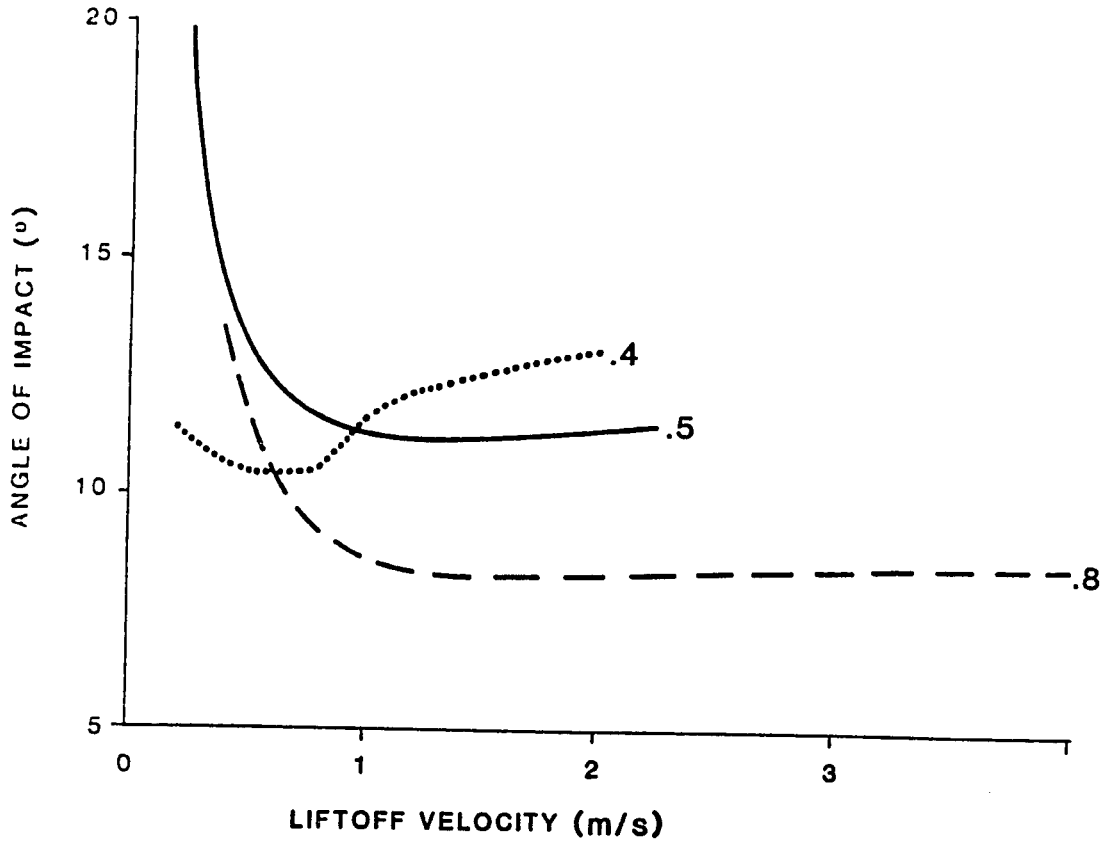

Figure 1.6. Angle of impact with the bed as a function of liftoff velocity, for u_*=.4,.5, and .8 m/s. D=.25mm, α=90.

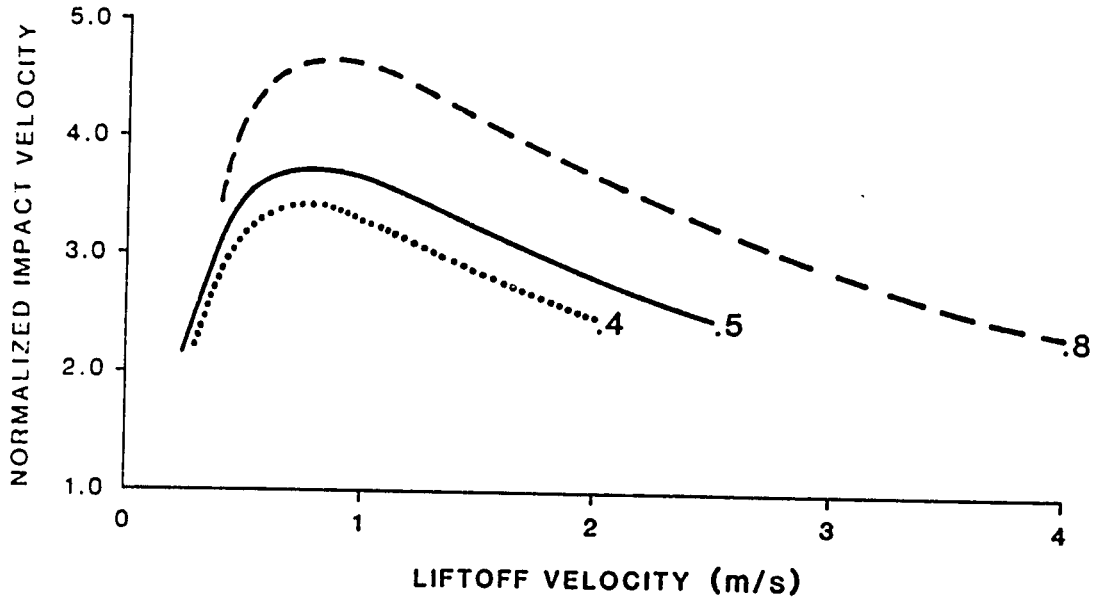

Figure 1.7. Impact velocity relative to liftoff velocity U_{pim}/U_{po}, as a function of liftoff velocity, for u_*=.4,.5, and .8m/s. D=.25mm, α=90.

grains, resulting in the rounding and frosting of grains, and in the production of dust fragments.

1.5 CONCENTRATION AND MASS FLUX PROFILES

The concentration and mass flux as functions of height for the identical trajectory case invariably show distinct maxima at the top of the trajectory (figure 1.8a and b). Our model also gives us access to the vertical variation of the mean horizontal particle velocity (summed over upward and downward portions of the trajectory), which is now measureable (Schmidt,1977). Given the vertical profiles of the mass flux, $q_m(z)$, and concentration, $c(z)$, the mean horizontal particle velocity becomes:

$$\overline{u}(z)=\frac{q_m(z)}{\rho_p\, c(z)} \tag{1.14}$$

The mean horizontal particle velocity, expressed as a fraction of the wind speed at the top of the trajectory, decreases from roughly .5 at the bed to .3 at the top of the hop for typical saltating quartz grains of diameter D=.25 mm (figure 1.9). These proportions increase with both increasing ejection velocity and decreasing particle size and density. Snow grains of the same size, for example, attain 70 % of the wind velocity at the top of the hop, and average 90 % of that velocity at the bed.

1.6 PROBABILISTIC ASPECT OF THE SALTATION MODEL

The peak of the mass flux profile at the top of the hop is clearly due to the vertical concentration gradient that reflects the amount of time a particle spends in any height increment, dz. These patterns in concentration and mass flux are clearly unrealistic, however, because all particles are assumed to travel identical trajectories. Indeed, abundant experimental data reveal monotonic declines in these quantities

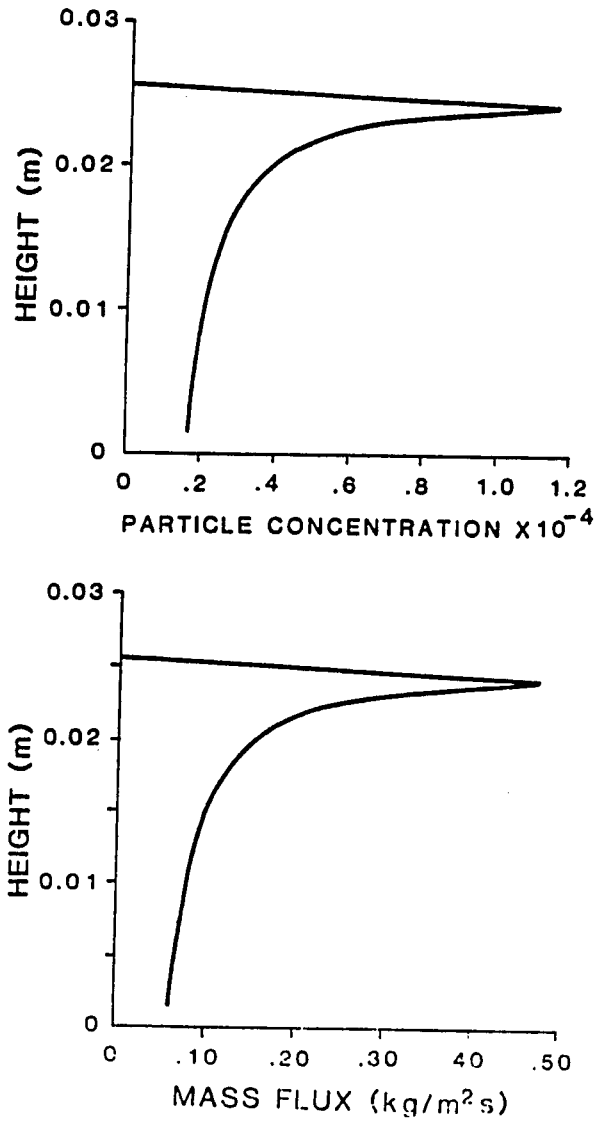

Figure 1.8. Particle concentration (a), and mass flux (b) profiles with height, for the identical trajectory case, showing distinct maxima at the top of the trajectory. D=.32mm, $u_* = .53$m/s, $w_o = .74u_*$, $\alpha = 90$.

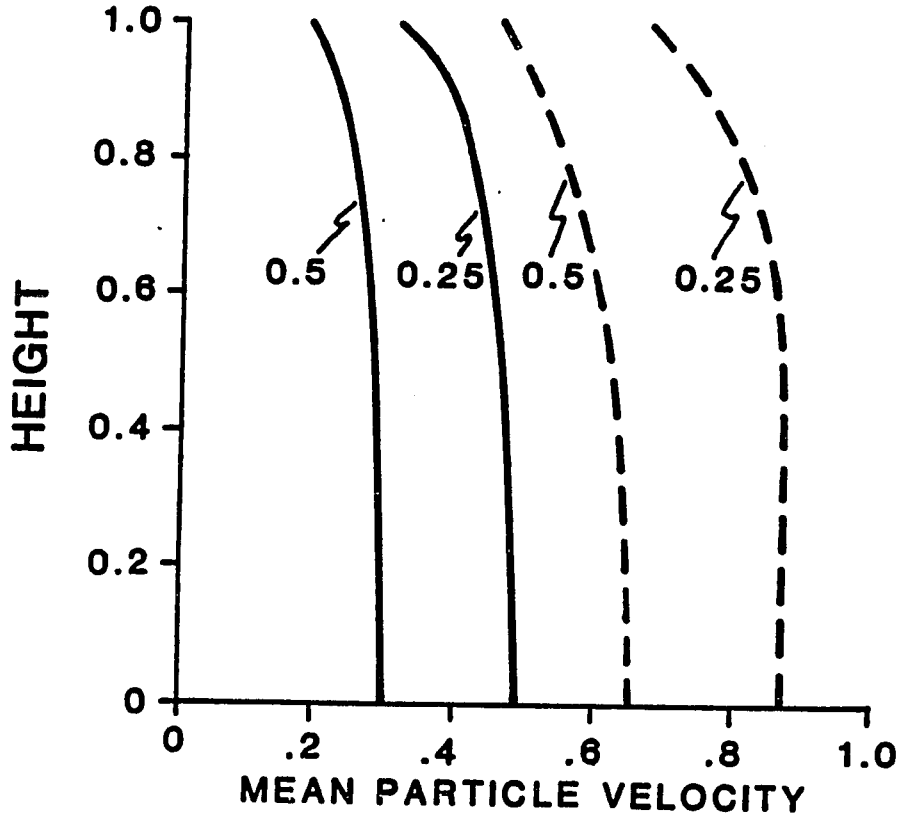

Figure 1.9. Mean particle velocity relative to the wind velocity at the top of the trajectory, as a function of height (normalized with trajectory height), in the identical trajectory case. Labels refer to particle diameter in mm. Dashed lines represent data for snow, solid for quartz. $w_s = u_* = .5$m/s, and $\alpha = 90$ in all cases.

with height during saltation of both sand and snow (Williams,1964; Takeuchi,1980; White, 1982; Greeley et.al.,1983). Williams(1964) shows mass flux profiles above mixed grain size beds decay exponentially with height. Takeuchi(1980) claims saltation profiles fall off exponentially, while suspension profiles fall off as power laws with height. White(1982) and Greeley and coworkers(1983), too, conclude that the dependence of mass flux with height is exponential, regardless of the wind and bed conditions.

The differences between such measured profiles and those calculated with the simple identical trajectory model motivates us to include in the model the inherent stochastic elements of ballistic collisions at the bed. Measurements from filmed saltation trajectories in wind tunnel experiments (White and Schulz,1977,figure 6) clearly show a wide range of initial conditions, presumably due to complex interactions of impacts with a with loose, granular bed capable of significant deformation. Liftoff speeds range from essentially zero to four or five times the shear velocity of the air, and liftoff angles range between 20 and 100 degrees from the horizontal.

Following Ungar and Haff (1985), we propose that the essense of the stochastic ejection of grains from the bed may be represented by a probability distribution of the vertical liftoff speeds, the most important determinant of the trajectory shape. As a preliminary numerical experiment, we divided the probability density of liftoff speeds into ten distinct classes, assigning probabilities in accordance with a two parameter gamma function fit to White and Schulz's distribution of lift-off speeds (figure 1.10):

$$P(w_o)=\frac{27}{2}\left(\frac{1}{.96u_*}\right)\left(\frac{w_o}{.96u_*}\right)^3 exp\left(-3\left(\frac{w_o}{.96u_*}\right)\right) \qquad (1.15a)$$

where $.96u_*$ is the most probable vertical liftoff speed, and $\frac{27}{2}$ ensures that the integral of the probability density is unity. As only the distribution of initial speeds was reported, estimates of the vertical components of the liftoff velocities were obtained by multiplying all speeds by the sine of 50 degrees, the reported mean liftoff angle. (In essense, this calculation assumes the distribution of liftoff angles is independent of liftoff speed.) Noting the photographic method by which White and Schulz measured their distribution of initial conditions, and the inherent difficulty of

resolving individual trajectories very near the bed, it is highly likely that a large portion of trajectories with low initial vertical velocities were not counted. A second fit to the White and Schulz data was therefore made assuming an exponential form of the distribution, also shown in figure 1.10:

$$P(w_o) = \frac{1}{.63u_*} exp\left(-\frac{w_o}{.63u_*}\right) \tag{1.15b}$$

where $.63u_*$ is now the mean liftoff velocity. The two empirical relations for mass flux as a function of shear velocity and grain size were again used to set the total number of particles ejected per unit area of bed per unit time, N. The number of particles traversing each trajectory is then $NP(w_o)dw_o$.

A representative mass flux profile is presented in figure 1.11, together with measured mass flux data reported by Williams (1964) for his "intermediate" shear velocity case (.53m/s). The grain diameter corresponds to the mean grain size in his "symmetrical" grain size distribution (.32mm). The discontinuous nature of the profile introduced by our gross discretization of the continuous probability density has been smoothed. Now both concentration and mass flux decrease with height, much as the experimental data. The best accord with the measured fluxes is obtained using the exponential form of the probability distribution of liftoff velocities, and White's form of the mass flux relation.

The distribution of the liftoff velocities of the form represented by our equations 15a and 15b result in distributions of hop lengths shown in figure 1.12 for various shear velocities. The broad distribution becomes even more dispersed as the shear velocity increases. The lack of a sharp maximum in the probability distribution at finite hop lengths casts doubt on the connection between "mean path length" and ripple wavelength that has been repeatedly suggested by previous workers (e.g. Bagnold,1941; Ellwood et.al.,1975).

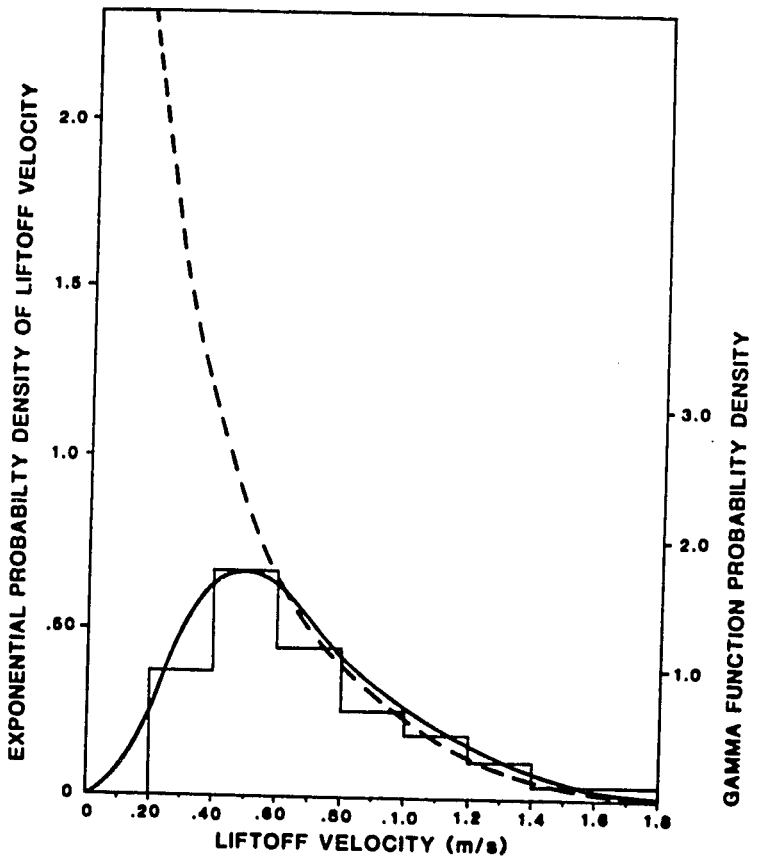

Figure 1.10. Probability distribution of liftoff velocity. Histogram is White and Schulz (1977) data from photographs of 57 particle trajectories, with $u_* = .396$m/s, D=.35-.71mm. Solid line is best fit gamma distribution (eqn.1.15a); dashed line is best fit exponential distribution (eqn.1.15b). Vertical component of liftoff velocity is obtained by multiplying liftoff velocity by sine of the mean liftoff angle (50 degrees).

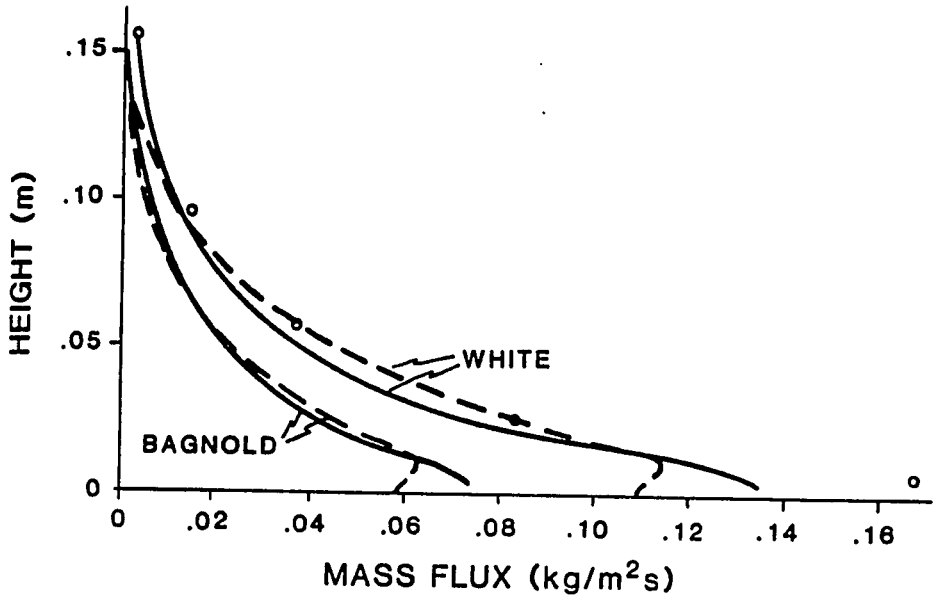

Figure 1.11. Calculated and measured (circles) mass flux profiles for Williams's (1964) "symmetric" grain size distribution, "intermediate" velocity run ($u_* = .53$m/s). Curves are smoothed versions of 10-trajectory simulations, using a single grain size equivalent to the mean reported size (D=.32mm). Continuous lines refer to exponential distribution of liftoff velocities (eqn.1.15b); dashed lines refer to gamma distribution (eqn.1.15a). Labels refer to mass flux relations used: Bagnold (eqn.1.13a), and White (eqn.1.13b).

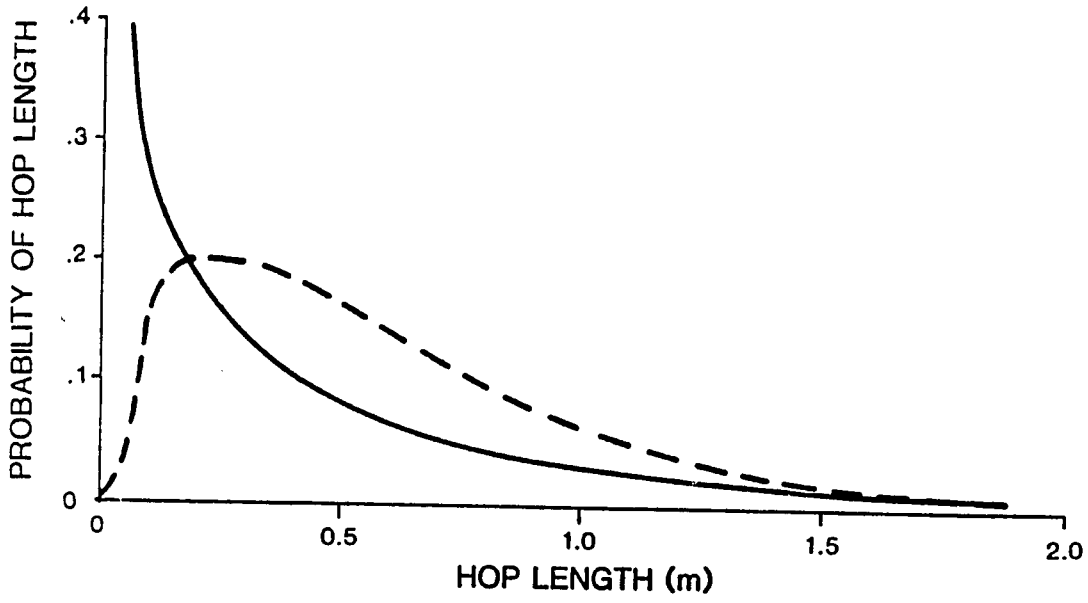

Figure 1.12. Broad distribution of hop lengths for exponential and gamma distributions of liftoff velocity, in the simulation of Williams's "symmetric, intermediate" case.

1.7 MULTIPLE GRAIN SIZES IN SALTATION

An obvious extension of the saltation model involves the incorporation of several different grain sizes, each comprising a different fraction of the bed, i_b. An analysis of Williams's (1964) wind tunnel data shows that for a given shear velocity, the mass flux decreases with height at a rate that increases with grain size. This strongly implies that high liftoff velocities become considerably less likely as grain size increases. We propose the following admittedly tentative argument to account for this effect. If the kinetic energy delivered to the bed by impacting grains is uniformly available for the consequent ejection of any grain in the bed, we would expect the smallest grains to be ejected at the highest average velocities. To incorporate this effect simply in the model, we assume that each particle size has identical mean kinetic energy upon ejection from the bed. This requires that the mean velocity of particle size "i" be inversely proportional to the square root of its mass, M_i:

$$(\overline{U_{po}})_i = (\overline{U_{po}})_{ref} \left(\frac{M_{ref}}{M_i}\right)^{\frac{1}{2}} \tag{1.16}$$

where $(\overline{U_{po}})_{ref}$ is the mean liftoff velocity for a reference grain of mass M_{ref}.

We use White and Schulz's (1977) distribution to set the reference conditions, i.e. the dependence of the mean liftoff velocity on shear velocity for a reference grain size, D=.35mm, yielding $(\overline{U_{po}})_{ref} = .84u_*$. Again adjusting for the mean liftoff angle yields $\overline{w_o} = .63\ u_*$. Once the mean vertical velocity has been set, the exponential probability density function (equation 15) is fully determined. The total mass flux of each grain size, Q_i, is taken to be simply the product of the total mass flux, Q, with the weight fraction of that grain size in the bed, i_b. The total flux is again determined using Bagnold's mass flux relation, calculated using the mean grain size of the bed.

This inferred grain size dependence has been assessed by comparing our calculated mass flux profiles with profiles for individual grain sizes derived from experimental data (Williams,1964). Specifically, figure 1.13 shows the results for a "symmetric" grain size distribution, with $\overline{D} = .32$mm, subjected to an "intermediate" shear

velocity, $u_* = .53$m/s. The mass flux gradients closely parallel the measured gradients, implying that our assumed grain-size dependence of the liftoff velocity probability densities accounts for much of the grain size effect, for grains ranging in size from about .1 to .6 mm. Again a better correspondence is obtained between measured and calculated profiles using White's mass flux relation than using Bagnold's.

1.8 SUSPENSION

As in most treatments of steady state eolian suspension, we begin with the simple balance of gravitational settling and turbulent diffusion of sediments (Budd,1966; Shiotani and Aria,1971; Gillete,1972):

$$\frac{\partial}{\partial z}(K_s(\frac{\partial c_s}{\partial z})) = -s(\frac{\partial c_s}{\partial z}), \tag{1.17}$$

where K_s is the effective diffusion coefficient for the sediment, s is the concentration-weighted average settling velocity of the sediment, and c_s is the total volumetric sediment concentration. In the absence of sediment sources and sinks, integration of equation 17 yields

$$K_s \frac{\partial c_s}{\partial z} = -sc_s \tag{1.18}$$

The effective diffusion coefficient for the sediment is then assumed to be equivalent to that for momentum ($K_s = K$), which varies linearly in the boundary layer characterized by the logarithmic velocity profile ($K = ku_* z$, with k von Karman's constant, 0.4). The equation may then be integrated to yield

$$c_s = c_a(\frac{z}{z_a})^{\frac{-s}{ku_*}} \tag{1.19}$$

where c_a is the total concentration at a reference height z_a.

A more complete analysis (Smith,1977; Long,1981) produces equations for the concentration of each grain size in the system:

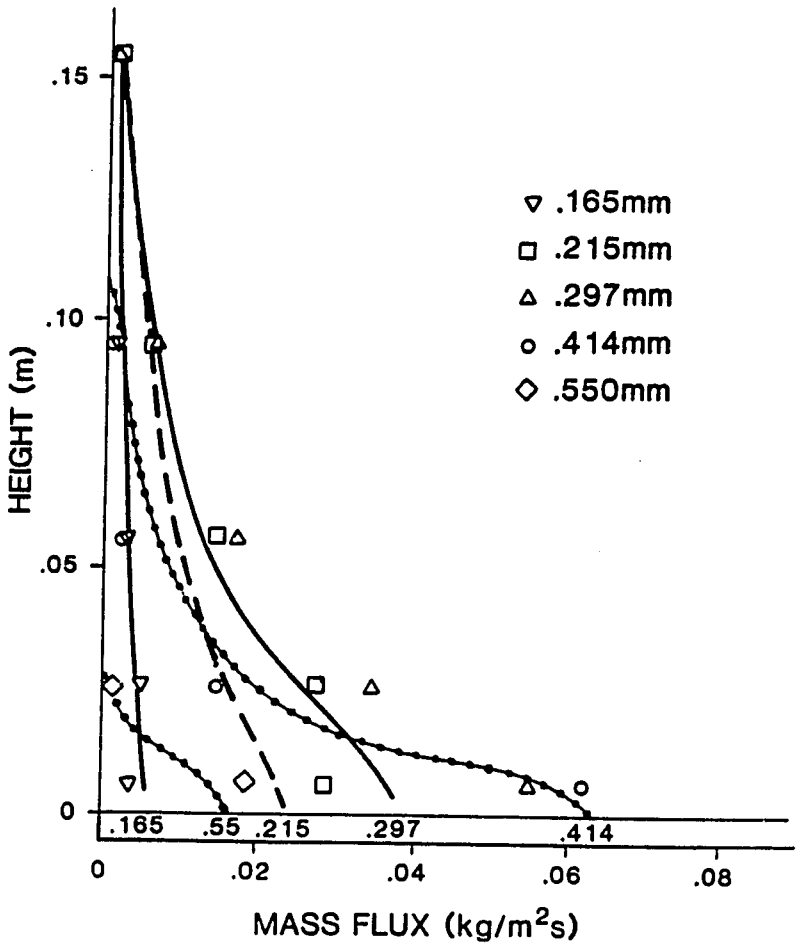

Figure 1.13. Calculated and observed mass flux profiles for five grain sizes in Williams's "symmetric-intermediate" case. Symbols represent fluxes measured at specific heights; curves represent calculated mass fluxes for the grain diameters labelled at the base of the curves, using the exponential distribution of liftoff velocities, the scaling of liftoff velocity with size (equation 16), and White's mass flux relation. The sum of these curves corresponds well to the profile calculated using the mean diameter (D=.32mm), shown in figure 1.12.

$$c_n = (c_n)_a \frac{(1-c_s)}{(1-c_s)_a} \exp \int_{z_a}^{z} -\frac{s_n}{k u_* z} dz \qquad (1.20)$$

where $(c_n)_a$ is the concentration of sediment size class n at the reference height, and s_n is the settling velocity of size class n. This reduces to a power law relation for each size fraction:

$$c_n = (c_n)_a \frac{(1-c_s)}{(1-c_s)_a} \left(\frac{z}{z_a}\right)^{-p_n} \qquad (1.21)$$

where the power $p_n = \frac{s_n}{k u_*}$ is often called the Rouse number (Guelphenbaum and Smith,1985). This resembles closely equation 19 for the total suspended concentration, but now the settling velocity used is that of a single grain size (figure 1.14), rather than a concentration-weighted average. The total concentration is coupled to that of individual size classes through the $(1-c_s)$ terms. Much of the departure of individual size class concentration profiles from the simple power law relation reflects the upward fluid velocity caused by the continuous settling of particles.

The total concentration profile is then simply the sum of the individual concentration profiles:

$$c_s = \frac{(1-c_s)}{(1-c_s)_a} \sum_{n=1}^{n=i} (c_n)_a \left(\frac{z}{z_a}\right)^{-p_n} \qquad (1.22)$$

It departs from the power law relation (equation 19) because, at each level, the concentration field is dominated by different grain sizes, and hence by different power law behavior.

1.9 LOWER BOUNDARY CONDITION

To calculate concentration profiles, the sediment concentration at some reference level, $(c_n)_a$, must be properly assigned. Though the shapes of the concentration, and mass flux profiles are fixed by the theory, the magnitude of each depends on this boundary condition, which will reflect the saltation process near the bed.

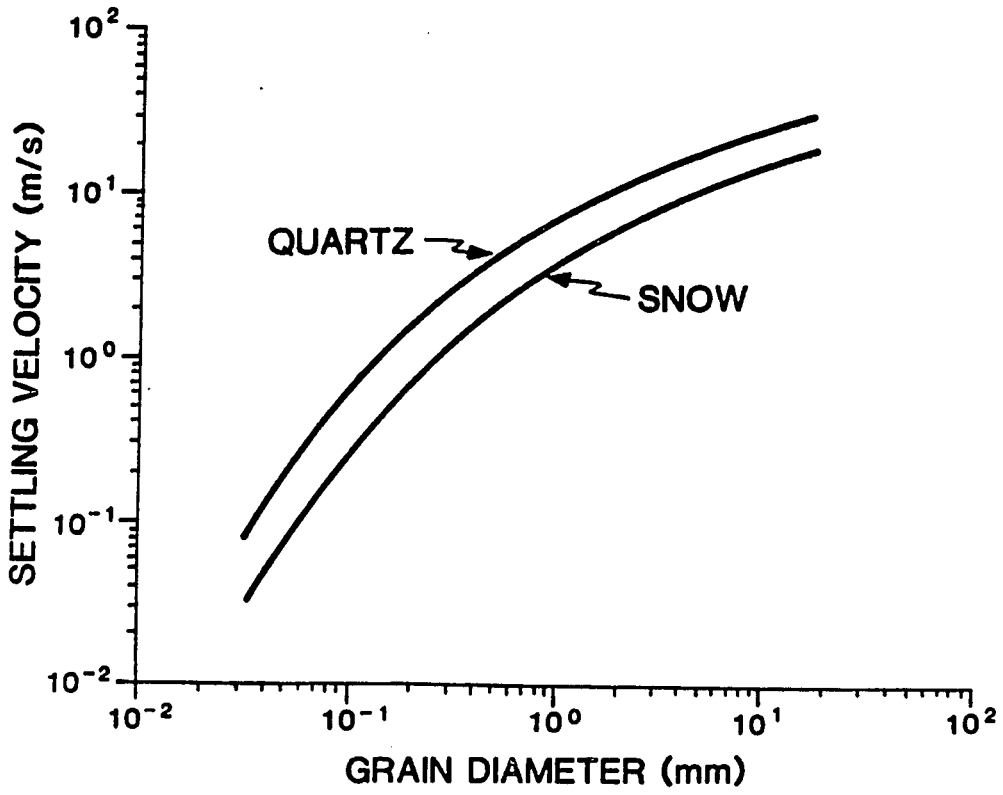

Figure 1.14. Calculated settling velocity as a function of grain diameter, for spherical particles of quartz (ρ_p =2650 kg/m^3), and of ice (ρ_p =917 kg/m^3).

Thus a full treatment of eolian sediment transport will require an explicit coupling of the saltation and suspension problems. In the absence of such a model, previous workers in suspended sediment studies have simply relied upon experimental data to set the lower boundary condition (Gillette et al.,1974 in air; McTigue,1983 in water), or have used order of magnitude estimates of the relative magnitude of saltation and suspension fluxes (Greeley et al.,1982 on Mars).

We follow the work on aqueous systems by Smith (1977), who parameterizes the concentration of size class n at a reference level as

$$(c_n)_a = \frac{(c_n)_b \gamma S}{1+\gamma S} \tag{1.23}$$

where S is a non-dimensional excess shear stress, $S = \frac{\tau_b - \tau_c}{\tau_c}$, with τ_c the critical shear stress needed to entrain sediment of size class n, $(c_n)_b$ is the concentration of the size fraction in the bed, and γ is a free coefficient. This formulation behaves properly at the high and low excess shear stress asymptotes: as $S \rightarrow \infty$, $c_{n\,a} \rightarrow c_{n\,b}$, and as $S \rightarrow 0$, $c_{n\,a} \rightarrow 0$. γ is set by comparison with specific sets of field or experimental data (Smith and McLean (1977) argue $\gamma = O(10^{-2})$ for medium sands in water.)

We redefine the excess shear stress to account for the difference between the fluid dynamic threshold shear stress, τ_{cf}, and the impact threshold, τ_{ci}. As recognized long ago by Bagnold(1941), the distinction is important for eolian sediment transport because of the dominant effect of saltation impacts in mobilizing particles off the bed. In the presence of mixed grain sizes in the bed, impacting grains will eject small grains that would otherwise require much higher boundary shear stresses to move (figure 1.15). Gillette and coworkers(1972,1974) have shown conclusively that winds over agricultural soils will suspend the finer grains as soon as some grains begin saltation. It follows that the production rate of small grains from the surface, and hence the reference level concentration ought to vanish as the boundary shear stress drops well below the threshold necessary to cause saltation of the most susceptible grains: τ_{cmin} (see figure 1.15); and that given a saltation event, the smaller grains are more readily mobilized into suspension. A more appropriate form for the excess shear stress may therefore be

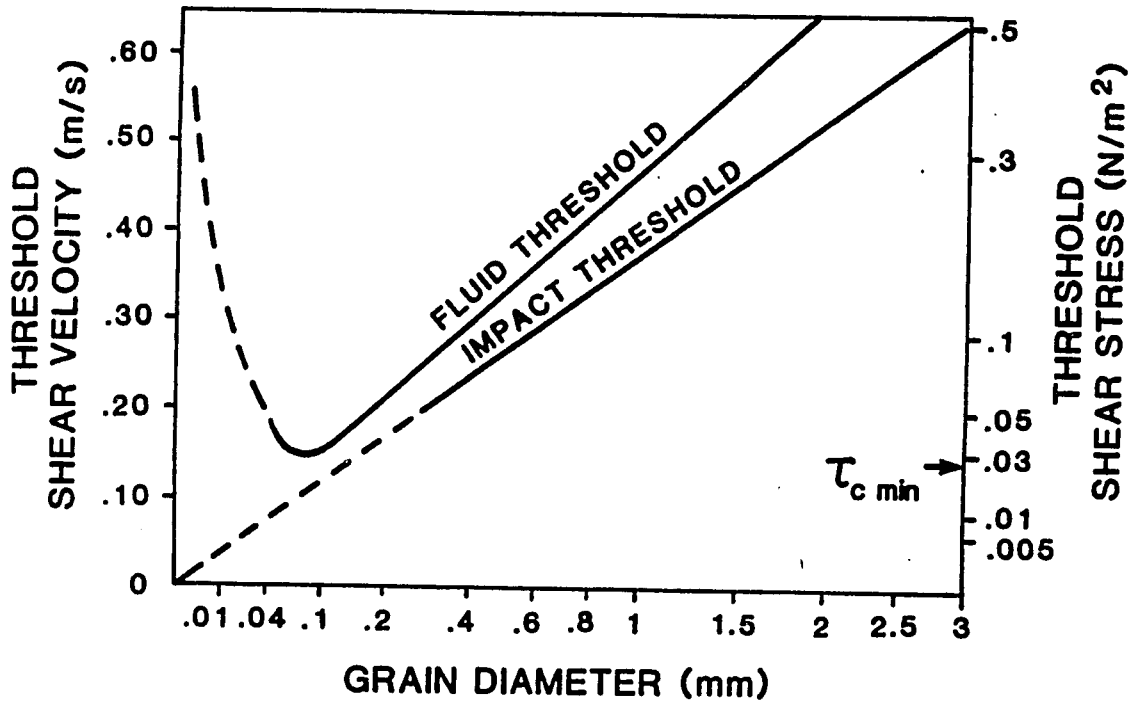

Figure 1.15. Threshold shear velocity and threshold shear stress as functions of grain diameter, showing "impact" and "fluid" thresholds (after Bagnold,1941). τ_{cmin} is the minimum shear stress needed to initiate motion of the most readily transported grains.

$$S = \left(\frac{\tau_b - \tau_{ci}}{\tau_{ci}}\right) \tag{1.24}$$

Here the hysterisis characteristic of eolian sediment transport is neglected; nonetheless, this form might be expected to apply at shear stresses characteristic of the experiments discussed in this paper, which are well above τ_{cmin}. The critical impact shear stress, τ_{ci}, was modelled by Bagnold (1941) as

$$\tau_{ci} = A\,\rho_p\,gD \tag{1.25}$$

where A is an empirical coefficient equal to 0.0064. This reflects clearly the growing ease of dislodging smaller grains.

It is difficult to assess the validity of this suspension model using the published data sets on blowing sand and dust because they either fail to provide the pertinent grain size information, or they integrate over highly variable wind conditions. Instead, we evaluate model predictions by comparing them to extensive data available in the blowing snow literature (Budd et.al.(1966), Oura(1967), Takeuchi(1980), Schmidt (1982,1984), and Brown and Decker(1983)). Though here too the grain size distribution in the bed is often not reported, sufficient detail in the grain size distribution and mass flux profiles with height is made available, and the run durations are characteristically short.

For the few Byrd runs (Budd et.al.,1966) for which the near-surface grain size distribution and wind velocity data were available, best fits to the concentration and mass flux profiles were obtained using the fluid threshold form of the excess shear stress, with $\gamma = 1.4\text{x}10^{-5}$ and $z_a = .04$m (see figure 1.16a). Our confidence in this parameterization is not high, because the grain size distribution of the bed itself was not given, but a γ of order 10^{-5} provides reasonable fits to other Byrd runs (figure 1.16b). That this same calibration fits well the data reported in Takeuchi (1980), in Schmidt(1982b), and in Decker and Brown (1983), lends further confidence to its value as a proper treatment for blowing snow. The curvature of the total concentration profile is well accounted for by explicit incorporation of several grain sizes in the analysis, removing the need for invoking a "variable fall velocity", as did Budd(1966).

Using the impact threshold form of the excess shear stress did not adequately simulate concentration profiles. Best fits to the Byrd data using this form of the

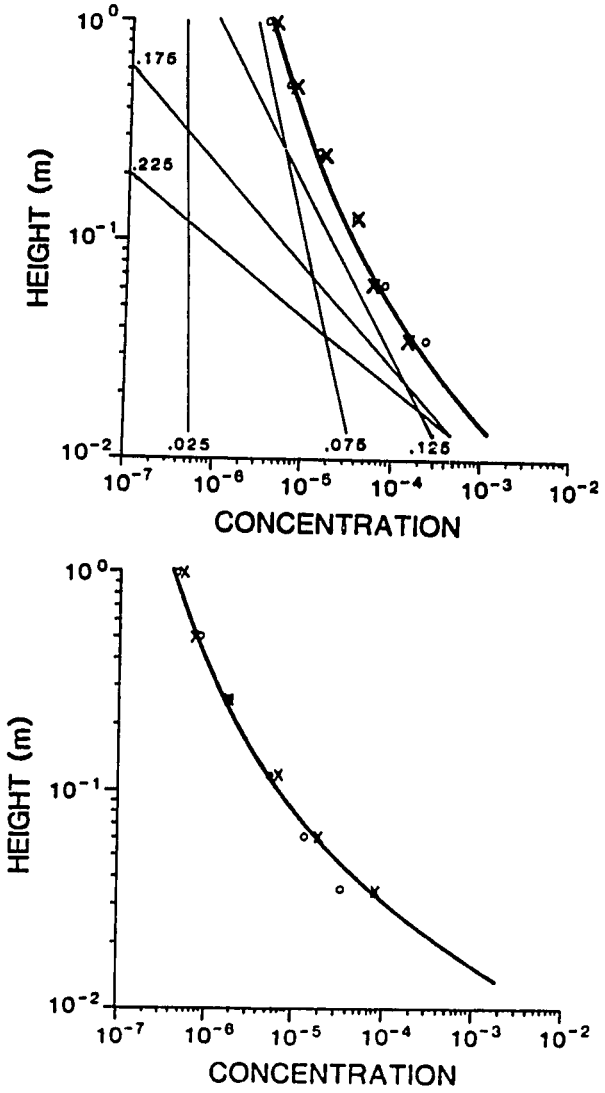

Figure 1.16 (a) Observed concentrations for Byrd runs 118 (x's), and 121 (o's), and calculated profiles for five grain sizes (labelled in mm),using $u_* = .67$m/s, $\rho_p = 917$ kg/m^3, the fluid threshold form of the excess shear stress, and $\gamma = 1.4 \times 10^{-5}$. The fraction of the bed, i_b, represented by each grain size was .01,.10,.45,.31,and .13 for grains of diameter .025,.075,.125,.175 and .225 mm, respectively. The bold curve is the sum of the five individual profiles.
(b) Observed and calculated total concentration profiles for Byrd runs 110 ($u_* = .43$m/s)(x's), and 112 ($u_* = .42$m/s)(o's). Calculations use $u_* = .425$m/s, and other parameters as in figure 1.16a.

excess shear stress were obtained only when the concentrations of the finest grain size class were artificially reduced by an order of magnitude. For reference heights again assumed identical among grain sizes, at z_a=.04, the best fit corresponds to γ=2.2$\times 10^{-6}$.

1.10 RESULTS OF THE SUSPENSION ANALYSIS

The profiles of concentration and mass flux for the snow suspension case illustrate well many of the expected properties. In all cases the matched logarithmic wind structure described in the saltation section was used. Concentration profiles for individual size classes deviate little from expected power law decays with height, implying that the $(1-c_s)$ term has little importance. This is indeed expected, as c_s is $0(10^{-4})$. The total concentration profiles, however, deviate markedly from a single power law, reflecting the vertical variation of the mean grain size , and, hence, of the effective mass diffusion coefficient. The vertical gradient in the total concentration should always decrease with distance from the bed, as progressively smaller grains, with lower settling velocities, dominate the concentration field.

To assess the applicability of the model, and of the calibration of γ derived from the blowing snow literature, to the case of blowing dust, data from dust storms in the Slims River Valley were used as input (Nickling,1978,1983). We attempted first to match run #10, as the reported wind velocities for this run show the least deviation from a logarithmic profile (u_*=.67, z_{out}=.007). (Note that in Nickling's (1978) figure 1.8 the "mean flow rate" should be expressed in mg/m^2s, rather than in mg/cm-s as labelled.) Good fits were obtained using γ=1.7x10^{-7}, and γ=2.2x10^{-8}, respectively, for fluid and impact threshold forms of the excess shear stress. Resulting concentration, mass flux, and mean grain size profiles for another run (#9) are shown in figure 1.17, along with Nickling's reported profiles.

Although the fits are generally good, the concentration and mass flux gradients are consistently underestimated, indicating that the model tends to overestimate the importance of fine particles in the profile. As in the case of blowing snow, the

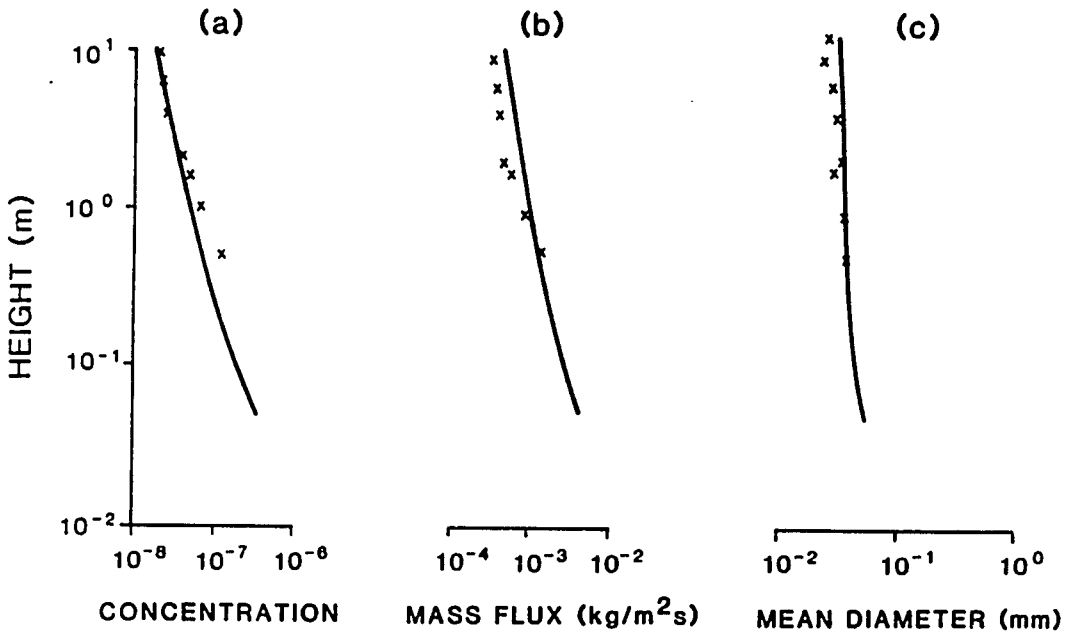

Figure 1.17. Calculated and observed concentration, mass flux, and mean diameter as functions of height for Nickling's Run 9, using $u_* = .52$m/s, and the impact form of the excess shear stress with $\gamma = 2.2 \times 10^{-8}$. Grains of diameters .031,.054,.067,.077, and Nickling's(1978) textural data.

overestimate is more extreme when the impact version of the excess shear stress is used.

1.11 DISCUSSION

Though the existing data sets on suspension of fine grained minerals are not sufficient to test the model adequately, the data on blowing snow transport supports well the simple proposed parameterization of the reference level concentrations, yielding both proper shapes and magnitudes of the total concentration profiles. It is apparent that most of the departure of the total concentration profiles from a single power law is accounted for by the variation in the mean grain size with height. Moreover, it appears that the role of stratification, ignored in this preliminary treatment, must be relatively minor, at least for the environmental conditions represented by the data sets (with total concentration-imposed density gradients only of order 10^{-3} near the bed), and that the diffusivities of mass and momentum can indeed be equated. Analysis of aqueous suspension, in which the data sets are more robust, supports this latter contention, the ratio K/K_s ranging between 1.0 and 1.3, and averaging 1.15 close to the bed (McTigue,1983). At present, incorporation of this effect is included in our calibration of γ.

The problem of the assignment of a reference level concentration focuses attention on the coupling of saltation and suspension mechanisms. Mass transport near the bed is dominated by extraction of momentum from the air by accelerating particles, and transfer of large fractions of that momentum to the bed via impacts. In contrast, mass transport well above the bed is dominated by a diffusion-like mechanism driven by vertical velocity fluctuations. The situation is analogous to that of fluid flow near a boundary, where the physics governing the momentum transfer well away from the boundary are different (turbulent) from those near it (viscous). The physics of momentum transfer in both regions in the fluid is well enough understood that their respective solutions may be matched, generating a continuous momentum or velocity profile.

We do not yet know enough about the mass transfer process that feeds small suspendible grains into the flow. The present parameterization neglects the hysterisis in the threshold velocity characterisic of eolian sediment transport, introducing uncertainties that should be largest as shear stresses drop below τ_{cmin}. With our present knowledge of the coupling between saltation and suspension, reference level concentrations must still be established using semi-empirical methods as employed in this paper.

In aqueous suspension research the top of the saltation layer is often taken as the lower limit of applicability of the diffusion region (e.g. Yalin,1972; Smith,1977). Such a ceiling is more definable for an aqueous saltation layer, where saltation heights are typically of order 2-3 grain diameters. In contrast, our analysis and many experimental data on eolian saltation, show that significant numbers of saltating grains reach heights several tens of centimeters above the bed. There must therefore be a transition region at intermediate heights characterized by significant contributions from both suspension and saltation. A "saltation layer" is most naturally defined as the region in which mass flux due to saltation dominates. Gillette and Goodwin (1974) argue that there is a grain size dependent height, estimated to range from .15 to .50 m above the surface, below which the diffusion theory of suspension is not justified. Their measured concentration profiles of three size fractions (their figure 1.2), shows their limits to be overly conservative for typical transport events over agricultural soils; comparison with theoretical profiles is good to within about .10 m of the bed in each case. To within the accuracy of the Byrd data set on blowing snow, the snow data seem to compare well with theory to within 3 cm of the bed, the lowest level of measurement.

The mechanics involved in ejecting small particles from a bed clearly include both ballistic and aerodynamic forces. Gillette et.al.(1972) suggest "sandblasting" is the dominant mechanism once saltation begins. Under intense bombardment a mixed grain size bed is incapable of hiding small particles in a laminar sublayer, as this layer is continuously disrupted by impacts; in addition, large impact stresses can rupture cohesive bonds that tend to retain fine particles in the bed. Even under moderate transport conditions, ($u_* = .5$m/s for D=.3mm) each grain must be ejected every 1-10 seconds ($N = O(10^6)$). This would favor the impact threshold over the

fluid threshold as the appropriate critical shear stress used in the formulation of the "excess shear stress", S. That the fluid threshold gives better fits to the Byrd data on blowing snow is unexpected, though the threshold for snow is arguably a complex function (Schmidt,1980).

Mismatches of the predicted and measured concentration gradients when the full reported grain size spectrum of the bed is used may arise from the tendency for the smallest fraction to travel as aggregates. The processes of collection and mechanical seiving can result in over-representation of the finest fractions by the breakage of weak interparticle bonds produced either by water or by salts. In addition, as sampling of the bed was done only occasionally, and not in coincidence with a storm, the possible effects of time dependent armoring of the bed, important in both saltation and suspension processes, are neglected.

1.12 RESEARCH SUGGESTIONS

The primary role of empiricism in the model is to evaluate scaling factors. Most importantly, we resort to empirical mass flux relations for assessing N (equations 11 and 12), the number of saltating particles ejected from the bed per unit area per unit time; and to suspension mass flux measurements at a given height to set γ, the free coefficient in the reference level concentration (equation 23). The choice of an appropriate form for the probability distribution of saltation liftoff velocities is presently derived from a single wind tunnel experiment using a single grain size bed (White and Schulz,1977); extrapolation to other grain sizes and to mixed grain size beds rests upon unverified energy arguments. Though the reference level suspension concentrations seem adequately parameterized, the mechanics by which small grains are ejected into the flow need experimental elucidation.

Well designed wind tunnel experiments are recommended, involving simple mixtures of two grain sizes subjected to shear velocities such that 1) both sizes are saltating, and 2) one size is clearly saltating ($p_* >> 2.5$), while the other is clearly in suspension ($p_* << 2.5$). Simple experiments measuring the ejection velocities resulting

from single impacts with a granular bed will aid in constraining the probability distribution of liftoff velocities important in the saltation process. In addition, any field experiments performed with the intent of constraining or testing the suspension theory must 1) be of short duration relative to the variability of the wind, 2) include concentration, mass flux and wind velocity measurements at several heights above the bed, and 3) include careful local and periodic sampling of the bed materials subjected to the wind.

3.13 CONCLUSIONS

We developed a simple general model of eolian sediment transport, including both saltation and suspension modes. In figure 1.18 we present the resulting mass flux and concentration profiles for a realistic mixture of grain sizes subjected to a shear velocity such that several grain sizes are saltating, and several are in suspension. The "saltation layer height" is that level below which saltation fluxes dominate. Both saltation and suspension processes result in monotonic declines in mass flux and concentration with height, at rates that generally increase with grain size. In saltation, this results from the dependence of the liftoff velocity distribution upon the particle mass, and in suspension it results from the variation of the settling velocity relative to the vertical velocity fluctuations of the wind.

The importance of understanding the physics of stochastic grain-bed interactions cannot be understated, because they ultimately control (1) profiles of concentration and mass flux in saltation, and (2) the production rate of suspendible grains from a mixed grain size bed: i.e. the important coupling between suspension and saltation.

We have clarified several aspects of eolian sediment transport theory. The relative importance of saltation and suspension in the concentration and mass flux at any height above the bed is now available. Stratification effects are ignored in the present analysis, though the quality of the fits obtained argue strongly against the importance of stratification under the environmental conditions represented by the

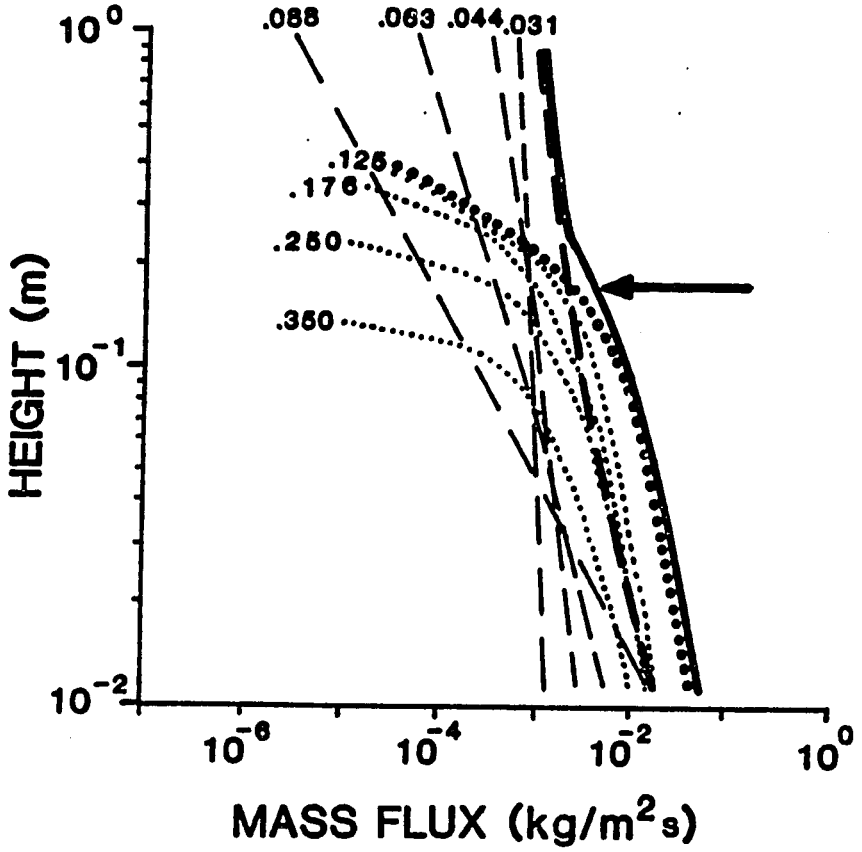

Figure 1.18. Combined saltation and suspension mass flux profile (solid line on extreme right) for u_*=.6 m/s, and a fine sandy soil with grains of diameter and .05 fraction of the bed, respectively. Individual mass flux curves (light dotted lines for saltation, light dashed lines for suspension) are labelled with the corresponding grain diameter, in mm. Total saltation and total suspension fluxes are represented by heavy dotted and heavy dashed lines, respectively. Arrow marks "saltation layer height", where the total mass fluxes from suspension and saltation are equivalent.

existing field data. The role of the saltation process in altering the wind profile, and the relative importance of saltation and suspension in performing eolian erosion can be analyzed readily within the framework of this model; results and implications will be presented in a companion paper.

CHAPTER 2

EOLIAN SEDIMENT TRANSPORT AS A STOCHASTIC PROCESS: THE EFFECTS OF A FLUCTUATING WIND ON PARTICLE TRAJECTORIES

Eolian sediment transport must be considered a stochastic process because (1) the trajectories of individual grains are affected to varying degrees by turbulent (random) fluctuations of the wind; and (2) the impacts of these grains with a granular bed results in subsequent ejections whose number and velocities may be known only in a probabilistic sense.

Previous analyses of saltating grains (e.g. Anderson and Hallet, 1986; Jensen and Sorenson, 1985; Willetts and Rice, 1985; White and Schulz, 1977) have proceeded by assuming that saltation trajectories respond effectively only to the mean wind (i.e. that they are deterministic in the sense that they are determined entirely by the initial conditions of liftoff speed and angle). In this end-member case, the stochastic problem reduces to a determination of the distribution of these initial conditions (Anderson and Hallet, 1986).

Previous models of suspension transport of sedimentary particles in turbulent fluids (e.g. Smith, 1977 in water; Nickling, 1978, and Gillette, 1974 in air) have relied heavily upon the analogy between mass and momentum transfer within the fluid, allowing treatment of the system of air and particles as a continuum. Whether the analysis uses principally continuity arguments (e.g. Smith, 1977; Anderson and Hallet, 1986) or mixture theory, wherein the interaction forces are identified within the equations of motion for both fluid and particulate phases (e.g. McTigue, 1983), the resulting analytic solutions for the particle concentration within the near-bed region show concentration falling off as height above the bed raised to a power. This power, p, (the Rouse number) is a simple function of the settling velocity of grains and the shear velocity of the fluid.

All such treatments require either a single measured concentration, or an analytic expression for a reference level concentration, in order to establish the magnitude of the concentrations. In a sense, this serves as a surrogate for a source term at the bed. Simple expressions for the reference level concentrations have been

generated for transport of both dust and snow by air (Anderson and Hallet, 1986). Though these provide a means of predicting first order suspension concentrations in a given wind, our confidence in the extension of the meager data sets available to other sites is not high. A more physically based model of the source term in the suspension transport problem is needed.

Observations of eolian sediment transport in mixed grain size soils (Gillette et al., 1972, 1974, 1978) have clearly demonstrated that suspension of the fine grain size fractions commence whenever the first (generally larger) grains begin to saltate. This implies a coupling of saltation and suspension processes, previously envisaged by both Bagnold (1941) and Gillette (e.g. 1974), wherein large, high-energy impacting grains mobilize a mixture of grain sizes from the bed.

In order to place eolian saltation and suspension on an equal footing, to emphasize the similarity in the physics of the two processes, and to make the coupling between the processes more explicit, we need to develop models for the grain-bed and grain-wind interactions.

The mechanics of ballistic impacts into a multiple-grain size bed is currently being addressed by Haff and coworkers (e.g. Mitha et al., 1985; Werner and Haff, 1985, 1986), using physical and numerical experimental techniques. The desired outcome from this research is a "splash function" (Ungar and Haff, 1986) characterizing the ejection rate of each grain size fraction from the bed, and the probability distribution of its velocities.

A suspension trajectory is comprised of random excursions of a particle that represent the particle's response to random fluctuations in the wind velocity. These give rise to the diffusive nature of suspension transport. In general, the problem is extremely complex in that the types of statistical data needed to constrain the air velocity field the particle experiences are very difficult to measure. The point of view is neither Eulerian nor Lagrangian: the particle does not experience the same fluctuations one would measure at a fixed point in space (Eulerian); nor, in general, is the particle travelling at exactly the velocity of the fluid (requiring a Lagrangian statistical description). Large particles, whose mean horizontal velocity is far less than that of the air, will experience a statistical field of turbulence more Eulerian in character

than smaller particles whose slip relative to the air is diminished. In addition to this difficulty, even the Eulerian turbulent velocity field is poorly known near the bed of a natural system. Nonetheless, we may proceed with caution, with the aim of capturing the essense of the problem through appropriate simplifications.

The problem may be broken into two steps: the response of a particle to a given change in air velocity, and the air velocity history itself. First, we analyze the response of small particles to a single step change in velocity, and show that for small particle Reynolds numbers the particle response may be expressed as a simple linear differential equation. A characteristic response time, τ_r, emerges, representing the sensitivity of a particle to a change in the wind velocity. The expression for the velocity history of the particle then becomes a convolution integral; the particle velocity history becomes a dampened version of the air velocity history it experiences, the damping being a function of the response time.

Second, we discuss the effects of a realistic wind velocity history. Particle trajectories are shown to depend on the Eulerian statistics of the flow at each height above the bed, characterized by the standard deviation of the vertical velocity fluctuations, and the local dissipation of energy within the flow. Trajectories and resulting concentration profiles are presented and are shown to approximate closely the expected power law behavior. Currently the ejection rate, N, is chosen through comparison of calculated and empirically derived reference level concentrations.

With a working model of vertical air velocity fluctuations in hand, the trajectories of larger grains -- involving particle Reynolds numbers well above the Stokes range -- are calculated in order to assess the importance of these fluctuations in modifying saltation trajectories. The resulting distribution of trajectory lengths for a single set of initial conditions may be used to define more formally saltation and suspension. A method of estimating the proportions of each grain size class expected to travel in each of these modes is then suggested, based upon a "saltation parameter", defined as the ratio of the hop time to the response time.

2.1 PARTICLE RESPONSE TO CHANGES IN THE WIND VELOCITY

The local balance of forces yields an equation for the acceleration of a particle:

$$\frac{dU_p}{dt} = -g + \frac{F_d}{m} \tag{2.1}$$

where U_p is the particle velocity, g the acceleration due to gravity, F_d the drag force, and m the particle mass. As the particle-fluid density ratio, $\frac{\rho_p}{\rho_a}$, is of order 1000 for sediment in air, we may safely neglect (1) forces due to pressure gradients in the fluid surrounding the particle caused by particle accelerations, (2) "virtual" or "added mass" effects -- the force required to accelerate a particle-volume of fluid out of the way before the particle can replace it --, and (3) the "Basset history term", which accounts for the effects of deviations in the flow pattern from steady state (see Hinze, 1975, p.463-464). Also neglected are lift forces due to particle buoyancy, to velocity gradients in the flow, and to particle spin (the Magnus force). We have a general equation for aerodynamic drag,

$$F_d = \frac{1}{2}\rho_a C_d A \mid U_{rel} \mid U_{rel} \tag{2.2}$$

where ρ_a is the air density, C_d is the drag coefficient, and U_{rel} is the relative (vector) velocity of the particle and the air. Recalling that at low Reynolds numbers ($Re = \mid U_{rel} \mid D/\nu$) the drag coefficient $C_d = 24/Re$, the drag formula reduces to

$$F_d = \beta f U_{rel} \tag{2.3}$$

where

$$\beta = 3\pi\rho_a \nu D \tag{2.4}$$

and departure of f from a value of 1 represents deviation from the Stokes drag law. Hence, in the low Reynolds number asymptote ($f \approx 1$), the drag force scales with the relative velocity of the particle and the air, and with the particle diameter. The acceleration equation then becomes

$$\frac{dU_p}{dt} = -g + Af U_{rel} \tag{2.5}$$

where

$$A = \frac{18\rho_a \nu}{\rho_p D^2} \tag{2.6}$$

Note that A has dimensions of inverse time.

With this simplified version of the acceleration equation, we now introduce a fluctuating component to the local wind. For the moment, suppose we may decouple the vertical and horizontal components of velocity; let us investigate the effects of vertical velocity fluctuations on a particle essentially travelling at the horizontal velocity of the fluid. We may rewrite the acceleration equation as a scalar equation in the vertical velocity component of the particle, w_p, and of the air, w:

$$\frac{dw_p}{dt} = -g + Af\,(w - w_p) \tag{2.7}$$

The effects of steady gravitational settling, and turbulent accelerations of the air may be separated by defining $w = \overline{w} + w'$, and $w_p = \overline{w_p} + w_p'$, where bars denote steady or average quantities, and primes denote fluctuating quantities. Since the mean of the vertical velocity fluctuations of the air must be zero, ($\overline{w} = 0$), we have

$$\frac{d\overline{w_p}}{dt} + \frac{dw_p'}{dt} = -g - Af\,(\overline{w_p}) - Af\,(w' - w_p') \tag{2.8}$$

Note that in the absence of turbulence, the vertical particle velocity will approach the settling, or terminal velocity ($\frac{d\overline{w_p}}{dt} = 0$). For particles small enough such that the Reynolds number at their settling velocity is small (<10), $f \approx 1$, and the settling velocity may be approximated by $s = \frac{g}{A} = \frac{\rho_p g D^2}{18\rho_a \nu}$. As the approximation holds well for fine sand and smaller, we shall hereafter consider only the low Reynolds number, $f \approx 1$ case. After the terminal velocity has been reached, the only relevant acceleration of the particle is due to turbulent fluctuations of the air, leaving

$$\frac{dw_p'}{dt} + Af w_p' = Af w' \tag{2.9}$$

For the low Reynolds number case, this becomes a first order, linear, non-homogeneous ordinary differential equation with a solution in the form of a convolution:

$$w_p' = \int_0^t e^{-A(t-u)} A w'(u)\, du \tag{2.10}$$

for $\overline{z_p} > 0$, where $\frac{d\overline{z_p}}{dt} = \overline{w_p}$, and where $z_p = 0$, $\overline{w_p} = w_{po}$, and $w_p' = 0$ at $t = 0$. As expected, vertical fluctuations of particle velocity are smoother than those of the air.

To interpret the parameter A, we impose a simple step change in the air velocity, of magnitude w_*, effective at $t = 0$. The resulting particle velocity is

$$w_p' = \int_0^t A e^{-A(t-u)} w_* \, du \tag{2.11}$$

or

$$w_p' = w_*(1 - e^{-At}) \tag{2.12}$$

We see that the particle velocity has attained $(1 - \frac{1}{e})$ of the new vertical air velocity when $At \approx 1$, inspiring the definition of a response time, $\tau_r = \frac{1}{A} = \frac{D^2 \rho_p}{18 \rho_a \nu}$. For example, $\tau_r = 8 \times 10^6 D^2$ for quartz in air. (See figure 2.1.)

Such response times have been defined previously in the particulate transport literature (see, for instance, Soo, 1967; Hinze, 1972, 1975; Lumley, 1957; Peskin; 1959); all such treatments show the dependence on the square of the particle diameter. In some cases (e.g. Hinze, 1972), a response time appropriate for high particle Reynold's number is presented as well, in which the dependence is linear in the particle diameter, but becomes dependent upon the relative velocity between the particle and the air. This introduces a non-linearity in the governing equation, and greatly complicates the analysis.

By responding much less sensitively to the high frequency turbulence than to the low, the particle acts as a low pass filter to the turbulent energy spectrum of the wind. This is readily seen (following treatments of Hinze, 1975, and Soo, 1972) by calculating the Fourier transform of the vertical components of the air and particle

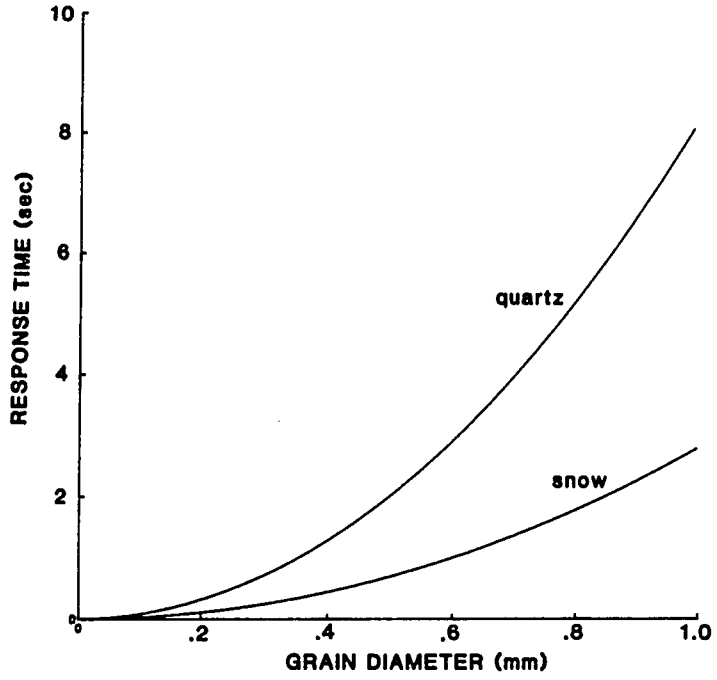

Figure 2.1. Response time of particles of two densities (corresponding to quartz and snow) to changes in the velocity of the surrounding air.

velocities, w and w_p (with the primes dropped):

$$w(t) = \int_{-\infty}^{\infty} \tilde{w}(\omega) exp(i\omega t) d\omega \tag{2.13}$$

and

$$w_p(t) = \int_{-\infty}^{\infty} \tilde{w}_p(\omega) exp(i\omega t) d\omega$$

where ω is the frequency of the turbulence, and $(w, \tilde{w})$, and $(w_p, \tilde{w}_p)$ constitute the Fourier transform pairs for the air and particle vertical velocities, respectively. Homogeneous, stationary turbulence is assumed. Substituting these expressions into equation 2.9, and setting $f = 1$, yields the relation between the Fourier transforms as a function of frequency

$$\tilde{w}_p(\omega) = \left[\frac{\left(\frac{A}{\omega}\right)^2 - i\,\frac{A}{\omega}}{\left(\frac{A}{\omega}\right)^2 + 1}\right] \tilde{w}(\omega) \tag{2.14}$$

The amplitude of the particle response, represented by the real part of (14), depends sensitively upon the ratio of the inverse response time, A, to the turbulent frequency, ω. This is plotted in figure 2.2a; the grain size and frequency dependence is made more explicit in figure 2.2b. Two asymptotes illustrate the dependence:

(1) for $\frac{A}{\omega} >> 1$ (small particles, low frequency turbulence),

$$\tilde{w}_p \approx (1 - \frac{\omega}{A} i)\, \tilde{w} \tag{2.15}$$

The response amplitude is essentially that of the air, (see figure 2.1) but a slight phase shift is expected, which diminishes as the particle size or the turbulence frequency diminishes; the particle closely follows the air parcel.

(2) for $\frac{A}{\omega} << 1$ (larger particles, high frequency turbulence)

$$\tilde{w}_p \approx ((\frac{A}{\omega})^2 - \frac{A}{\omega} i)\, \tilde{w} \tag{2.16}$$

The magnitude of the response is drastically diminished, and a similar phase shift occurs. Given, then, a spectrum of turbulence, characterized by a spectral energy density function $E(\omega)$, particles of different sizes will act to modify (or filter) this

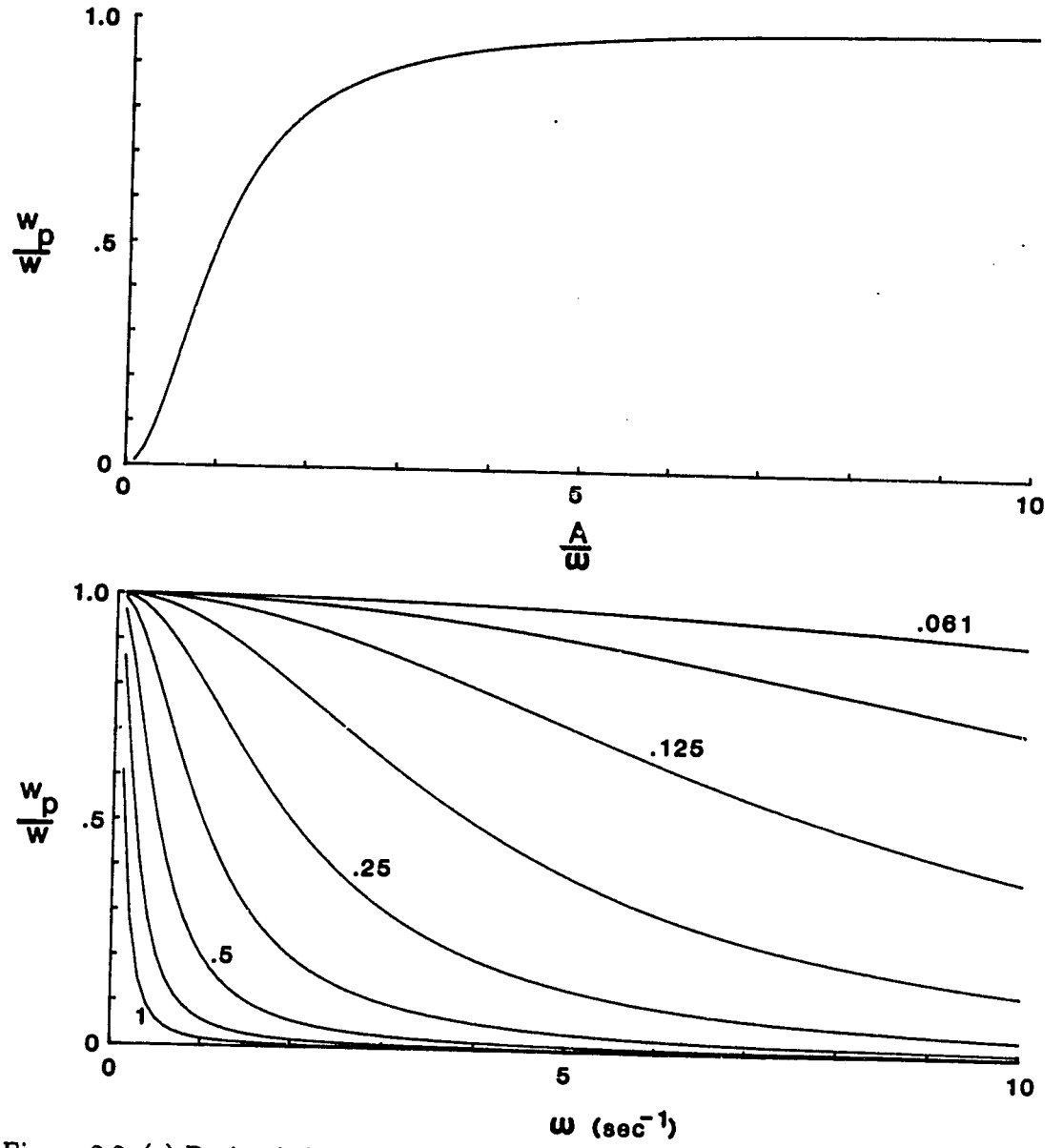

Figure 2.2. (a) Ratio of the amplitude of particle response, w_p, to amplitude of wind velocity fluctuation, w, as a function of the ratio of inverse particle response time, A, to frequency of wind fluctuation, ω.
(b) Ratio of particle response amplitude to wind fluctuation amplitude, plotted as a function of the frequency of wind fluctuation for several grain diameters (labelled, in mm). Particle density is that of quartz, 2650 kg/m^3.

energy, resulting in an energy density function for the particle, $E_p(\omega)$, that is relatively depleted in high energy frequency content.

Though such treatments go on to address the ratio of particle to fluid diffusivities, their restriction to homogeneous turbulence diminishes their usefulness to the geological sediment transport problem. The approach taken here is to model individual trajectories, which "see" turbulence whose statistics vary strongly with distance above the ground. The velocity history of a fluid element is addressed in the following section.

2.2 AIR VELOCITY FLUCTUATIONS

Calculation of suspension trajectories requires a knowledge not only of the mean wind profile, but of structure of the velocity fluctuations. Suspension trajectories are most easily visualized as a random process calculated by subdividing the particle motion into a number of time increments; at each time increment new horizontal and vertical velocities of the surrounding air must be chosen from a probability distribution that depends upon the height above the bed, and, in general, upon the air velocity at previous time steps (i.e. there is some memory in the system, which imposes an auto-correlation in the velocity structure). We wish ultimately to derive an expression for the auto-correlation structure of the wind velocities to which a solid particle is subjected throughout its trajectory. This requires three levels of analysis. First (Section 2.2a), an expression is proposed to account for the velocities to which an *air parcel* is subjected in homogeneous turbulence. Second (Section 2.2b), modifications of this formulation are made which allow treatment of the more realistic case of (nonhomogeneous) turbulence within the lowermost portions of the atmospheric surface layer. Third (Section 2.2c), further refinement is made to account for the fact that the particle does not remain within a single air parcel, but rather slips from one air parcel to another throughout the trajectory.

2.2a Air parcel trajectories in homogeneous turbulence

For the first analysis, we follow work on cloud droplet formation (Jonas and Bartlett, 1972) that required calculation of air parcel trajectories in homogenous turbulence. For a wind with an Eulerian distribution of vertical velocities characterized by a gaussian distribution with zero mean and standard deviation σ_w, a rate of dissipation of energy per unit mass, ϵ, and a prior vertical velocity w_{i-1} at $t=t_{i-1}$, the vertical velocity at $t_i=t_{i-1}+\Delta t$ is:

$$w_i = w_{i-1}\, exp\,(-\frac{\epsilon \Delta t}{2\sigma_w{}^2}) + n_i\,\sigma_r \tag{2.17}$$

where

$$\sigma_r{}^2 = \sigma_w{}^2(1-exp\,(-\frac{\epsilon \Delta t}{\sigma_w{}^2}))$$

and n_i is a random number to be chosen from a distribution with zero mean and unit standard deviation. The exponential expression on the right hand side of (17) represents the correlation between velocities at two times, $R(\Delta t)$. By inspection it may be verified that as $\epsilon \to 0$, the velocity distribution becomes a delta function centered about the original vertical velocity, and that as $\epsilon \to \infty$, the distribution becomes identical to the Eulerian distribution (see figure 2.3).

The Jonas and Bartlett formalism is the discrete version of the stochastic differential equation

$$dw = -\alpha\, w\, dt + \sigma\, dW_t \tag{2.18}$$

where

$$\alpha = \frac{\epsilon}{2\sigma_w{}^2} \qquad \text{and} \qquad \sigma = \sqrt{\epsilon dt}$$

Equation 2.18 is a form of the Langevin equation (see, for instance, Uhlenbeck and Ornstein (1930, p.872)) originally formulated to describe the incremental changes in velocity of a Brownian particle in a viscous fluid. In the original form the first term on the right hand side represents the drag arising from the asymmetry of molecular collisions due to the particle's velocity. The second term represents the purely random impulses remaining after subtraction of this asymmetry.

To interpret the extension of the Langevin equation to the problem of the

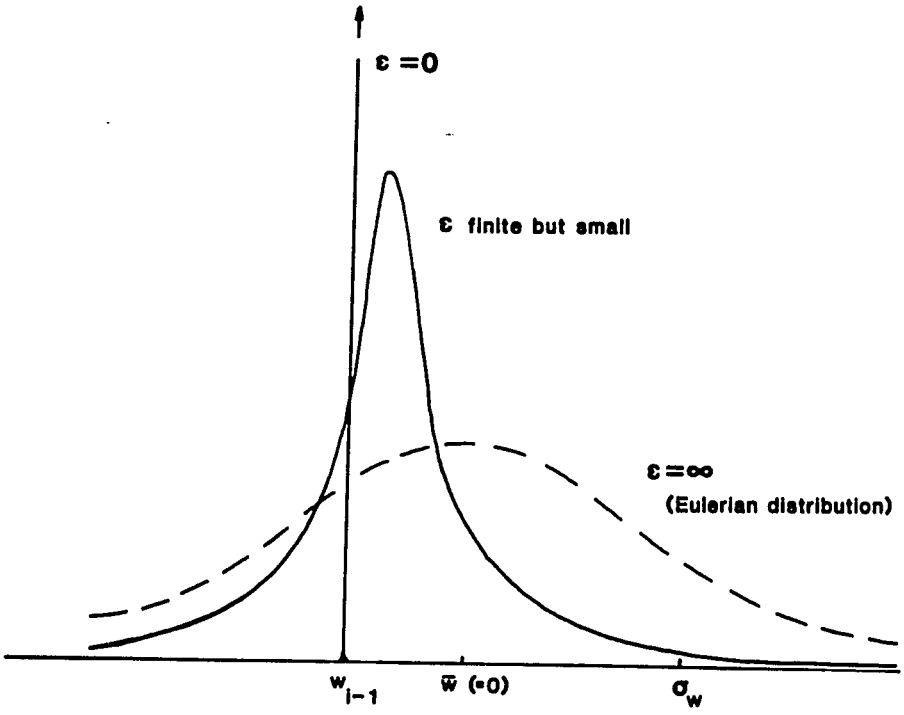

Figure 2.3. Probability distributions of vertical velocities to be chosen from at time step i, given that the velocity at time $(i-1)$ is $w_{(i-1)}$. If there is no dissipation of energy in the flow (i.e. if $\epsilon=0$), the velocity at any time step will be the same as that in the last. This results in a delta function centered at $w_{(i-1)}$. On the other hand, if there is infinite dissipation in the flow, there is essentially no memory from one time to the next, and the velocity distribution at any time must be chosen from the Eulerian distribution, characterized by a mean $\bar{w}=0$, and standard deviation σ_w. For finite dissipation increasing from zero, the distribution is characterized by a mean that shifts from $w_{(i-1)}$ toward $\bar{w}$, and a standard deviation that shifts from 0 toward σ_w. The memory from one time step to the next becomes less and less perfect.

motion of a neutrally buoyant air parcel subjected to turbulence, it is useful to define a Lagrangian time scale, $T_l = \frac{2\sigma_w^2}{\epsilon}$ ($= \frac{1}{\alpha}$ in equation 2.13b), the period during which the velocity of an air parcel is auto-correlated. Formally, this is an integral time scale, derived by integrating the autocorrelation of the vertical velocity, $R(\tau)$, with respect to the time lag, τ.

$$T_l = \int_0^\infty R(\tau) d\tau \tag{2.19}$$

with $R(\tau) = \frac{\overline{w(t)w(t+\tau)}}{\sigma_w^2} \approx e^{\frac{-\tau}{T_l}}$.

2.2b Air parcel trajectories in the atmospheric boundary layer

The above treatment holds formally only for homogeneous turbulence; the boundary layer near the bed clearly violates this assumption. It has recently been argued (van Dop and others, 1985) that the simple extension of the Jonas and Bartlett form of the Langevin equation to the inhomogeneous or unsteady cases (involving changes in the turbulence statistics with height or time) may not be appropriate in some cases, and can lead to physical inconsistencies as serious as violation of mass conservation. In particular, such models resulted in an inordinate accumulation of fluid within regions of low turbulent intensity. Van Dop and others (1985) reviewed the recent literature and proposed a variant of the Langevin equation (2.18) to mitigate these problems:

$$dw = (-\frac{w}{T_l} + a_1)dt + a_2^{\frac{1}{2}} dW_t \tag{2.20}$$

where a_1 and a_2 represent the spatial and temporal gradients of the turbulent statistics: $a_1 = \frac{\partial \sigma_w}{\partial z}$, and $a_2 = \frac{2\sigma_w^2}{T_l} + \frac{\partial \sigma_w}{\partial t} + \frac{\partial \overline{w^3}}{\partial z}$.

We now seek expressions for how the rate of dissipation and the magnitude of the velocity fluctuations vary with height. Both theoretical and experimental work on turbulent boundary layers (see summary in Hinze, 1975, p.587-770) demonstrate that dissipation almost exactly balances production of turbulent kinetic energy by the

mean flow very near the bed (i.e. that advection and diffusion of turbulent energy can be ignored very close to the bed). The rate of energy production per unit volume, E, may be modelled as the product of the mean shear rate of the fluid, $\frac{\partial \overline{U}}{\partial z}$, with the turbulent (Reynolds) stresses, $-\rho\overline{u'w'}$. An eddy viscosity model of the turbulent stress yields

$$-\rho\overline{u'w'} = \rho K\frac{\partial \overline{U}}{\partial z} = \rho k u_* z\frac{\partial \overline{U}}{\partial z} \tag{2.21}$$

The rate of energy dissipation per unit mass then becomes

$$\epsilon = \frac{E}{\rho} = k u_* z\left(\frac{\partial \overline{U}}{\partial z}\right)^2 \tag{2.22}$$

Near the ground surface in neutrally stable conditions [in the "inertial sublayer" of O(100m) , or more strictly, within the "constant stress" layer of O(20m)(Tennekes, 1984)], the shear rate may be approximated as $\frac{\partial \overline{U}}{\partial z} = \frac{u_*}{kz}$, which yields both the final form for the dissipation structure

$$\epsilon = \frac{{u_*}^3}{kz} \tag{2.23}$$

and, upon integration, the logarithmic wind velocity profile. Dissipation is high very near the bed, decreases monotonically with height above the bed, and is very sensitive to the shear velocity.

Numerous studies of turbulence within the atmospheric surface layer demonstrate that in neutral conditions the standard deviation of vertical velocity fluctuations remains virtually constant. According to Hunt (1984):

$$\sigma_w = b_2 u_* \tag{2.24}$$

where b_2=1.3±0.1. Divergence from this value is expected under both stable (air density decreasing with height; b_2 decreases with height) and unstable (air density and b_2 increasing with height) conditions (see Hunt, 1982, p.239, fig.6.4).

Referring, then, to van Dop and others' proposed stochastic differential equation (20), we see that in the neutral surface layer, $a_1 = \frac{\partial \sigma_w}{\partial z} = 0$. The first term in a_2 is simply the dissipation rate, ϵ. However, little is known about the third moment, or

skewness, of the vertical velocity distribution within the surface layer. In the steady case ($\frac{\partial \sigma_w}{\partial t} \approx 0$), and in the absence of large variations in the skewness ($\frac{\partial \overline{w^3}}{\partial z} \approx 0$), $a_2 = \epsilon$, and the van Dop formulation collapses to the Jonas and Bartlett form, eqn. 2.13b. Caution is certainly warranted, however, in any attempt to apply the Jonas and Bartlett formalism to either stable or unstable conditions. In these more general cases, more must be known about the higher moments of the velocity field, and equation 2.14 should be used.

We proceed with the simplifying assumptions that the atmospheric boundary layer is both steady and neutrally stratified. The Lagrangian time scale representing the correlation between vertical velocities may be written: $T_l = b_1 \frac{z}{u_*}$, where b_1 is a dimensionless constant. The correlation between vertical velocities at two times should increase with distance from the bed, and should decrease rapidly with increasing u_*. Combination of equations 16 and 17 yields $b_1 \approx 1.4$. Actual measurements of b_1 range roughly an order of magnitude, with 1.4 the upper bound. In neutral conditions within the surface layer, Hanna (1984, p.284) suggests $b_1 \approx .38$, which is within the range (.25-.40) proposed by Hunt and Weber (1979).

2.2c Divergence between particle and air parcel trajectories

A further refinement is needed when the solid particles become massive enough for their velocities to differ significantly from those of an air parcel, making our use of the lagrangian velocity history of the air parcel, characterized by T_l, inappropriate as a model for the air velocity history to which the solid particle is subjected. This effect has been addressed in the past by various researchers (see summary in Hinze, 1972, 1975), and has been variously called the filtering, slip, crossing-trajectories, and probability of encounter effects. In all cases it is recognized that non-buoyant particles will effectively move from one parcel of fluid to an adjacent one.

The time a particle spends in an air parcel depends upon its relative velocity with respect to that parcel of air, and the characteristic dimensions of the parcel.

Following the work of Hunt and Nalpanis (1986), one may define a new correlation time scale, T_l^*, that accounts for this effect. We expect the modified time scale to be shorter than the lagrangian time scale, T_l; the velocities to which a solid particle is subjected will be less well correlated than those to which a fluid element is subjected.

The asymptotic behavior expected is: $T_l^* \rightarrow T_l$ as the relative velocity goes to zero, or as the eddy size goes to infinity, on the one hand, and $T_l^* \rightarrow T_e$ as the relative velocity approaches σ_w, where T_e is the Eulerian correlation time (that time scale derived from the auto-correlations measured at a fixed point). Earlier theoretical work on the relation between the Eulerian and Lagrangian time scales (e.g. Hanna,1972; Pasquill,1974) implies that $\frac{T_l}{T_e} \approx 4$, while experiments of Snyder and Lumley (1971) demonstrate that the ratio is at least greater than 3. Hence, $T_l^* = T_l/4$ should be a lower limit for the modified correlation time.

Several functional forms of the modified Lagrangian time scale have been proposed. Arguing that earlier forms failed to fit the experimental data of Snyder and Lumley (1971), Hunt and Nalpanis (1986) proposed the form

$$T_l^* = T_l \left[1/\left(1+A_1\left(\frac{U_{rel}}{\sigma_w}\right)^{2/3}\left(\frac{T_l}{\Delta t}\right)^{1/3}\right)\right] \qquad (2.25)$$

where U_{rel} is the relative velocity of the particle and the air parcel (here $U_{rel}\,\Delta t$ is an approximation for the slip between the air and the particle during the time step, Δt), and A_1 is a dimensionless constant of O(1) that must be set for the chosen time step. The Hunt and Nalpanis formula was developed with the following rationale (Hunt, personal communication, 1986; Hunt and Nalpanis, 1985). The solid particle and air parcel positions initially coincide, but proceed along divergent trajectories owing both to particle settling, and to the imperfect response of the particle to changes in the air velocity, represented by equation 2.12. Along the air parcel trajectory the auto-correlation of velocities is simply $R(\Delta t) = exp\left(-\frac{\Delta t}{T_l}\right)$. The auto-correlations of the fluid velocities experienced by the *particle*, however, depend not only on the ratio $\frac{\Delta t}{T_l}$, but on the ratio of the particle slip relative to the air with some spatial correlation scale, L_w. This correlation length may be constructed from time and velocity

scales: $L_w = T_l \sigma_w$ (Hunt and Nalpanis, 1986). For small time steps ($\Delta t < T_l$), Hunt and Nalpanis use the Kolmogoroff similarity hypothesis and the approximation that the particle slip relative to the air at the end of the time step may be written $U_{rel}\,\Delta t$ to derive (25). We modify their equation only slightly by substituting the *calculated* slip over the previous time step, arriving at

$$T_l^{\,*} = T_l\,[1/(1+A_2\frac{T_l}{\Delta t}(\frac{slip}{L_w})^{2/3})] \tag{2.26}$$

Note that the Hunt and Nalpanis form is recovered if $slip = U_{rel}\,\Delta t$. Equation 26 yields higher correlations between velocities than the Hunt and Nalpanis form; the calculated slip will always be less than the that calculated from $U_{rel}\,\Delta t$, owing to the particle's response to the newly imposed wind velocity at the beginning of the time step, as represented by equation 2.12.

2.3 SUSPENSION TRAJECTORIES

Suspension trajectories are calculated by coupling the history of air velocities encountered by the particle, with the analytical expression for the particle response to a single velocity fluctuation developed in section 2.1 (eqn.2. 12), all of which is superimposed on the particle's tendency to settle at a velocity, s, in response to gravity. For a given shear velocity of the wind, u_*, and grain diameter, D, a time step, Δt, is chosen such that $\frac{\Delta t}{\tau_r} < 1$. Initial conditions are then chosen for each trajectory: initial horizontal and vertical position, x_{po} and z_{po}; initial particle ejection speed, V_{po}, and ejection angle, α, are used to calculate initial horizontal and vertical components of particle velocity, u_{po} $(=V_{po}\,cos\,(\alpha))$, and w_{po} $(=V_{po}\,sin\,(\alpha))$. At each subsequent time step, $t_i = i\,\Delta t$, wind velocity, particle velocity and position are then calculated using the following recursive relations:

$$w_i = w_{i-1}\,exp\,(-\frac{\Delta t}{T_l^{\,*}}) + n_i\,\sigma_w\,(1-exp\,(-\frac{\Delta t}{2T_l^{\,*}})) \tag{2.27a}$$

where in the first time step

$$w_1 = n_1 \sigma_w \tag{2.27b}$$

with n_1 a random number on the interval (0,1), and $\sigma_w = b_1 u_*$.

$$w_{p(i)} = w_{p(i-1)} + [(w_i - w_{p(i-1)})(1 - exp(-\frac{\Delta t}{\tau_r}))] \tag{2.27c}$$

$$z_{p(i)} = z_{p(i-1)} - s\,\Delta t + w_i\,\Delta t - (w_i - w_{p(i-1)})\tau_r(1 - exp(-\frac{\Delta t}{\tau_r})) \tag{2.27d}$$

$$u_i = \overline{U}(z_{p(i)}) = [\frac{u_{*t}}{k}\ln\frac{z_{p(i)}}{z_o}, \frac{u_*}{k}\ln\frac{z_{p(i)}}{z_{ost}}]^+ \tag{2.27e}$$

$$u_{p(i)} = u_{p(i-1)} + (u_i - u_{p(i-1)})(1 - exp(-\frac{\Delta t}{\tau_r})) \tag{2.27f}$$

and

$$x_{p(i)} = x_{p(i-1)} + u_i\,\Delta t - (u_i - u_{p(i-1)})\tau_r(1 - exp(-\frac{\Delta t}{\tau_r})) \tag{2.28g}$$

Calculations continue until $z_{p(i)} < z_o$, i.e. until the particle re-encounters the bed. In the equation for the mean wind profile (27e), z_o is the Nikuradse roughness $\approx D/30$, and z_{ost} is the sediment transport roughness, which, following Owen (1964), is approximately $.02\frac{u_*^2}{2g}$, and u_{*t} is the critical shear velocity for sediment transport. The + outside the brackets requires taking the maximum of the two values, and therefore represents the matched logarithmic profile used in previous studies (e.g. Anderson and Hallet, 1986).

2.4 CONCENTRATION PROFILES

The volumetric concentration (volume of particles per unit volume of air) may be considered the product of a scalar with the probability density of encountering a particle in the volume element of concern. The scalar includes the volume of a single particle, and the rate at which particles are ejected from from the bed. In the deterministic treatment of saltation, trajectories are completely characterized by the initial

conditions of speed, angle and spin at liftoff. Assuming that a set of particles travel along identical trajectories, the concentration of a particle size fraction, j, with mean particle volume V_j, within the height element $(z-\Delta z, z]$, is defined such that the ejection rate, N_1, is one grain per unit area of bed per unit time, and that the initial conditions for each trajectory are identical. This may be written

$$c_j(z, w_{po}) = N_1 V_j \left(\frac{1}{|<w_p(w_{po})>|_+} + \frac{1}{|<w_p(w_{po})>|_-}\right) \tag{2.28}$$

(see Anderson and Hallet, 1986, eq.9), where $<w_p(w_{po})>$ is the average vertical velocity of the particle in crossing the height element, and the + and – subscripts denote the ascending and descending crossings, respectively (see figure 2.4a).

The total concentration at any specific level is then the weighted sum, over all possible initial conditions, of such identical trajectory concentrations; the weights are the probability densities of each initial condition. As the most important initial condition in determining the trajectory shape is the initial vertical velocity of the particle, w_{po}, the concentration may be written:

$$c_j(z) = \frac{N_j}{N_1} \int_0^\infty c_j(z, w_{po}) p(w_{po}) dw_{po} \tag{2.29a}$$

(after Anderson and Hallet, 1986, eq.10), or in summation form:

$$c_j(z) = \frac{N_j}{N_1} \sum_{m=0}^{m^*} c_j(z, w_{po})_m \; p(w_{po})_m \; \Delta w_{po} \tag{2.29b}$$

where N_j is the number of particles of size fraction j ejected per unit area of bed per unit time, m increments the initial vertical particle velocity, m^* being its maximum, and $p(w_{po})\Delta w_{po}$ the proportion of grains ejected with vertical velocities in the range $[m\,\Delta w_{po}, (m-1)\Delta w_{po}]$. In the absence of a model for the grain-bed interaction, the ratio $\frac{N_j}{N_1}$ is set by appeal to empirical equations for total mass flux (Anderson and Hallet, 1986).

This formalism can be extended to the suspension case by making two modifications. First, while an ideal saltation path may cross a given height increment either zero or two times, a suspension trajectory may cross it any even number of times. Second, as the suspension trajectories are stochastic rather than

deterministic, meaning that for a single set of initial conditions there are many different trajectories possible, we must ensemble average over many realizations of the process to determine the average concentrations to be expected from a single set of initial conditions.

The first simply involves extending the summation of equation 2.28 to become, for a single suspension trajectory (see figure 2.4b).

$$c_j(z,w_{po}) = N_1 V_j \sum_{k=1}^{k^*}\left(\frac{1}{|<w_p(w_{po})>|_k}\right) \tag{2.30}$$

where the subscripts refer to the k th crossing of the height element, and k^* is the total number of crossings made during this particular trajectory. For fixed time and height increments, Δt and Δz, respectively, this may be represented as

$$c_j(z,w_{po}) = N_1 V_j \frac{\Delta t}{\Delta z} \sum_{k=1}^{k^*}\eta_k(z) \tag{2.31}$$

where η_k is the number of time increments spent in the k th crossing of the height element.

Ensemble averaging over n^* suspension trajectories, each with identical initial conditions, we arrive at the generalized version of equation 2.18 [which reduces to (2.18) with $k^*=2$ and $n^*=1$]:

$$c_j(z,w_{po}) = N_1 V_j \frac{\Delta t}{\Delta z}\left[\frac{1}{n^*}\sum_{n=1}^{n^*}\left(\sum_{k=1}^{k^*}\eta_k\right)\right] \tag{2.32}$$

The extension to total concentration is then perfectly parallel with the saltation case, meaning equation 2.29 may again be utilized to calculate $c_j(z)$.

In the absence of a physical model of the grain-bed interaction, concentration profiles must be scaled with the use of an empirically derived formula for a reference level concentration (e.g. Anderson and Hallet, 1986, eqn.22):

$$c_a = c_b \frac{\gamma S}{1+\gamma S} \tag{2.33}$$

where the excess shear stress $S = \frac{\tau_b - \tau_c}{\tau_c}$, and the dimensionless coefficient $\gamma = 1.7\times10^{-7}$ and 7.8×10^{-6} for dust and snow, respectively. This formalism yields

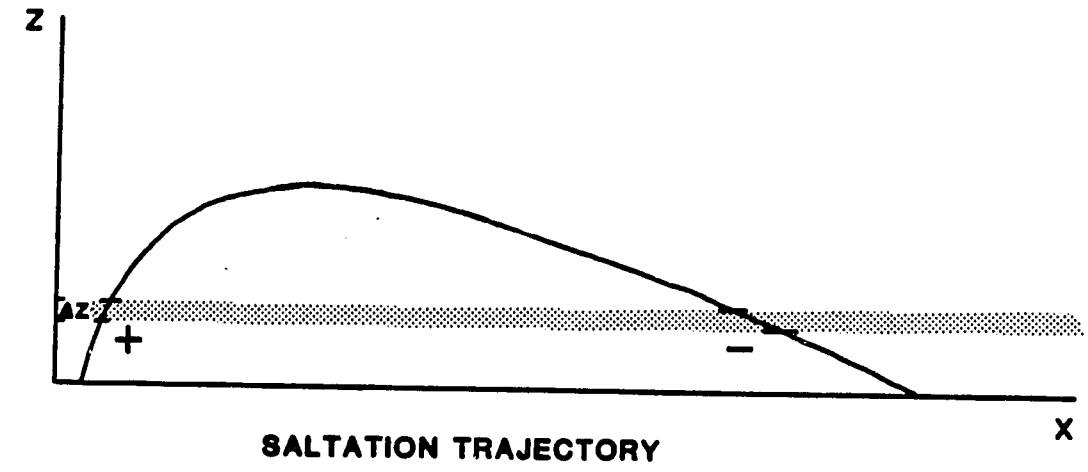

SALTATION TRAJECTORY

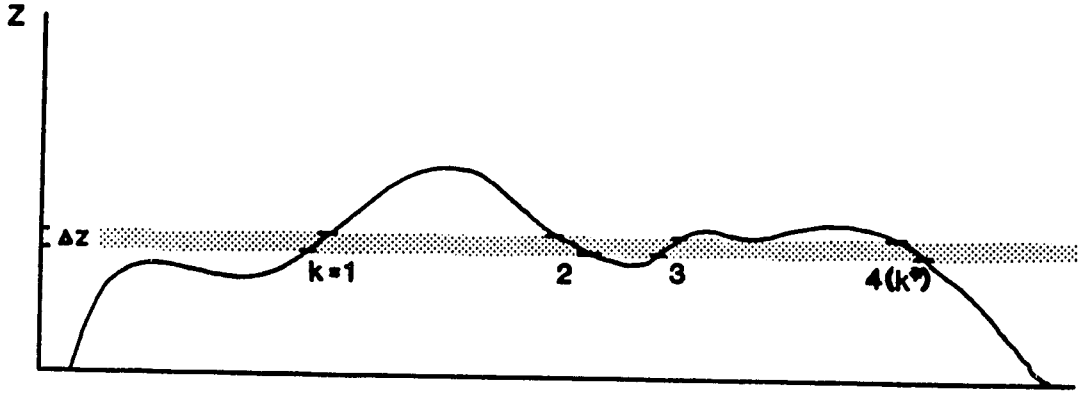

SUSPENSION TRAJECTORY

Figure 2.4. (a) Schematic saltation trajectory. The height element Δz is shaded to illustrate the ascending (+) and descending (-) crossings to be taken into account in calculations of concentration.
(b) Schematic suspension trajectory. Four crossings of the height element Δz are noted, making $k^* = 4$ in the notation of equations 2.30-2.32.

$$\frac{N_j}{N_1} = \frac{c_a(emp)}{c_a(calc)} \tag{2.34}$$

where N_1=1 is the initially assigned value of the ejection rate, $c_a(emp)$ is the empirically calibrated reference level concentration from equation 2.33, and $c_a(calc)$ is the calculated concentration for the interval $(z_a-\Delta z, z_a)$.

2.5 SUSPENSION RESULTS

Concentration profiles are calculated from runs with 1000 trajectories, 25 of which are shown in the corresponding x-z plots (see figures 5a-5d). The power laws corresponding to the appropriate Rouse number ($p=\frac{s}{ku_*}$) are plotted as well. The concentration profiles show encouragingly good fits for the range of Rouse numbers associated with suspended grains, i.e. $p<2.5$, or, equivalently, for particles with settling velocities less than the shear velocity of the air. Best fits are obtained using b_2=1.3, b_1=.5, A_2=0.5. The results are quite sensitive to both b_1 and A_2.

Interestingly, the fit deteriorates well above the bed, falling off much more rapidly than the power law appropriate for the near-bed region. This results from the time limit imposed (for computer-cost reasons) upon the trajectory calculations: those trajectories that do not re-impact the bed within this limit, t_{max}, are not completed. Given the time constraint, there exists some finite height above which no grains will have reached. The steady state profile will not have extended into this region. Recognizing that the process is essentially a diffusive one, we may construct an approximate "diffusion height scale", z_D, using the mean eddy diffusivity, $\bar{K}$, and the time limit:

$$z_D = \sqrt{\bar{K} t_{max}} \tag{2.35}$$

Taking $\bar{K} \approx ku_* \frac{z_D}{2}$ leaves $z_D \approx ku_* \frac{t_{max}}{2}$. A single run with the time limit quadrupled nearly quadrupled the region of near-bed power law behavior, supporting this development.

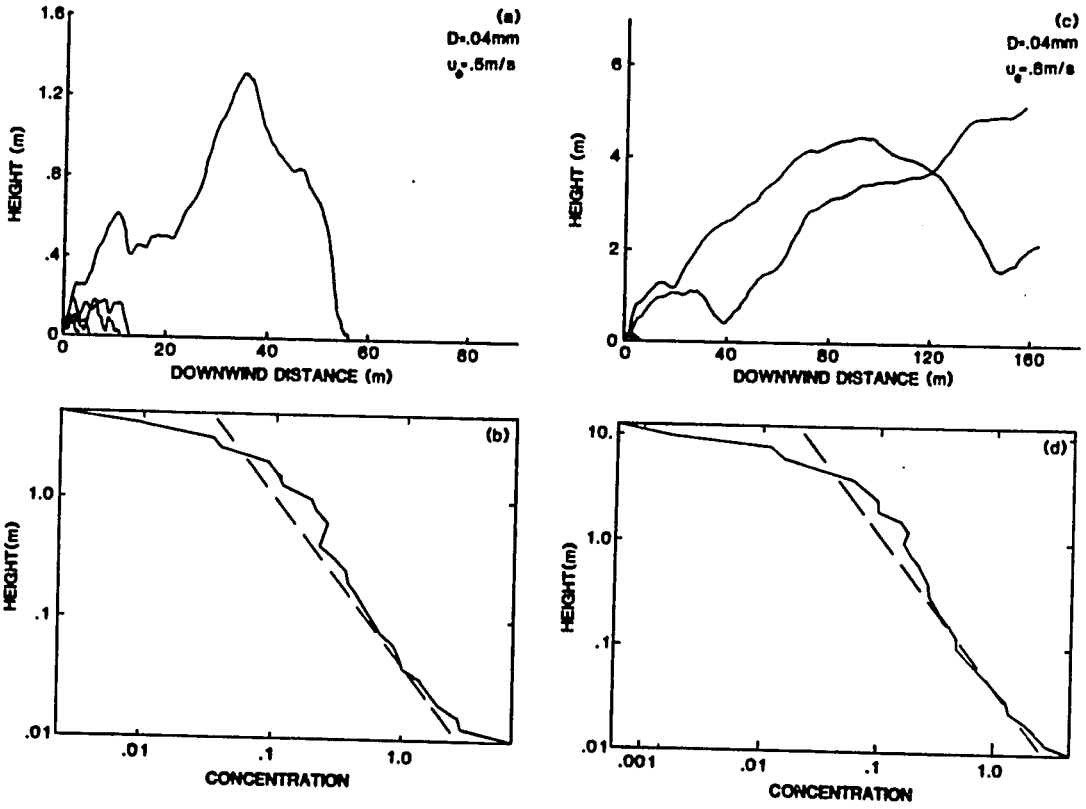

Figure 2.5. (a,c) Suspension trajectories for (a) D =.04mm, u_*=0.5m/s, and (c) D =.04mm, u_*=0.8m/s.
(b,d) Concentration profiles corresponding to suspension trajectories in (a) and (c), respectively, with corresponding power law fits using the Rouse numbers, (b):p =.71, and (d): p =.44, shown as dashed straight lines. Concentrations are normalized with respect to a reference level concentration at z=.04m (see Anderson and Hallet, 1986). See text for discussion of divergence from the power law with height.

Though this result was expected, it is worth pointing out that the implications are important in interpreting field data. The implied time dependence of the concentration profile may be translated into spatial dependence through the mean wind velocity; there should exist a similarly enhanced decay of concentration above some height at any specific distance downwind from the point where sediment transport conditions begin. This is the "fetch effect" described in the blowing snow literature (e.g. Takeuchi, 1980).

2.6 SALTATION, SUSPENSION, AND MODIFIED SALTATION

For a given wind profile, the suspension trajectory algorithm suggested above becomes invalid for particles large enough to produce particle Reynolds numbers well beyond the Stokes range ($R > 10$, say). A more general algorithm incorporating the full functional range of the drag coefficient on the Reynolds number (used, for instance, in the saltation model of Anderson and Hallet, 1986) is then used in the computations. Otherwise, initial conditions are set, and turbulent velocities are chosen according to the procedure summarized above. Figures 6a,b,c represent trajectories calculated using a single set of initial conditions, and the parameters giving the best fits for the suspension profiles.

The trajectories of different grain sizes resulting from calculations incorporating more realistic fluctuating wind velocities prompt a more formal definition of saltation and suspension. For a given particle size and shear velocity of the wind, a set of calculated trajectories with identical initial conditions (i.e. realizations of the trajectory process) gives rise to a distribution of trajectory lengths and times that may be represented by their mean and standard deviation. Choosing the hop length as an appropriate, and easily measurable characteristic outcome of the process, we may say that the particular set of initial conditions gives rise to *saltation* if

$$c = \frac{\sigma_\lambda}{\bar{\lambda}} < c_1 \tag{2.36a}$$

where $\bar{\lambda}$ and σ_λ are the mean and standard deviation, respectively, of the hop length,

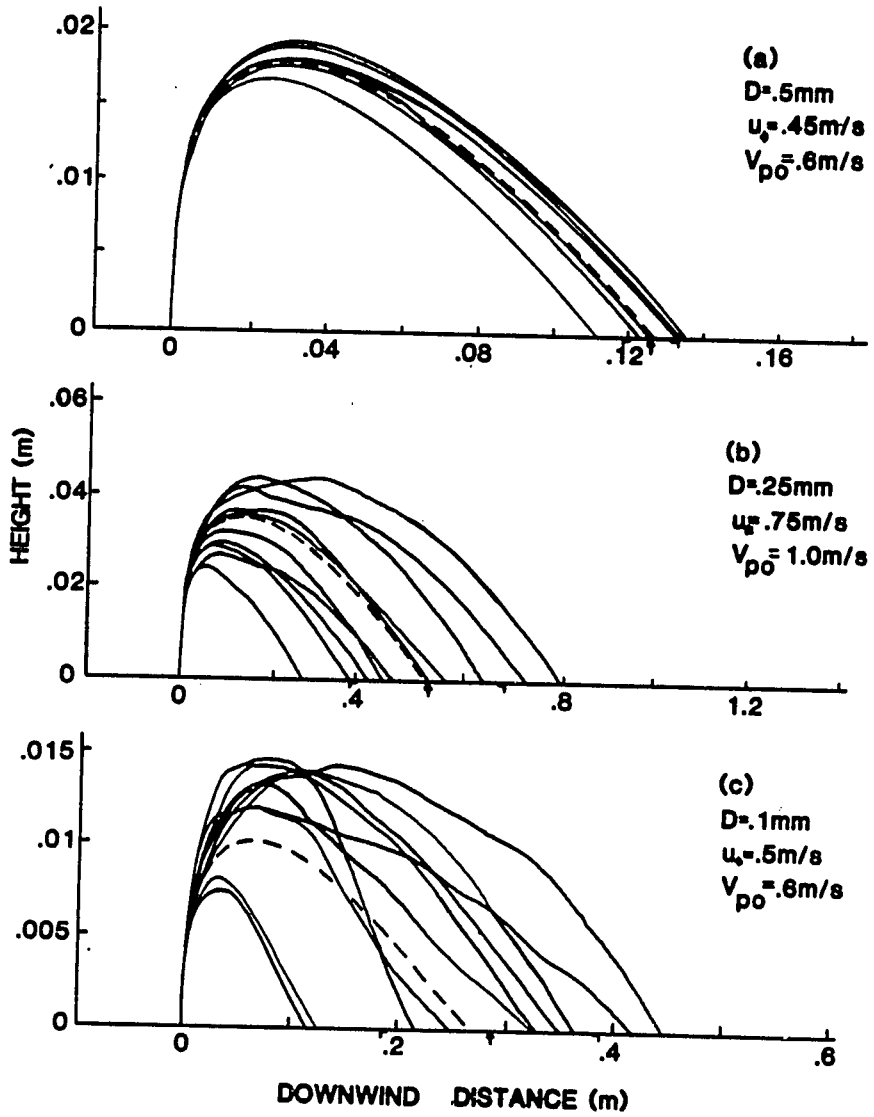

Figure 2.6. Saltation trajectories with turbulent wind component included. All trajectories are given identical initial conditions of liftoff angle (90 degrees), and spin (0). Initial vertical speed is noted. Mean hop length of twenty calculated trajectories is marked with an arrow; brackets indicate one standard deviation. Note exaggerated vertical scales.
(a) D =.5mm, u_* =.45m/s, V_{po} =.6m/s: P_s =16.4.
(b) D =.25mm, u_* =.75m/s, V_{po} =1.0m/s: P_s =2.46.
(c) D =.1mm, u_* =.5m/s, V_{po} =.6m/s: P_s =.66.

and c_1 is an arbitrary constant much less than unity. Similarly, the initial conditions give rise to *suspension* if

$$\frac{\sigma_\lambda}{\bar{\lambda}} > c_2 \tag{2.36b}$$

where c_2 is an arbitrary constant of order one. The region between c_1 and c_2 may then be called *modified saltation*, after Hunt and Nalpanis (1986).

Ultimately, we would like to know the proportions of a particular size fraction likely to be transported in each of these modes. Once the limiting constants c_1 and c_2 are chosen, this determination would require a knowledge of the distributions of initial velocities for each grain size fraction, and extensive trajectory calculations of the sort described here. Ideally, however, we would like to characterize these fractional transport modes without the complicated trajectory calculations. A predictor of the ratio c is therefore needed, in the form of a parameter to be composed of grain size, wind speed, and initial conditions. In the past, this role has been played by the Rouse number, p, which represents the ratio of the particle settling speed to the shear velocity of the fluid. When this ratio falls significantly below unity (i.e. $p << 2.5$) the particles in this size class are to be considered suspended. Similarly, if $p >> 2.5$ the grains are to be considered saltating. Note, however, that this parameter does not incorporate the initial conditions explicitly: the entire population of grains in a certain size class is either saltating or it is suspended. An alternate scaling involves the two important characteristic times in the problem: the response time, τ_r (developed in section I), and the particle hop time, τ_h. In the absense of nongravitational forces, the duration of a single particle trajectory is $\tau_h = \frac{2w_{po}}{g}$, where w_{po} is the vertical component of the liftoff velocity. A "saltation parameter", P_s, may be defined as the ratio of the response time to the hop time:

$$P_s = \frac{\tau_r}{\tau_h} = \frac{D^2 \rho_p g}{36 \rho_a \nu w_{po}} \tag{2.37}$$

When $P_s >> 1$, the grain will not be aloft for long enough to react significantly to vertical velocity fluctuations of the air, and the trajectory will be a smooth *saltation*; conversely, when $P_s << 1$, the vertical velocity fluctuations will dominate the trajectory; the *suspension* trajectory will diverge significantly from the smooth, single-

maximum trajectory characteristic of saltation. [*Note that for small particles, the settling velocity may be approximated by $s = g\tau_r$. The saltation parameter may then be rewritten as $P_s = \frac{s}{2w_{po}}$, which collapses to the Rouse number for a specific initial velocity: $w_{po} = 0.2u_*$.]

The trajectory calculations presented in this paper may be used to identify the relation between the saltation parameter, P_s, and the expected variation of trajectory lengths for a specific set of initial conditions, represented by c. This relationship is presented in figure 2.7 for various wind speeds. Inspection of figure 2.7 reveals a natural break in the functional relationship, motivating a choice of c_1=0.3 and c_2=1.0. Once these limiting constants have been chosen, we may identify the corresponding saltation parameters, $P_{s(1,2)}$. We define the critical vertical liftoff velocities, $w_{po(1,2)}$, as those giving $P_s = P_{s(1,2)}$:

$$w_{po(1,2)} = \frac{D^2 \rho_p g}{36 \rho_a \nu} P_{s(1,2)} \tag{2.38}$$

Determination of the fraction of each grain size class expected to travel in each mode then requires the knowledge of the distribution of the initial velocities, w_{po}. This may be expressed as

$$p(w_{po})dw_{po} = \frac{1}{\overline{w_{po}}} exp\left(-\frac{w_{po}}{\overline{w_{po}}}\right)dw_{po} \tag{2.39}$$

where $\overline{w_{po}}$ is inversely proportional to the square root of the particle mass (Anderson and Hallet, 1986). We may now estimate the fraction, S, of grains of a particular size that will be suspended in a wind of a given shear velocity:

$$S = \frac{\int_{w_{po(2)}}^{\infty} p(w_{po})dw_{po}}{\int_{0}^{\infty} p(w_{po})dw_{po}} = \int_{w_{po(2)}}^{\infty} p(w_{po})dw_{po} \tag{2.40}$$

since $p(w_{po})$ is a proper probability density. This is plotted in figure 2.8 for both quartz and snow and for a variety of shear velocities, with a choice of c_2=1.0.

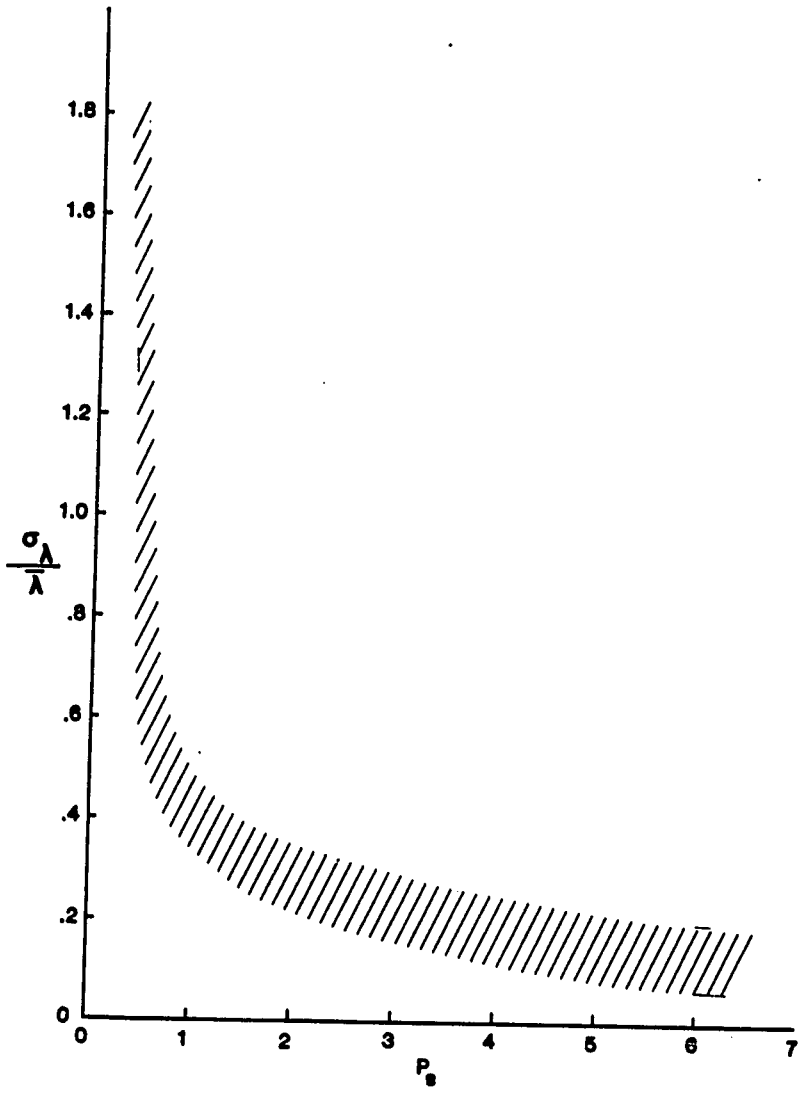

Figure 2.7. Ratio of standard deviation of hop lengths to mean hop length, shown as a function of the saltation parameter, P_s. The scatter indicated by the cross-hatched region indicates that the particular ratio of hop time and response time does not account for the entire range of particle behavior; a more complex dependence including the shear velocity of the wind, acting through an averaged lagrangian time scale, would perhaps be more appropriate.

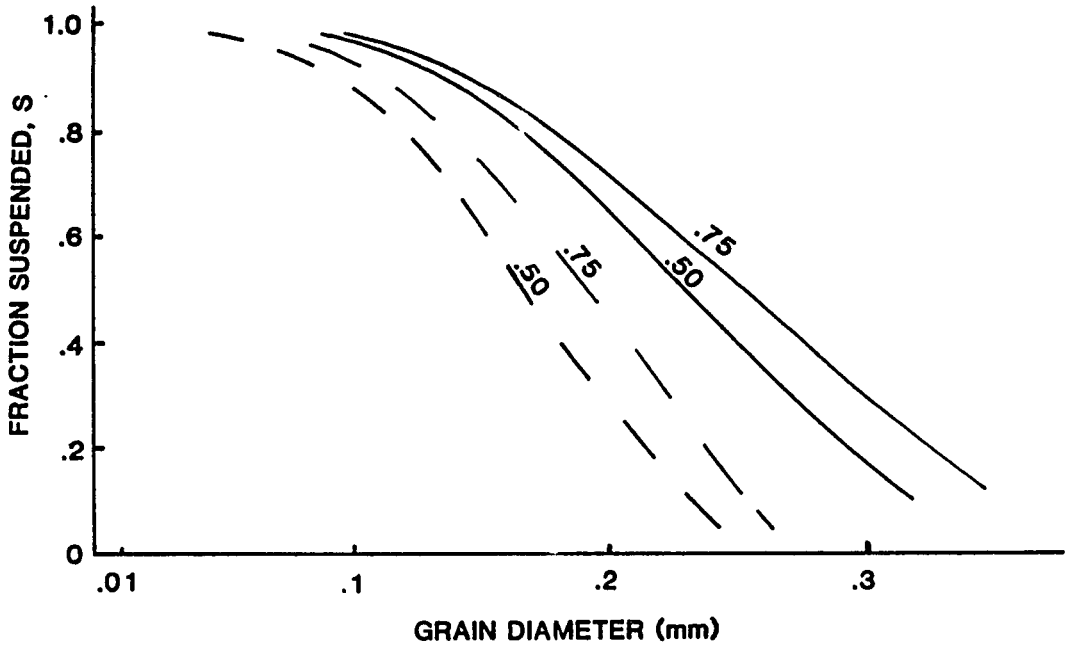

Figure 2.8. Fraction of grains expected to be suspended, S, as a function of grain diameter. Both quartz [dahsed (density 2650 kg/m^3)], and snow [solid (density 917 kg/m^3)] are shown subjected to two shear velocities (labelled, in m/s). The chosen probability distribution of liftoff velocities is exponential, and depends upon grain size as proposed in Anderson and Hallet (1986).

2.7 CONCLUSIONS

We have attempted to address the effects of turbulent fluctuations of the wind velocity on particle trajectories involved in eolian sediment transport. For a given wind condition, a broad range of particle behavior, spanning the continuum between saltation and suspension, results from (1) the distribution of grain sizes in the bed, and (2) the range of initial velocities with which each particle size may be ejected from the bed. Several important time scales emerge from the analysis: the particle response time, τ_r, the hop time, τ_h, and the lagrangian auto-correlation time scale, T_l (or its modified version, T_l^*). For small particles in moderate winds (where the particle Reynolds number remains in the Stokes range), a simple analysis based upon the particle response time captures the essense of the particle's response to fluctuations in the surrounding air velocity. Using a stochastic model of wind velocity history, based upon the langevin equation, and modified to account for the particle's slip relative to the air parcel, particle trajectories are produced with associated concentrated profiles that match well with the power law behavior expected from continuum suspension theory. The region within which the steady (power law) profile accurately describes the suspension concentration grows in height downwind from the position where sediment transport conditions are initiated; concentrations fall off very rapidly above this region. In the absence of a model for the stochastic grain-bed interaction, the ejection rate that sets the source strength, or the concentration at some chosen reference level, must be set empirically, as for instance in Anderson and Hallet (1986).

Larger particles require use of the full functional dependence of the drag coefficient on the Reynolds number. Modification of a numerical saltation trajectory model (Anderson and Hallet, 1986) to account for wind velocity fluctuations allows assessment of trajectory variations as a function of grain size, initial conditions, and wind velocity. As expected, trajectory variations diminish with grain size, and increase with both ejection velocity and wind velocity. A means of estimating the fraction of grains of a particular diameter that will participate in true saltation, true suspension, and some intermediate transport mode, here called "modified saltation", is suggested. Any quantification, however, again requires a knowledge of the

probability distribution of ejection velocities of each grain size in the bed, re-emphasizing the importance of the grain-bed interaction.

Clearly, the analysis presented here is a preliminary attempt to incorporate the complexities of turbulence in the atmospheric boundary layer into a sediment transport model. The intent is not so much to present an alternative to the much simpler eddy-diffusion theory as to clarify some of the physics that gives rise to individual particle trajectories, and, collectively, to the diffusive nature of suspension transport. We stress that there is a continuun between saltation and suspension, and that the "modified saltation" region of this continuum, which for some transport conditions and grain size distributions may be quite important, is made accessible only by combining the available saltation trajectory models with the sort of wind velocity fluctuation history addressed herein.

CHAPTER 3

MODIFICATION OF THE WIND PROFILE DUE TO SALTATING GRAINS

Prediction of particle concentration, mass flux, and kinetic energy flux caused by wind requires accurate calculation of particle trajectories, which in turn requires a detailed knowledge of the wind velocity profile. By Newton's third law, the force exerted on transported grains by the wind results in an equal and opposite force on the air, which acts to retard the near-bed air velocities during sediment transport. A theoretical model for the magnitude and distribution of the resulting stress imposed upon the wind by saltating grains is necessary to establish the relative magnitude of the three contributions to the overall drag over a mobile sand bed: saltating grains, stationary grains on the bed, and form drag due to ripples. In the *eolian* sediment transport system, the vertical region within which the velocity profile is modified by sediment transport is of the order of centimeters, making detailed measurement of the velocity structure possible. Unfortunately, there is little hope for a comparable collection of such data for aqueous saltation, as it is confined to within a few grain diameters of the bed (e.g., Wiberg and Smith, 1985).

In the lowest 10 m of the atmospheric boundary layer the shear stress, τ_b, is approximately constant (Tennekes, 1984). Within this region, but well above the heights of the roughness elements, a logarithmic velocity profile is expected to exist, dependent upon a single velocity scale, u_*, and a single length scale, z_o. The velocity scale is the shear velocity, u_*, defined as $\sqrt{\tau_b/\rho_a}$, where ρ_a is the air density. The shear stress, in turn, is governed by larger scale atmospheric circulation, driven by pressure gradients imposed largely by differential solar heating of the atmosphere. In the absence of large bedforms, the length scale setting the logarithmic velocity profile is proportional to the diameter of the grains in the bed: $z_o = D/30$.

Sediment transport alters the effective roughness of the bed in two ways: first, the horizontal acceleration of transported grains extracts momentum from the wind, and second, the formation of ripples in the bed imposes a form drag on the wind. The resulting sediment transport roughness, z_{ost}, measured by extrapolating the velocity profile outside the sediment transport region to the $U=0$ axis (see figure 3.1),

has been shown to depend on the shear velocity [after Owen (1964, figure 3) for sand in air; extended by Kind (1976) for snow in air]

$$z_{out} = \alpha \frac{u_*^2}{2g} \tag{3.1}$$

with $\alpha \approx .02$, (ranging from .011-.038 [Owen, 1964]). Since in the absence of non-gravitational forces, a grain leaving the bed with velocity u_* reaches a height of $\frac{u_*^2}{2g}$, the success of Owen's formulation implies that the roughness is no longer proportional to the size of the stationary roughness elements in the bed, but rather to some typical hop height of a saltating grain.

Wind velocity measurements *within* the saltation region, show significant deviations from the logarithmic profile. Velocity gradients nearest the bed are reduced from those expected by extrapolating the outer flow toward the bed, and result in ln(z) - U plots of wind profiles that are convex upward. This curvature corresponds to Bagnold's (1941) "kink" in the profile, which occurs typically on the order of one to a few centimeters above the bed. As stressed by Gerety (1986), such near-bed deviations from the logarithmic velocity profile during seidment transport have led to incorrect assessment of the shear velocity during experimental work in wind tunnels. All too often, the slope of the least-squares fit to the ln(z)-U plot, from which the shear velocity is calculated, incorporates at least in part the region in which saltating grains are expected to impose a systematic departure from the simple logarithmic profile. Correct assessment of the shear velocity is essential, for instance, in the development of the correct functional dependence of the total mass flux on the shear velocity (e.g., Bagnold,1941; White, 1979).

A full model of the modification of the wind profile by saltating grains must therefore be able to predict both this curvature of the profile, and the altered effective roughness of the bed. As emphasized by Ungar and Haff (1986), a complete steady state saltation model must include iteration through a wind-velocity profile feedback loop, as the altered wind profile will change the suite of particle trajectories, which in turn result in a new wind profile, etc.

Although it has long been recognized that the modification of the wind profile results from the extraction of momentum from the wind by the saltating grains,

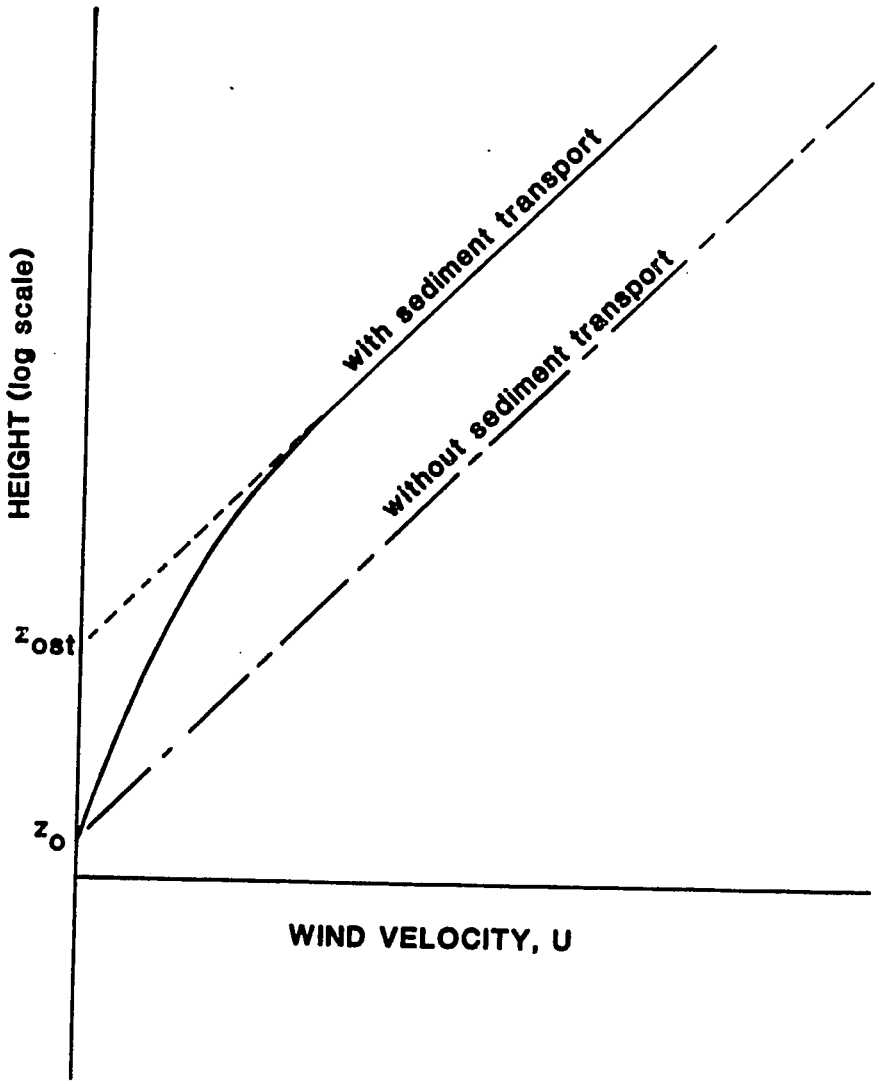

Figure 3.1. Schematic wind velocity profiles. Note logarithmic scale for height; straight lines represent logarithmic profiles. Sediment transport modifies the near-bed profile by extracting momentum from the wind, resulting in alteration of effective roughness from z_o to z_{ost}. The far field shear velocity is calculated from the slope of the profile well away from the bed: $u_* = k\,[U(z_2)-U(z_1)]/[ln\,(z_2)-ln\,(z_1)]$, with k (=0.4) von Karman's constant.

previous attempts to incorporate this effect have suffered from serious oversimplification of the saltation process. Most notably, Owen (1964) assumed that all particles trace identical trajectories. It is now clear, however, that the probabilistic nature of the grain-bed interaction leads to a broad distribution of initial conditions for particle trajectories, and to large gradients in particle concentration, mass flux, and kinetic energy flux with height above the bed (e.g., Anderson and Hallet, 1986; Anderson, 1986; Jensen and Sorenson, 1985; Nalpanis, 1986; Sorenson, 1986; Willetts and Rice, 1986). This structure is expected to be reflected in the force profile imposed by the acceleration of transported grains.

Two recent attempts have been made to calculate wind profiles during sediment transport (Ungar and Haff, 1986; Sorensen, 1986). Ungar and Haff, in their interesting analysis of the saltation problem, confine their calculations to the simplest possible case that yet retains all the important elements of the problem. At any shear velocity, they force their solution to yield only one particle trajectory. As the grain-bed interaction, characterized by their "splash function", is independent of wind speed, i.e. the same liftoff velocity is retained for a particular grain impact velocity no matter what the wind structure is, the single trajectory allowed at each shear velocity must have the same impact velocity. This requires that each such trajectory experience the same net acceleration by the wind. They argue, therefore, that in accord with Bagnold (1941, p.59) "no matter how hard the wind is made to blow ... the wind velocity at a height of about 3 cm remains almost the same. Moreover, at levels still closer to the ground the wind velocity actually falls as the wind above is made stronger." Ungar and Haff's computed profiles show this behavior. It remains to be seen whether similar results can be obtained for a more realistic range of particle trajectories, arising from a more realistic grain - bed interaction, or "splash function."

Sorenson's treatment of wind velocities during sediment trasnport allows a realistic range of particle trajectories. The principal contrast with the formalism presented below lies in the nature of the postulated "closure" relation between the fluid stress and the shear rate, discussed further in section 3.4.

In this paper the equations for the change in the wind velocity due to a given force profile are first formulated, followed by an assessment of the force profile to be

expected during transport of a given grain size in a particular wind. The resulting wind profiles are then compared with the few existing accurately measured profiles.

3.1 MOMENTUM EQUATION FOR THE AIR

Within the saltating curtain, the assumption of constant shear stress breaks down, as the acceleration of massive grains imposes an additional force on the wind. Following the formulation of Ungar and Haff (1986), we identify a horizontal body force on the wind, $F_s(z)$, acting in the upwind ($-x$) direction due to the acceleration of the grains by the air. This appears explicitly in the turbulent Navier-Stokes equations as an additional force term:

$$\rho_a \frac{\partial U}{\partial t} + \rho_a U \cdot \nabla U = -\nabla p + \nabla \cdot \tau_T - \rho_a g - F_s \tag{3.2}$$

where ρ_a is the air density, U is the mean horizontal wind velocity, g is the acceleration due to gravity, and τ_T is the turbulent (Reynolds) shear stress. Given steady ($\frac{\partial}{\partial t} \approx 0$), horizontally uniform ($U \cdot \nabla U \approx 0$) flow, and making boundary layer approximations ($\frac{\partial}{\partial z} >> \frac{\partial}{\partial x}, \frac{\partial}{\partial y}$), the equation for momentum in the downwind (x) direction collapses to:

$$\frac{\partial \tau_T}{\partial z} = F_s(z) \tag{3.3}$$

In the absence of saltating grains the right hand side vanishes, and the first integration yields $\tau_T = constant$. Identifying this constant as the shear stress imposed by the exterior flow, $\tau_b = \rho u_*^2$, making the common "closure hypothesis" that the turbulent stresses may be identified as the product of an eddy diffusivity, K, with the strain rate, $\frac{\partial U}{\partial z}$, and making the further assumption that the eddy diffusivity varies linearly with height, $K = k u_* z$, where k is von Karman's constant, a second integration yields the well known law of the wall, or logarithmic profile: $U = \frac{u_*}{k} ln(\frac{z}{z_o})$. Such conditions should apply throughout the profile in the absence

of sediment transport, and above the region within which grains are being appreciably accelerated by the wind during sediment transport, the difference between them being in the value of the effective roughness, z_o (see figure 3.1).

Within the saltation region, however, the stress on the wind must vary in the vertical direction as the force on the wind due to the extraction of momentum by saltating grains varies.

Assuming a constant total stress available for transporting momentum of either grains or fluid across any level z, the stresses may be partitioned according to (plotted schematically in figure 3.2)

$$\tau_b = \tau_T + \int_z^{z_{max}} F_x \, dz \tag{3.4}$$

where z_{max} is the maximum height to which a saltating grain travels in the given transport conditions. The first term on the right hand side represents the stress available to shear the air at the level z, or the flux of fluid momentum across that level; the second , also called the "grain stress", τ_g (Sorenson, 1986), represents the change in horizontal momentum of grains between their upward and downward crossings of the level z, or the flux of grain momentum across that level. We see that as the bed is approached from above, the grain stress increases, leaving less shear stress available to shear the fluid.

Integration of equation 3.3 yields

$$\tau_T = \int_0^z F_x(z)dz + \tau_{sf} \tag{3.5}$$

where τ_{sf} is the fluid stress at the bed, or the skin friction, part of which may be taken up by form drag due to ripples, as discussed further in section 3.4.

By combining equations 3.4 and 3.5, we see that the skin friction, or the shear stress exerted on the bed by the wind, is simply the far-field shear stress minus the *total* change in horizontal momentum of *all* grains ejected from a unit area of bed in a unit time:

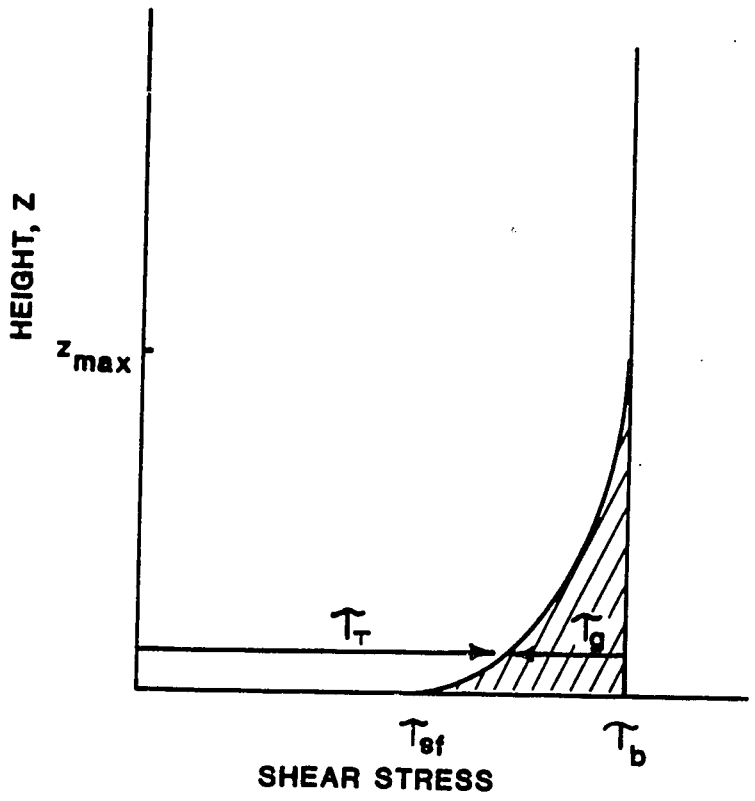

Figure 3.2. Schematic diagram of shear stress as a function of height. Well above the bed, the shear stress is approximately constant, at τ_b. As the bed is approached, the stress imposed by the acceleration of transported grains, τ_g, increases monotonically, resulting in a monotonically decreasing stress available to shear the fluid, τ_T. The skin friction, τ_{sf}, is the fluid stress at the bed.

$$\tau_{eff} = \tau_b - \int_0^{z_{max}} F_x \, dz \tag{3.6}$$

For a given exterior wind condition, characterized by τ_b, as the body force diminishes in magnitude, more fluid stress is made available at the bed for aerodynamic initiation of saltation, and conversely, as body force increases, the shear at the bed decreases. Owen (1964) hypothesized that the self-regulatory nature of eolian saltation arose from such a feedback, with skin friction held near the threshold shear stress necessary to entrain particles aerodynamically. It remains to test this hypothesis quantitatively.

We now seek an equation for the velocity gradient as a function of height, which when integrated will yield a velocity profile in equilibrium with sediment transport. Given the above relations between far field shear stress, skin friction, and grain stress, we need a constitutive relation between the turbulent stresses and the velocity gradient, and we need the body force profile, $F_x(z)$. For simplicity, we again postulate an eddy diffusivity closure: $\tau_T = \rho_a K \frac{\partial U}{\partial z}$, and retain the linear dependence of the eddy viscosity with height, $K = ku_* z$, that gives rise to the logarithmic velocity profile in the absence of sediment transport. However, referencing u_* to the total stress, τ_b, is no longer appropriate. We define a local, or effective shear velocity, referenced to the *local* turbulent stress, τ_T, as $u_{*eff} = \sqrt{\tau_T/\rho_a}$. Rearranging (3.5), and writing $\tau_T = \rho_a k u_{*eff} \frac{\partial U}{\partial z}$, yields:

$$\frac{\partial U}{\partial z} = \frac{1}{k \rho_a^{1/2}} \frac{\left[\tau_b - \int_z^{zmax} F_x(z) dz\right]^{1/2}}{z} \tag{3.7}$$

Note that above the region within which grains accelerate, i.e. $z > z_{max}$, or in the absence of sediment transport altogether, i.e. $F_x = 0$ everywhere, the numerator becomes $\sqrt{\tau_b}$, and the rate of shear becomes $\frac{\partial U}{\partial z} = \frac{u_*}{kz}$, which again yields the logarithmic profile, as required. Given the form of the force profile, derived in the next section, equation 3.7 is numerically integrated for a given shear velocity and grain size to yield the wind velocity profile throughout the saltation region. Note, however, that irrespective of the actual form of the force profile, the fluid stress, and hence the

effective shear velocity, will increase monotonically with height, giving rise to the convex upward U-ln(z) plots.

3.2 FORCE ON THE WIND DUE TO SALTATING GRAINS

Following the formalism established in previous work (Anderson and Haller,1986; Anderson,1986), the force due to identical trajectories with unit ejection rate is first calculated; the distribution of initial conditions and the actual ejection rate are then incorporated to yield a total force profile.

By Newton's third law, the force exerted on a particle by the wind must be equal and opposite to the force on the wind. Figure 3.3 illustrates the horizontal component of the force of the wind on a particle as a function of position along the trajectory, $f_x(z)=M(a_x(z))$, where a_x is the instantaneous horizontal acceleration of the grain, and M is the particle mass. The highest instantaneous force is attained early in the ascending limb of the trajectory, before the particle has been appreciably accelerated by the wind, and where the relative velocity between the particle and the air is greatest. The force on the particle becomes negative shortly before impacting the bed, indicating that the particle there is travelling faster than the wind.

Summing over the ascending and descending limbs of the trajectory, and assuming a single particle is ejected per unit area of bed per unit time, i.e. $N_1=1$, with initial vertical velocity w_o, we obtain the "identical trajectory" force on the wind:

$$F_x(z \mid w_o, N_1) = N_1 M\left(\frac{a_x}{|<w(w_o)>|_+} + \frac{a_x}{|<w(w_o)>|_-}\right) \qquad (3.8)$$

where w is the mean vertical particle velocity in crossing the height element $(z-dz, z]$, and the + and - denote upward and downward limbs of the trajectory, respectively. The upwind direction of the force is left implicit, and is taken into account by the sign convention in equation 2. The identical trajectory force profile displays a distinct maximum at the top of the trajectory (figure 3.4), similar to the maxima in particle concentration, mass flux, and kinetic energy profiles reported

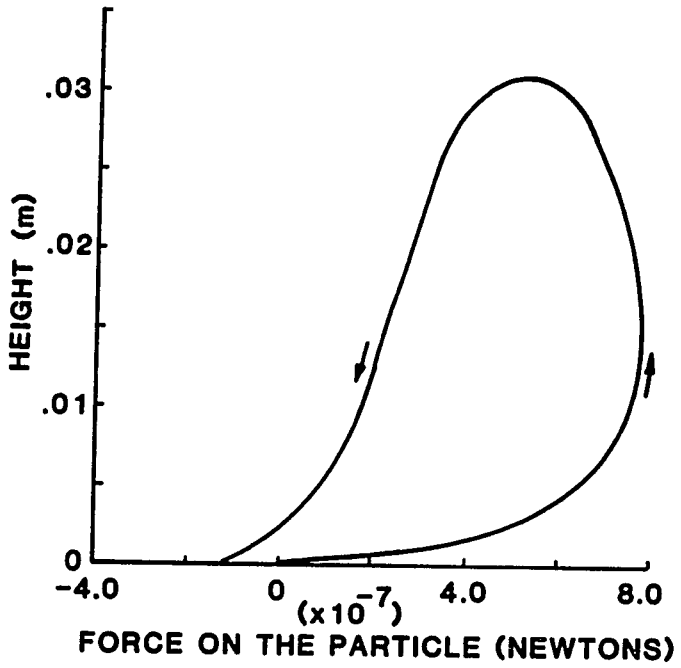

Figure 3.3. Force on the particle as a function of position within its trajectory, for $D = .25mm$, $u_* = .45m/s$, and vertical liftoff velocity, $w_{p_0} = .80m/s$. Up and down arrows denote ascending and descending segments of the trajectory.

earlier (Anderson and Hallet, 1986; Anderson, 1986). Although the instantaneous horizontal force on the particle peaks approximately one third of the way up the ascending limb of the trajectory, most of the particle's horizontal acceleration occurs near the top of the hop, where its vertical velocity is very low, and therefore where it spends the most time.

The "height of the effective fluid thrust" referred to in the saltation literature (Bridge and Dominic,1984; Abbott and Francis,1977; Schmidt,1984; Bagnold,1966) may be interpreted as the "center of gravity" of this body force profile, marked with the arrow in figure 3.4. Effective heights deduced from our trajectory calculations correspond to 80-85 percent of the trajectory height, in close agreement with calculations made from observed saltations in water (Abbot and Francis,1977); in their notation, $y_a = .836 y_{max}$.

The probability density of the vertical liftoff velocity, $p(w_o)dw_o$, and the actual number of particles ejected per unit area of bed per unit time, N, are now introduced to yield an integral equation for the total horizontal body force per unit volume on the wind due to the presence of saltating particles:

$$F_x(z) = \frac{N}{N_1}\int_0^\infty p(w_o)F_x(z \mid w_o, N_1)dw_o \quad [=] \frac{N}{m^3} \tag{3.9}$$

This is illustrated in figure 3.5, along with its integral, the grain stress, τ_g.

This force profile may be closely approximated by an exponential function: $F_x = F_{xo}\, exp(z/z^*)$. Hence, the *total* grain stress may be expressed as $(\tau_g)_{max} \approx z^* F_{xo}$, and the fluid stress may be written: $\tau_T = \tau_b - F_{xo} z^* exp(-z/z^*)$. A series of numerical calculations demonstrates that F_{xo} is a strong function of both grain size and shear stress, as expected, and that the height scale, z^*, is on the order of 1-3cm, implying that the effect of transported grains on the wind profile should vanish by 5cm, as is observed. The scale height is a reflection largely of the probability distribution of initial velocities, which is a strong function of grain size. According to Anderson and Hallet (1986), the mean vertical liftoff velocity, $\overline{w_{po}}$, goes inversely as the square root of the particle mass, and hence as $D^{-1.5}$; a similar inverse dependence is postulated by Sorenson and Jensen (1986).

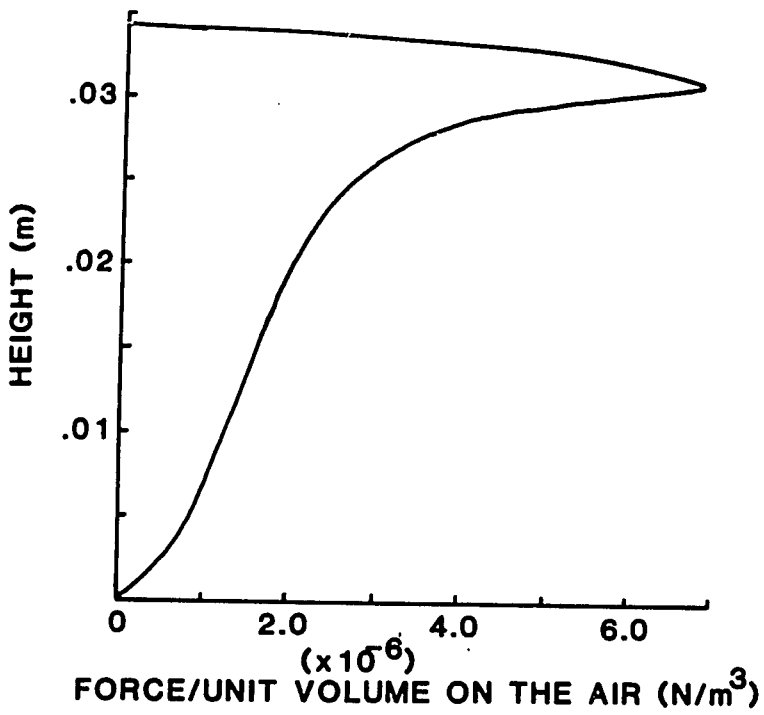

Figure 3.4. Force per unit volume on the air as a function of height. Same conditions as in figure 3.3. A single identical trajectory is initiated per unit area of bed per unit time, i.e. $N=1$. Arrow denotes the calculated "center of mass" of the force profile, at approximately 80 percent of the hop height.

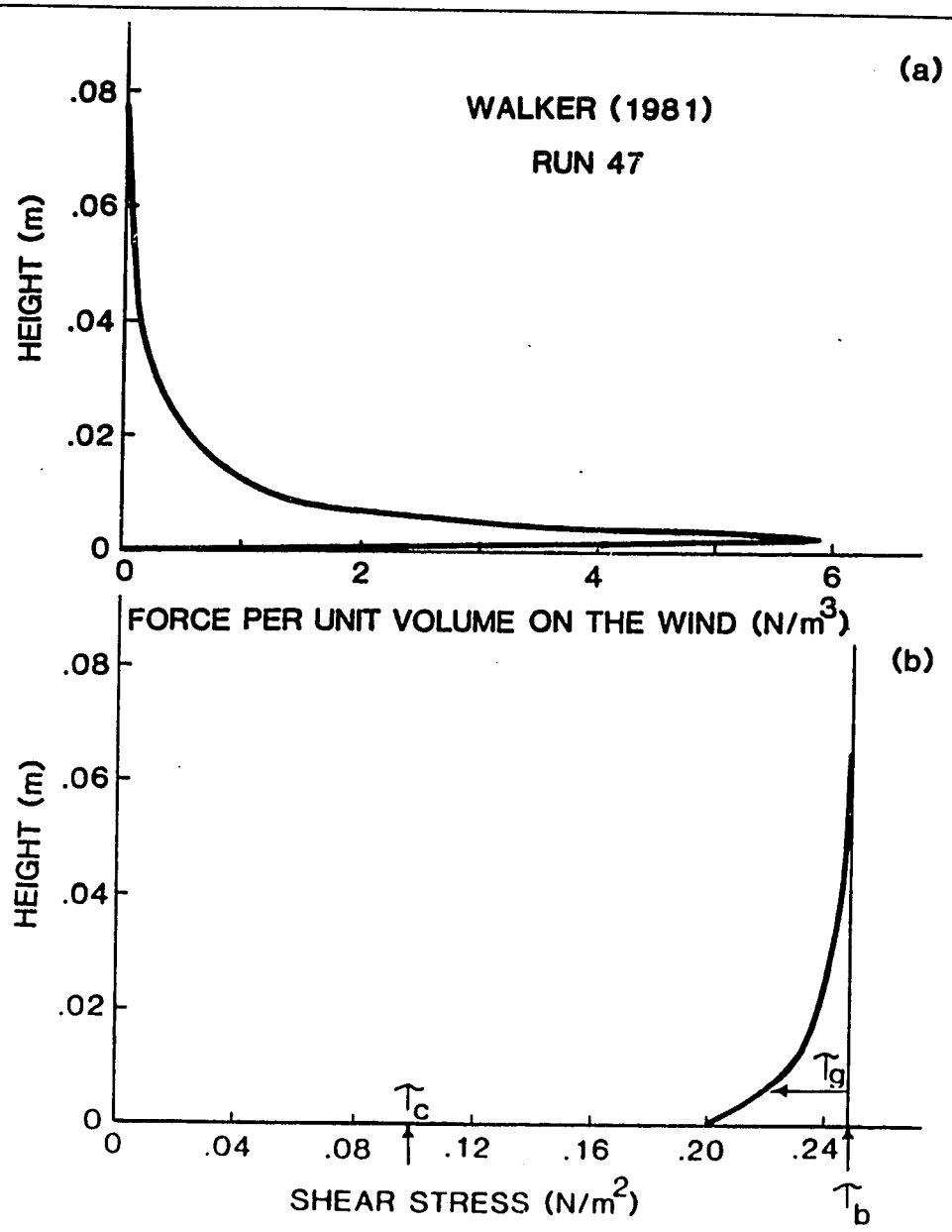

Figure 3.5. Profiles of (a) force on the wind due to saltating particles, and (b) the resulting "grain stress", τ_g, for Walker's (1981) run number 47: $u_* = .45 m/s$, $D = .25 mm$. Note the strongly decaying force as a function of height and its rapid decrease to approximately zero within a millimeter above the bed. The grain stress increases monotonically to a maximum at the bed, but is not sufficient to reduce the fluid stress to the calculated critical shear stress, τ_c, given the ejection rate used, N. See text for discussion.

3.3 RESULTS

Wind velocity profiles were calculated for conditions matching those reported for experiments by Walker(1981), and by Belly (1963). To evaluate u_*, two measured wind velocities were used, both well above the majority of the saltating grains, but below the top of the turbulent boundary layer in the wind tunnel (typically .10 and .20 m measurements were used from the Walker (1981) experiments). Saltation trajectories were then calculated using White's (1979) mass flux relation to determine the ejection rate, N, and a probability density of liftoff velocities, $p(w_o)dw_o$, chosen according to the formulation detailed in Anderson and Hallet (1986). The resulting wind velocity profiles are plotted in figure 3.6. In general the agreement with the measured velocities is encouraging.

Note that the curvature of the log profiles occurs over a broader region for smaller grains than for larger (contrast Walker's runs 7 and 55), reflecting the change of the scale height with grain size, already discussed. That the region within which the curvature occurs is relatively well simulated implies that the probability distribution of initial velocities is well captured by the Anderson and Hallet formalism.

3.4 DISCUSSION

As the magnitude of the force profile is directly proportional to the ejection rate, N, (see equation 3.9) the resulting wind velocity profiles are highly sensitive to the accuracy of the mass flux relation used to calculate N. Greeley and Iversen (1985, p.100, table 3.5) list many such relations that purport to capture the transport rate's dependence on both grain size and wind speed. To illustrate this sensitivity, figure 3.6b shows two velocity profiles that appear to be better fit by doubling the ejection rate above that calculated using the White (1979) mass flux formula. At present, without a theoretically based transport law, or a full physical description of the grain-bed interaction that gives rise to the steady state ejection rate, further testing

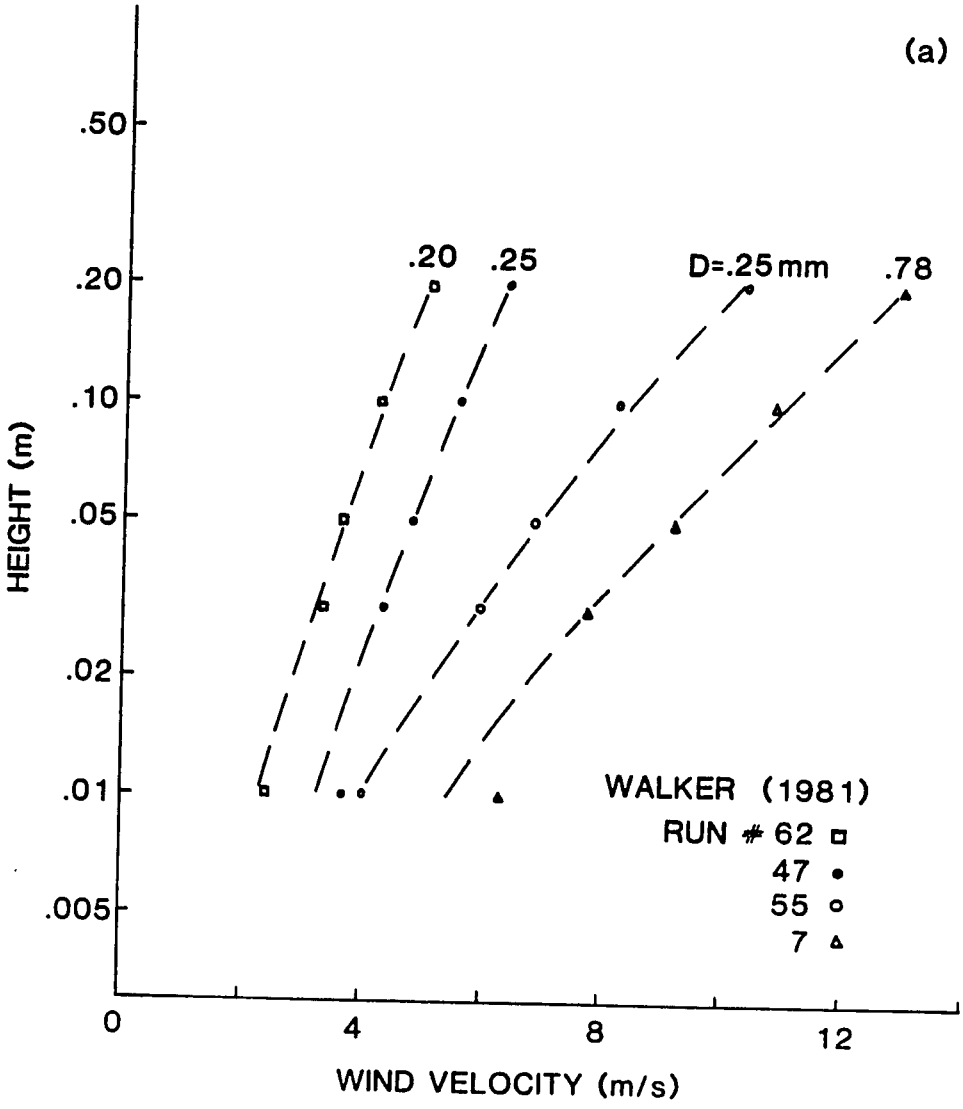

Figure 3.6. (a) Measured (symbols) and calculated (dashed lines) wind velocity profiles for representative runs from Walker's (1981) data set. Grain sizes are noted above each profile, in millimeters. Shear velocities calculated from measured wind velocities at .10 and .20 m heights.

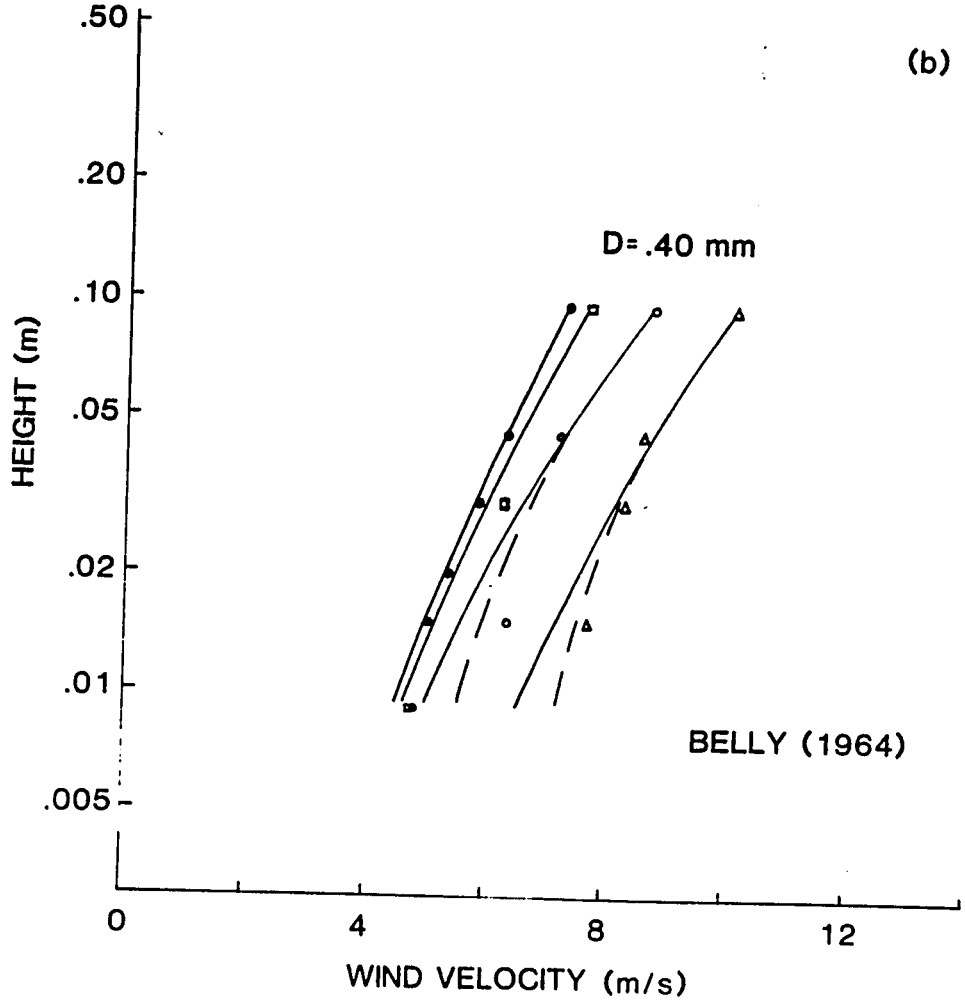

(b) Measured (symbols) and calculated (lines) wind profiles for Belly's (1964) data set, as reported in Gerety (1986). All runs use $D = .40mm$. Solid lines represent calculations using the ejection rate, N, from White's (1979) transport law; dashed lines represent doubling of this ejection rate for the higher shear velocity runs.

of the wind velocity profile formulation presented in this paper can only be made with data sets that include simultaneous mass flux and detailed wind velocity data.

Although extrapolation of both measured and calculated wind velocities made in the more accessible region well above the bed indeed tend to "focus" at a height on the order of millimeters, in accord with Bagnold's (1941, p.130) findings, note that neither measured nor calculated velocity profiles corresponding to increasing shear velocities over the same bed actually cross in these data sets. Of the available data sets [summarized in Gerety (1986)], less than half show such crossing of velocity profiles. The present model fails to predict this behavior, given the transport law used to set the ejection rate, N. This implies that Bagnold's "focus" is possibly an artifact of the inaccuracy with which both wind velocities and anemometer heights can be measured within a centimeter or so of the bed.

It can, however, be stated categorically that the those profiles showing inflections in semi-log space, as some of Bagnold's (1941) early profiles do, are suspect; given the physics of the problem, the stress available to shear the fluid, and hence the effective shear velocity, should increase monotonically away from the bed, yielding convex-upward wind velocity profiles in semi-log space. Inflections resulting from an initial decrease in effective shear velocity, followed by an increase in shear velocity, should not exist.

The additional reporting of the ripple dimensions in equilibrium with the measured profiles would help constrain calculations of their effect on the flow. In his experiments on the effect of sand movement on the surface wind, Bagnold (1941, p.57-58) produced wind profiles over a wetted sand bed that was previously "not only pitted with tiny bombardment craters a few grain diameters in size, but was made to undulate in the usual flat transverse ripples". The resulting U- ln(z) profiles for $u_* = .20\text{-}.62$m/s (p.58, figure 17) show little or no curvature between 2mm and 10cm above the bed, and all yield roughness heights closely approximately by $z_o = 2D/30$, where $2D$ is approximately the mean height of the impact craters (Bagnold, 1941, p.59).

It may be argued that the small surface slopes presented to the wind by these typically low aspect ratio bumps on the bed will tend to minimize the pressure

differences over the rippleform that result in form drag. The ripple index of eolian ripples, defined as the ratio of wavelength to height ($RI=\lambda/H$), is very high: both Bagnold and Walker measured mean ripple indeces of 30 to 70 in experiments with uniform grains. The shear stress exerted by a transverse ripple field with mean height, $\bar{H}$, and mean wavelength, $\bar{\lambda}$, may be written:

$$\tau_r = \frac{F_d}{A} = \frac{\frac{1}{2}\rho_a C_d \bar{H} W U_{ref}{}^2}{\bar{\lambda} W} \tag{3.10}$$

where W is a unit width parallel to the ripple crest, C_d is a drag coefficient, and U_{ref} is a reference velocity. This reduces to:

$$\tau_r = \frac{1}{2}\rho_a C_d (\frac{1}{RI}) U_{ref}{}^2 \tag{3.11}$$

where the inverse dependence on the ripple index is now apparent.

The choice of a linearly increasing eddy diffusivity within the saltation region follows more closely the treatments of Ungar and Haff (1986) and of Sorenson (1986), and diverges from that of Owen (1964), who claimed a constant eddy diffusivity would be appropriate. Owen made the plausibility argument that the intensity of turbulence and the mixing lengths of the turbulence were both dominated by wakes cast by saltating particles, and would be roughly constant within the saltation curtain. However, the concentration of particles in the flow is on the order of 10^{-2} to 10^{-4} near the bed (Anderson and Hallet, 1986; Gerety, 1986; Sorenson, 1986). It may therefore be expected that the nearby presence of a continuous rough bed will dominate over the wakes cast by these sparsely distributed particles in setting the length scale of the turbulence. The use of a linearly varying eddy diffusivity also allows a much simpler feathering of the saltation region with the constant stress region above, rather than requiring an abrupt change in the nature of the turbulence as suggested by Owen. This explicitly recognizes that the saltation region is neither physically isolated, nor even easily identified in the real world. The character of the saltation curtain is such that *all* profile quantities, including the force on the wind imposed by the accelerating particles, fall off rapidly away from the bed, as a consequence primarily of the heavily skewed nature of the probability density of liftoff conditions resulting from the complex grain-bed interaction.

That the shear velocity be tied to the *local* fluid stress, τ_T, rather than the total or far-field stress, τ_b, makes our treatment different from those of both Ungar and Haff (1986), and Sorenson (1986). Such a hypothesis has proven fruitful in aqueous systems, where the form drag due to multiple sets of bedforms is modelled with a corresponding number of matched logarithmic profiles, each characterized by a shear velocity referenced to the spatially averaged form drag associated with that particular bedform scale (e.g. Smith and McLean,1977). The present model identifies both the magnitude of the stress due to saltating grains, and its profile, allowing a smoothly varying wind profile rather than a matched logarithmic profile.

A further difficulty with Owen's formulation of the wind profile within the saltation region is that the no-slip condition is left unsatisfied. Using his formula, wind velocities at the bed remain of the order 7-8u_*. Though this has prompted earlier workers (e.g. Tsuchiya,1972) to justify use of a constant wind velocity (=8.5u_*) in the saltation layer, thereby simplifying trajectory calculations, we argue that the present formulation is considerably more realistic, is not computationally taxing, and provides a profile valid through the entire region of interest in sediment transport mechanics.

3.5 CONCLUSIONS

The formalism presented here for the modification of the wind velocity profile during sediment transport appears to be quite successful in fitting the few data sets available. We stress, however, that high quality data sets that would allow a full testing of the theory are scarce; highly accurate, and closely spaced simultaneous mass flux and wind velocity measurements are necessary to avoid the dependence of the model on transport laws developed previously. In addition, measurement of ripple cross-sectional shapes, perhaps using the simple shadow-based device reported elsewhere (Werner and others, 1986), would aid in assessing the role of form drag due to ripples in reducing the aerodynamic stress available for initiating saltation at the bed.

The method of modifying the wind velocity profile during sediment transport presented here is an integral part of the full sediment transport problem. Given aerodynamic initiation of sediment transport immediately following a rise in the far-field wind velocity, the resulting trajectories not only impact the bed with sufficient energy to produce a cascade of ballistically induced saltations, but they modify the wind velocity field experienced by these new trajectories. An iterative scheme similar to the one proposed by Ungar and Haff (1986), wherein both the grain-bed interaction and the grain-wind interaction are properly addressed, is necessary to close the problem entirely.

CHAPTER 4

EROSION PROFILES DUE TO PARTICLES ENTRAINED BY WIND: APPLICATION OF AN EOLIAN SEDIMENT TRANSPORT MODEL

Erosion by wind-driven mineral particles is responsible for the development of unusual geomorphic phenomena ranging from centimeter-sized ventifacts, to kilometer-long yardangs. Important observations of large scale erosion features include (1) the re-entrant vertical profiles that occur in the "prows" of some yardangs (for instance those at Rogers dry lake, California (Blackwelder,1935; McCauley and others,1977; Ward and Greeley,1984)), and in large ventifacts (see cover photograph, Greeley and Iversen,1985), that reflect maximum erosion well above the ground, and (2) fan-like fluting of upwind surfaces on large ventifacts (e.g. Sharp,1949; Lancaster,1984) (figure 4.1).

Profiles of erosion in lucite rods exposed to wind for 15 years (Sharp,1964,1980), and in fenceposts eroded in 24 hours during the December 1977 San Joaquin duststorm (Sakomoto-Arnold,1981; Wilshire and others,1981) display erosion maxima .10-.12m, and .10-.55m (average .24m) above the ground, respectively. Figure 4.2 illustrates Sharp's final reported profile, and two particularly well constrained examples of erosion profiles in San Joaquin fenceposts (B.Hallet,1981,pers.comm.). Though other fencepost profiles display more complex patterns of erosion, and the height measurement of the erosion maxima is surely complicated by the local deflation of the surface during the dust storm (H.Wilshire,1985,pers.comm.), most posts do display a single pronounced maximum. Wilshire and others (1981) report that wind velocities may have locally exceeded 300km/hr in the San Joaquin storm. Though collection of meteorological data has been "consistently defeated by the elements" in the Coachella Valley (Sharp,1980), 100-150km/hr winds probably occurred within the 15 year span of the experiment. Akerman (1980), working in Spitzbergen, reports similar profiles of erosion in plexiglas tubes and clay disks, with maxima 0.5-1.0m above the ground, and argues strongly that they result from impacts of snow grains during high winter winds.

The modelling of such erosion profiles has two principal scientific merits: (1) to understand better the erosion of natural objects, and (2) to test quantitatively the

Figure 4.1. 1 metre wide ventifact on Garnet Hill, Coachella Valley, California, showing prominent radial fluting at the upper edge of the upwind surface. View faces downwind.

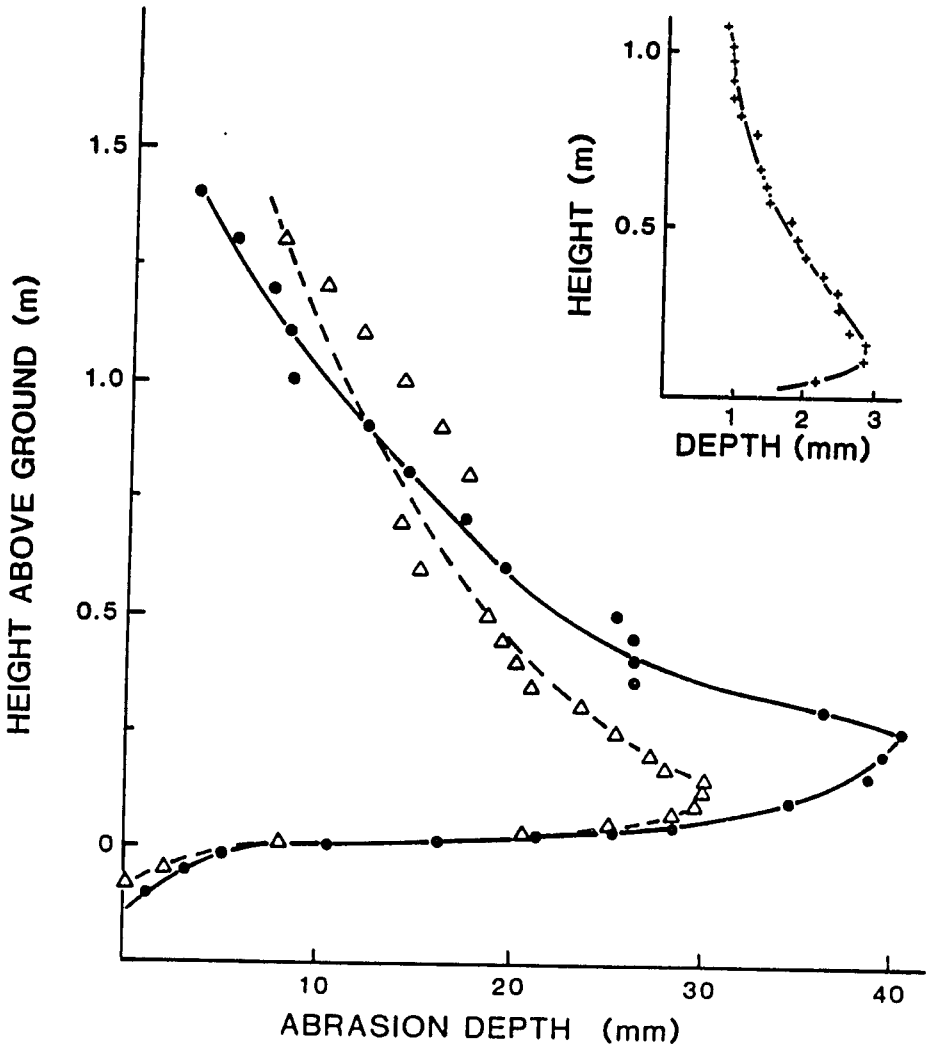

Figure 4.2. Erosion profiles measured in a lucite rod (upper figure, after Sharp,1980), and in two cedar fenceposts eroded during the 24-hour long San Joaquin dust storm of December 1977 (Hallet, unpublished data), measured parallel to wind direction. Note difference in the scales for abrasion depth. Fencepost profiles were measured from the *original* ground level, preserved as the upper limit of soil stain, and the lower limit of charring from grass fires, both still visible on the lee sides of the posts. Erosion below this level occurred as deflation on the order of .1 metre proceeded during the storm.

general model of eolian sediment transport (Anderson and Hallet,1986). This test of the transport model is an exacting one as it involves calculation of quantities very sensitive to the initial conditions in both saltation and suspension analyses. Natural obstacles are geometrically complex, and difficult to model without resort to calculations of three-dimensional air and sediment trajectories. In contrast, artificial obstacles in which the measured erosion profiles occur have a nearly cylindrical geometry that lends itself to simple quantitative analysis of the obstacle-flow interaction. In addition, while the erosion history of a natural object is difficult to decipher, that of manmade objects is often confined to one or several extreme events whose meteorological characterisitics can be inferred.

Several recent experiments have established the precise relation between erosion and impact parameters: grain diameter, D, density, ρ_p, speed, V, and angle of incidence, α (defined such that 90 degrees is a perpendicular impact). The mass of target material removed per impact, A, may be expressed as (Routbort and others, 1980; Scattergood and Routbort, 1983):

$$A = S_s \rho_p (V \sin\alpha - V_o)^n (D - D_o)^m \tag{4.1}$$

where S_s is the "susceptibility" of the material to erosion, dependent upon the density, hardness, and fracture-mechanical properties of the target and impacting materials, and V_o and D_o are the threshold particle speed and diameter needed to initiate erosion. Experiments on rates of target surface lowering yield values of n=2 and m=3 (Suzuki and Takahashi,1981; Greeley and others,1984), suggesting that the mass of material removed per impact is roughly proportional to the kinetic energy of the impact. In a more comprehensive study, Scattergood and Routbort (1983) show that the available data for erosion of a single silicon crystal at various impact angles collapse neatly using equation 1, with n=2.6, m=3.6, $D_o = 20\mu m$, and V_o essentially zero. Though these relations for erosion of single crystals are more complex than a simple function of kinetic energy, it is reasonable to assume that the mass removed per impact on most polycrystalline geological materials scales roughly with the kinetic energy of the impact. Note that in this case the susceptibility, S_s, becomes simply the mass of target material removed per unit kinetic energy. The model readily accepts alternate erosion "laws".

Sharp (1964,p.798) states "the zone of maximum wear does not correspond to the median saltation height, so it must represent the level at which grain size, number, and velocity combine to give the greatest energy of impact." We may now more precisely formulate this proposition by recognizing that it is the flux of kinetic energy to a surface that appropriately combines these variables. Defining the instantaneous horizontal flux of kinetic energy to a unit surface area perpendicular to the wind in unit time, q_{ke}, the mass of target material removed per unit surface area per unit time, $\dot{A}$, is taken to be simply

$$\dot{A} = S_e \, q_{ke} \tag{4.2a}$$

and the lowering rate of an impacted material surface, $\dot{L}$, is

$$\dot{L} = \frac{\dot{A}}{\rho_t} = \frac{S_e \, q_{ke}}{\rho_t} \tag{4.2b}$$

where ρ_t is the density of the target material.

The actual delivery of kinetic energy to a surface also depends upon particle diameter in that particles of differing sizes are variously deflected by the complicated airflow around an obstacle. Large particles with sufficient inertia effectively diverge from the flow and will more likely impact the surface than small particles, which follow more faithfully the flow streamlines that tend to parallel the surface. Theoretical studies of the paths of particles entrained in fluids around obstacles are numerous (e.g., Langmuir and Blodgett,1946; Morsi and Alexander,1972). They have been motivated by an assortment of both engineering and natural science problems, ranging from abrasion of propellor blades and of bird wingtips (Burtt,1981), to ice rime growth (e.g., Minsk,1980; Makkonen,1984), the collection of pollen by early seed plants (Niklas,1981;1985), and the capture of food by zooplankton (Strickler, 1982; Emlet and Strathman,1985).

Eolian abrasion, then, depends on four factors: (1) the distribution of kinetic energy flux due to both saltating and suspended grains in a steady, uniform wind; (2) the interaction of the wind with an obstacle and the relative decoupling of particles from the wind, allowing delivery of kinetic energy to the obstacle surface; (3) the temporal variations of the wind, and (4) the material properties of both the impactors and the exposed surface.

This report addresses the first two factors, providing a model for the instantaneous pattern of erosion of uniform materials. The magnitude of erosion depends on material properties, but the pattern of erosion does not. Full analysis of the abrasion of any specific obstacle would obviously entail integration over variable winds, and should allow the surface geometry of the obstacle to evolve. However, the erosion pattern will be shown to reflect closely the instantaneous profile inflicted during the highest winds.

As in the development of the general model of eolian sediment transport (Anderson and Hallet,1986), the saltation and suspension fluxes are treated separately. The kinetic energy flux due to a single saltation trajectory is first presented, followed by a summation over all particle trajectories, whose initial conditions are distributed in accord with experimental data (White and Schulz,1977). Suspension is treated first analytically, leading to general conclusions about the dependence of kinetic energy flux on both wind speed and particle size; then, a numerical simulation of a reference case is presented, wherein the kinetic energy flux is calculated for a realistic distribution of grain sizes subjected to a moderate wind. We then briefly analyse particle paths around a vertical cylindrical obstacle, to assess the relative efficiency of kinetic energy delivery to such obstacles by the various grain sizes. We conclude with a simulation of an instantaneous erosion profile due to both saltating and suspended particles expected during peak winds in the San Joaquin dust storm, and a discussion of the implications of the model regarding ventifaction.

4.1 KINETIC ENERGY FLUX DUE TO SALTATING GRAINS

We first calculate the vertical profile of kinetic energy flux due to a single saltation trajectory. The trajectory height is divided into equal increments, dz, and average horizontal and vertical particle velocities are recorded as it traverses each increment on both ascending and descending limbs of the trajectory. (See definition sketch, figure 4.3.) The "single trajectory kinetic energy flux" may then be written:

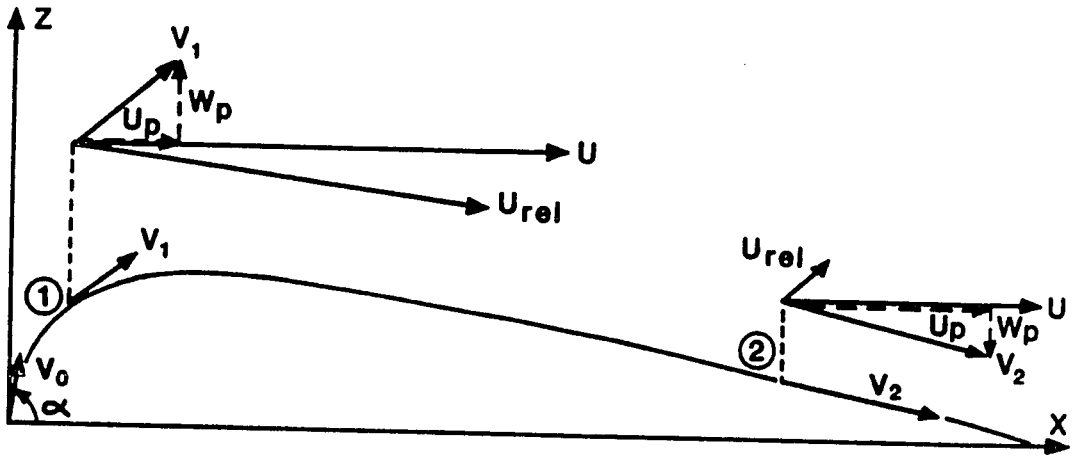

Figure 4.3. Definition sketch, showing particle velocity, V, air velocity, U, and horizontal and vertical components of particle velocity, u_p and w_p, respectively, at two positions along a saltation trajectory. The velocity, U_{rel}, of the particle relative to the air is also shown.

$$q_{ke\ 1}=\frac{1}{2}N_1M_p\left(\frac{V^2u_p}{|\ w_p\ |_+}+\frac{V^2u_p}{|\ w_p\ |_-}\right) \tag{4.3}$$

where the subscript "1" refers to the single trajectory case, the arrows refer to upward and downward portions of the trajectory, M_p is the particle mass, V is the particle speed ($=\sqrt{u_p{}^2+w_p{}^2}$), and N_1 is the number of grains ejected per unit area of bed per unit time (=1 in the single trajectory case).

The total flux of kinetic energy due to saltating grains is the sum of the single trajectory flux over all possible trajectories, weighted by the probability density of each trajectory. Approximating the probability density of trajectories with the probability density of vertical liftoff velocities, $p(w_o)$ (Anderson and Hallet,1986), the expression for kinetic energy flux becomes:

$$q_{ke}(z)=\frac{N}{N_1}\int_0^\infty p(w_o)q_{ke\ 1}dw_o \tag{4.4}$$

where N is now the actual ejection rate. Assuming that all particles travel identical trajectories is equivalent to approximating the probability density as a delta function. The kinetic energy flux profile then becomes simply the product of the ejection rate, N, with the single trajectory profile. More realistic probability densities are characterized by very high probability of small liftoff velocities, with progressively declining probability as liftoff velocity increases. Constrained by liftoff velocities reported by White and Schulz (1977), both exponential and gamma functions were tested (Anderson and Hallet,1986), the best fits to measured mass flux profiles being obtained with exponential distributions of the form

$$p(w_{po})=\frac{1}{\overline{w_{po}}}exp\left(-\frac{w_{po}}{\overline{w_{po}}}\right) \tag{4.5}$$

where $\overline{w_{po}}$ is the mean vertical liftoff velocity. The ejection rate, N, is set by equating the ratio N/N_1 with the ratio of the total mass flux computed using White's expression (1979), to the integral of the mass flux profile calculated assuming $N=N_1$. Calculated kinetic energy flux profiles for both the simple single trajectory case and the more realistic multiple trajectory case are shown in figures 4.4a and 4.4b, respectively.

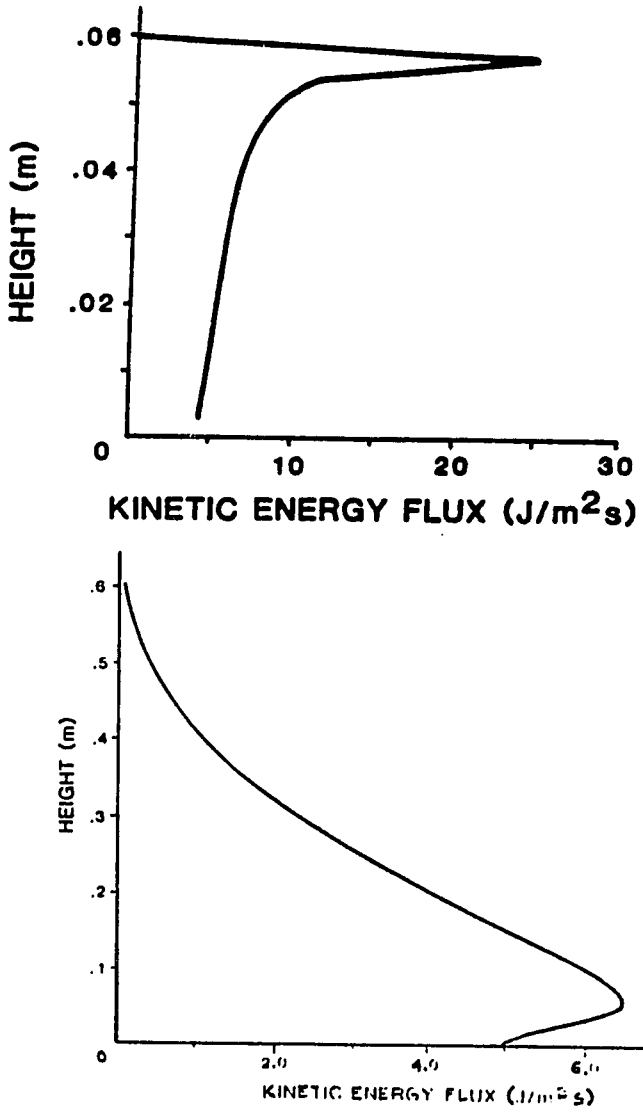

Figure 4.4. (a) Kinetic energy flux profile for single saltation trajectory case, with shear velocity $u_* = 1.0\text{m/s}$ ($u_* = (\frac{\tau_b}{\rho_a})^{\frac{1}{2}}$, where τ_b is the boundary shear stress, and ρ_a is the air density), $D = .25\text{mm}$, and liftoff velocity $V_o = 1.4\text{m/s}$. White's (1979) form of the mass flux relation was used to set $N = 1.6\text{x}10^6/m^2\text{s}$.
(b) Kinetic energy flux profile for multiple saltation trajectory case, with $u_* = 1.0\text{m/s}$, $D = .25\text{mm}$, and an exponential distribution of liftoff velocities prescribed in equation 6, with $\overline{V_o} = .63u_* = .63\text{m/s}$, and $N = 4.7\text{x}10^5/m^2\text{s}$.

As with the single trajectory concentration and mass flux profiles (Anderson and Hallet,1986), the single trajectory kinetic energy flux peaks sharply at the top of the trajectory, reflecting the large proportion of time the particle spends near the top of its trajectory. Summing many such profiles in the more realistic case -- corresponding to good fits with the observed mass flux profiles -- yields a less distinct maximum near the bed, above which the kinetic energy flux declines smoothly with height. Of course no erosion due to saltation occurs above the maximum trajectory height.

Multiple grain sizes in saltation may be incorporated using the grain size fractions in the bed, i_n, and assuming that the distribution of mean vertical ejection velocities, $\overline{w_{po}}$, for each grain size class, can be approximated from a simple kinetic energy argument (Anderson and Hallet,1986). Each grain size class is assumed to have identical mean initial kinetic energy, implying that large grains are ejected from the bed at lower velocity than small grains. Such a simple model provides good fits to mass flux profiles reported by Williams (1964) for multiple grain size saltation wind tunnel experiments. Resulting kinetic energy flux profiles for individual grain size classes, and the total kinetic energy profile due to saltation of a moderately well sorted sand are presented in figure 4.5. The shape of the resulting total profile peaks weakly near the bed, and declines smoothly above this.

4.2 KINETIC ENERGY FLUX DUE TO SUSPENDED GRAINS

In this section we develop an analytical expression for the kinetic energy flux, and analyze the height and strength of kinetic energy flux maxima due to each suspended grain size class. We then present a numerical calculation of the kinetic energy flux profiles for the entire range of particles mobilized by the peak winds observed during the San Joaquin dust storm.

Assuming the horizontal particle velocity roughly equals that of the wind, $U(z)$, (i.e. that the grains are in suspension), the kinetic energy flux due to grain size class n is:

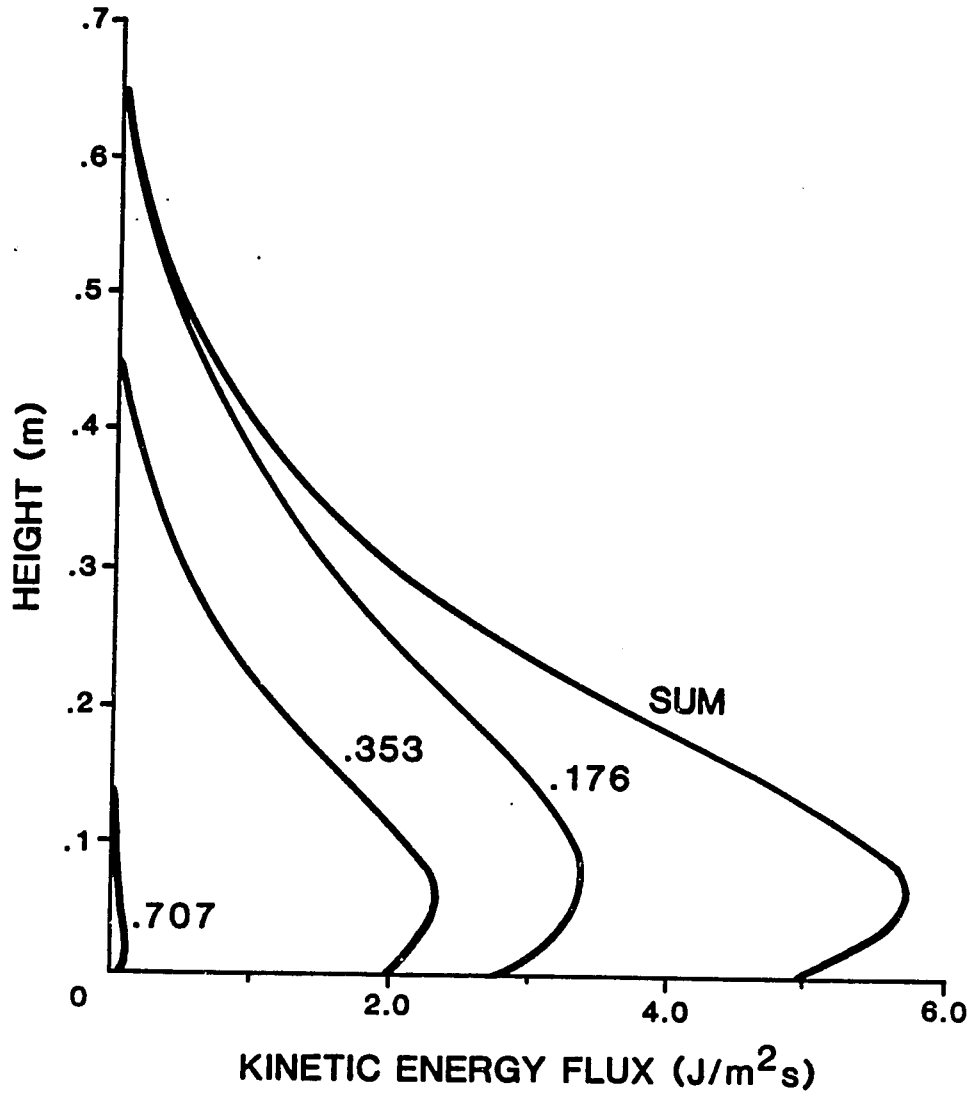

Figure 4.5. Multiple trajectory and multiple grain size calculations of the kinetic energy flux for saltation over a moderately well sorted bed with $\bar{D}$=.25mm, σ=.6ϕ, subjected to a shear velocity of 1.0m/s, using the exponential distribution of liftoff velocities, and White's mass flux relation. Grain sizes and fractions in the bed are: D=.707,.353,.176, and i=.05,.45,.45, respectively. The curve labelled "SUM" represents the summation of the contributions from all grain size fraction. Compare with figure 4.4b, calculated using only the mean grain size.

$$q_{ke} = \frac{1}{2}\rho_p\, c_n(z)\, U^3(z) \tag{4.6}$$

where again c_n is the volume concentration of grains of size class n. As the wind velocity increases with height, whereas concentration decreases with height, there must be a maximum q_{ke} for each grain size class at some height above the ground. Substituting expressions for concentration and for the wind velocity profile during sediment transport (Anderson and Hallet,1986), and neglecting minute stratification effects, gives

$$q_{ke} = \frac{1}{2}\rho_p\, (c_n)_a \left(\frac{z}{z_a}\right)^{-p_n} \left(\frac{u_*}{k} \ln \frac{z}{z_o}\right)^3 \tag{4.7}$$

where $(c_n)_a$ is the concentration at a reference level z_a, p_n is the Rouse number, defined as $\frac{s_n}{ku_*}$, with s_n the settling velocity of size class n, k von Karman's constant (=0.4), and u_* the shear velocity of the air. Neglecting substantial deviations from spherical shapes, particle settling velocities increase rapidly with diameter, from approximately .1m/s for quartz grains of .04mm diameter, to 10m/s for 2mm grains (Walker and others,1971; Anderson and Hallet,1986). The sediment transport roughness, z_o, is given by Owen(1964)

$$z_o = .0207\left(\frac{u_*^2}{2g}\right) \tag{4.8}$$

Calculated kinetic energy flux profiles, using a non-dimensionalized form of equation 7 (with $q_{ke}^* = \frac{q_{ke}}{\frac{1}{2}\rho_p (c_n)_a \left(\frac{u_*}{k}\right)^3}$, and $z^* = \frac{z}{z_a}$), are presented in figure 4.6 for p_n =0.5,1.0,2.0. The height of the maximum q_{ke} is obtained by setting $\frac{\partial q_{ke}}{\partial z} = 0$:

$$\frac{\rho_p (c_n)_a u_*^3}{2k^3} z_a^{p_n} \left(\ln^2\left(\frac{z}{z_o}\right)\right) z^{-p_n - 1} \left(3 - p_n \ln\left(\frac{z}{z_o}\right)\right) = 0 \tag{4.9}$$

Three solutions exist: $z = z_o$, $z = \infty$, and $z = z_o\, exp(3/p_n)$. The first two clearly correspond to minima, the first where the velocity vanishes, the second where concentration vanishes. The third solution corresponds to the expected maximum, and is strongly dependent upon both the shear velocity (through both p_n and z_o) and grain size (through the settling velocity in p_n). Substituting Owen's form for the

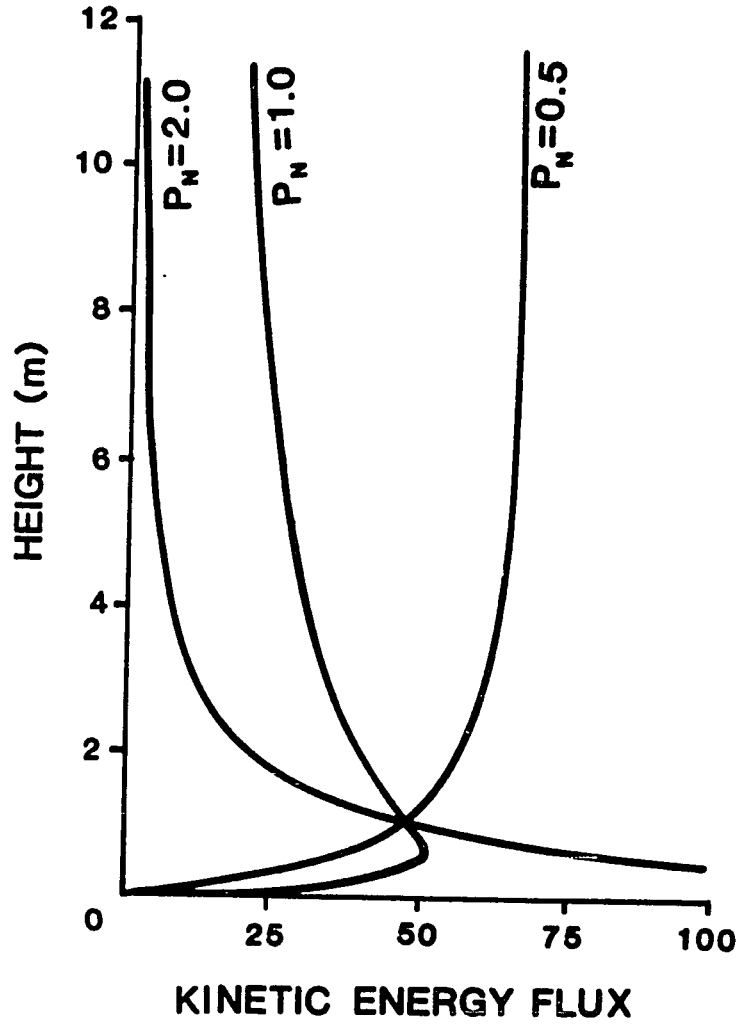

Figure 4.6. Non-dimensional form of the kinetic energy flux due to suspended grains, for Rouse numbers, p_n $(=\frac{\delta_n}{ku_*})$=0.5,1.0, and 2.0, corresponding to D =0.05,0.07, and 0.12mm, with u_*=1.0m/s, and z_a =.04m.

roughness, z_o, the height (in meters) of the kinetic energy flux maximum is:

$$z_{max} = 10^{-3} \times u_*^2 exp\,(1.2\frac{u_*}{\sigma_n}) \tag{4.10}$$

The sensitivity of the kinetic energy flux maximum to both shear velocity and grain size is illustrated in figure 4.7. Having determined the heights of the maxima, however, we must now evaluate the relative strengths of maxima corresponding to each grain size in a given wind. Equation 4.7, with $z = z_{max} = z_o\, exp\,(3/p_n)$, leads to:

$$q_{ke\,max} = \frac{27}{2}\rho_p (c_n)_a (\frac{u_*}{ekp_n})^3 (\frac{z_o}{z_a})^{-p_n} \tag{4.11}$$

The relative strengths of the kinetic energy maxima for various grain sizes are thus critically dependent upon u_*. Moreover, three terms are grain size dependent. The cubic term implies the maximum kinetic energy should increase dramatically as p_n, and hence grain size, decreases. Since the reference level z_a is typically an order of magnitude greater than the roughness height z_o, the last term decreases rapidly with grain size. Reference level concentrations, $(c_n)_a$, also decrease strongly with increasing grain size. Following work on aqueous suspension (Smith,1977), previous modelling of eolian suspension (Anderson and Hallet,1986) has shown that reference level concentrations may be parameterized using the weight fraction of sediment of size class n in the bed, i_n, and the excess shear stress, S, as expressed in the following equations:

$$(c_n)_a = c_b\, i_n \frac{\gamma S}{1+\gamma S} \tag{4.12}$$

where c_b is the total sediment concentration in the bed, a constant typically taken to be .65, and γ is an empirically derived constant. The excess shear stress may be written either as

$$S = \frac{\tau_b - \tau_{ci}}{\tau_{ci}} \tag{4.13a}$$

or

$$S = \frac{\tau_b - \tau_{cf}}{\tau_{cf}} \tag{4.13b}$$

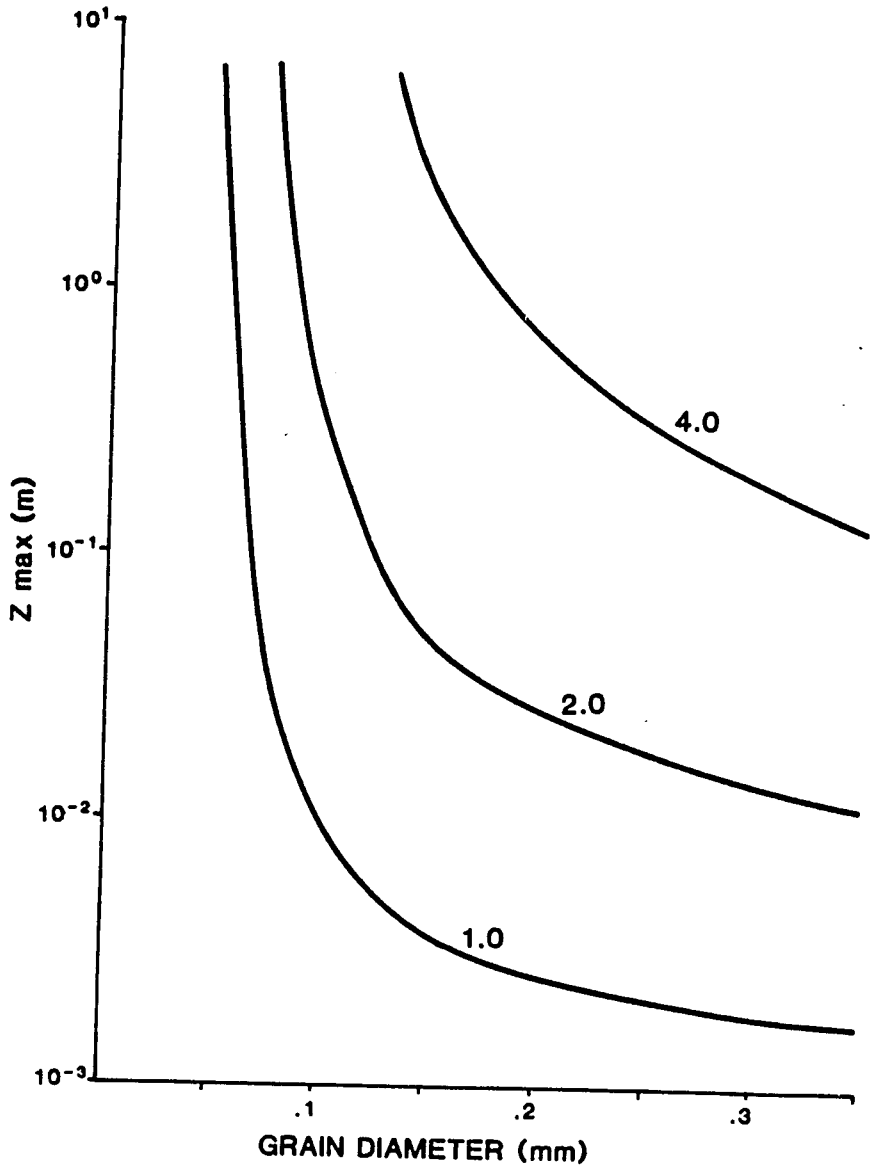

Figure 4.7. Height of the kinetic energy maximum, z_{max}, expected from suspension as a function of grain size and shear velocity, u_* (labels in m/s).

where τ_b is the shear stress at the bed, and τ_{ci} and τ_{cf} are, respectively, the impact and fluid threshold shear stresses (Bagnold,1941) necessary to entrain particles of size class n. Values of γ from first order eolian transport modelling (Anderson and Hallet, 1986) are 2.2×10^{-8}, and 1.7×10^{-7}, for impact and fluid forms of the excess shear stress, respectively, with $z_a = .04m$.

The relative strengths of the kinetic energy maxima are plotted in figure 4.8, for both forms of the excess shear stress, using again the reference case with $u_* = 1.0$m/s, and log-normal grain size distribution with $\bar{D} = .25$mm and a standard deviation $\sigma = .6\phi$, representing a moderately well sorted sand. Independent of the form of excess shear stress chosen, particles smaller than approximately .1mm (very fine sand) are responsible for the strongest kinetic energy maxima due to suspension. Combining these results with those for the grain size dependence of the heights of kinetic energy maxima, presented in figure 4.7, we expect that erosion due to suspended grains should peak meters off the ground during major wind storms characterized by shear velocities of 1-4m/s (corresponding to wind speeds of 11-64m/s 10m above the ground).

4.3 DEFLECTION OF PARTICLE PATHS: COLLECTION EFFICIENCY

Thus far we have neglected the deflection of both air and particle paths by the obstacle. In general, we might expect small suspended particles to be deflected more than large particles, thereby reducing their relative importance in the kinetic energy fluxes analyzed in the previous section. This should effectively reduce the calculated height of maximum erosion due to suspended particles. We develop in this section a simple model of particle paths around a vertical cylindrical obstacle, approximating the air streamlines by those predicted from inviscid flow theory. Both the separation expected at the lee of the obstacle, and the boundary layer of some finite thickness on the upwind side are neglected. The latter will be very thin owing to the presence of the favorable pressure gradient imposed by the obstacle, and hence should not

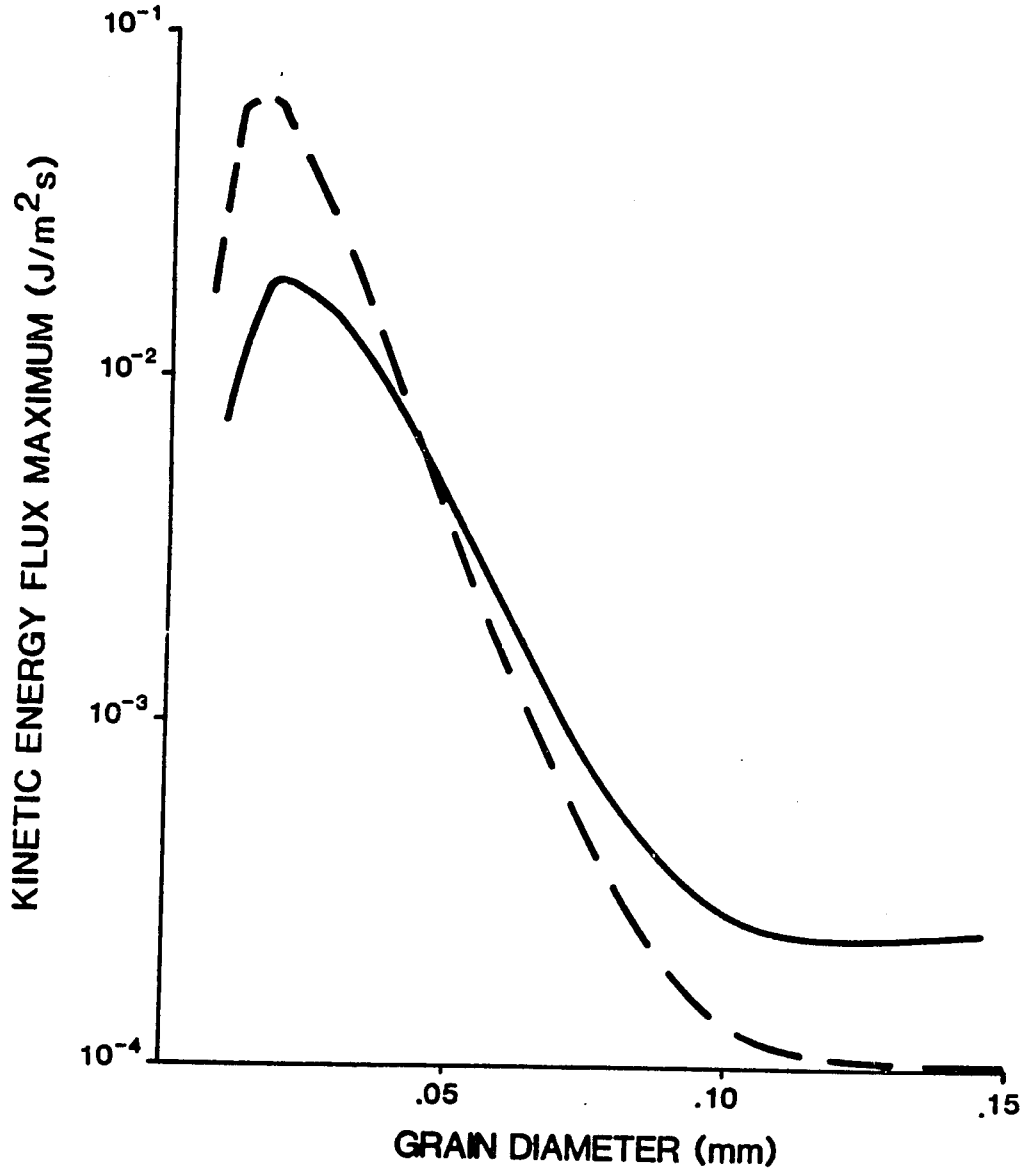

Figure 4.8. Maximum kinetic energy flux expected from suspension of different grain sizes, for u_*=1.0m/s, and a grain size distribution characterized by $\overline{D}$=.25mm, σ=.6ϕ. Only grains <.15mm (settling velocity = 1.0m/s=u_*) are considered suspended. Two forms of the reference concentrations are shown: impact form of excess shear stress (dashed), using γ=2.2x10^{-8}; and fluid form of the excess shear stress (solid), using γ=1.7x10^{-7}. Note logarithmic scale.

strongly affect the particle paths.

From inviscid flow theory (e.g., Morsi and Alexander,1972) the stream function is:

$$\psi = Uy - \frac{Ua^2y}{(x^2+y^2)} \tag{4.14}$$

where U is the free stream velocity at some height z in the flow, y is the horizontal distance perpendicular to the mean flow direction, and x is the distance downwind from the center of the vertical cylinder of radius a (see definition sketch, figure 4.9). The downwind and crosswind air velocity components may then be written, respectively:

$$u = \frac{\partial\psi}{\partial y} = U(1-\frac{a^2(y^2-x^2)}{(x^2+y^2)^2}) \tag{4.15}$$

and

$$v = -\frac{\partial\psi}{\partial x} = -2Ua^2(\frac{xy}{(x^2+y^2)^2}) \tag{4.16}$$

Given this wind field and a particle of diameter D and density ρ_p, its path may be calculated for any intitial position and speed. Morsi and Alexander (1972, p.198) show that "lift" forces due to shear in the flow may be neglected for a wide range of particle sizes and densities, leaving only the drag force to deflect particles. The equations of motion in both x and y directions may be written:

$$\frac{du_p}{dt} = \frac{1}{2}\rho_a C_d \frac{A_p}{M_p} \mid U_{rel} \mid (u-u_p) \tag{4.17}$$

and

$$\frac{dv_p}{dt} = \frac{1}{2}\rho_a C_d \frac{A_p}{M_p} \mid U_{rel} \mid (v-v_p) \tag{4.18}$$

where A_p and M_p are the cross sectional area and mass of the particle, respectively, $\mid U_{rel} \mid = \sqrt{(u-u_p)^2+(v-v_p)^2}$, and the drag coefficient C_d is a well known function of the particle Reynolds number, $Re = \frac{\mid U_{rel} \mid D}{\nu}$, as tabulated in Morsi and Alexander (1972) for spherical grains. Suspended particles are assumed to be travelling at the free stream velocity as their initial condition.

Numerical integration of particle paths is carried out using simple forward time stepping, with instantaneous drag coefficient, particle acceleration, velocity and position calculated at each step. Representative particle paths are shown in figure 4.9 for two grain sizes and a free stream velocity representative of the winds recorded in the December 1977 San Joaquin dust storm. The 41m/s velocity corresponds to that expected at a 1.0m height, during a wind regime characterized by u_*=4.0m/s, corresponding to an amemometer reading at 4m of approximately 200km/hr (Wilshire and others,1981). The collection efficiency, E_c, is defined (Langmuir and Blodgett,1946) as the ratio of the number of particles that actually impact an obstacle surface with the number that would pass the cross section in the absence of the obstacle. This may be expressed simply as the ratio of linear measures B and a, shown in figure 4.9, such that $E_c = B/a$ (Stallabrass and Hearty,1967). In figure 4.10 the collection efficiency is presented as a function of D for these two free stream velocities.

In an early study of ice riming, Langmuir and Blodgett(1946) proposed the expression of E_c in terms of a non-dimensional "inertia parameter", K, defined as

$$K = \frac{\rho_p D^2 U}{18 \rho_a \nu a} \tag{4.19}$$

It conveniently expresses the ratio of the response time of a particle to changes in wind velocity, $\tau_D = \frac{\rho_p D^2}{18 \rho_a \nu}$, with a characteristic time arising from the flow geometry, $\tau_c = \frac{a}{U}$. As K becomes large, a particle cannot react in time to deflect appreciably from its path, while at some sufficiently small K ($<1/8$, Langmuir and Blodgett, 1946), the collection efficiency effectively vanishes. For quartz particles entrained in air and impinging on a cylindrical obstacle with radius .05m in a free stream velocity of 41m/s, this corresponds to grain diameters of 4.4μm (see figure 4.10). Particles smaller than .025mm deliver only half of their available kinetic energy to the surface of the obstacle at the 1m height. The collection efficiency for a particular particle size varies with height, with relatively low efficiencies very near the bed, where the characteristic time available to deviate around the obstacle, τ_c, increases, while the particle response time, τ_D, remains constant.

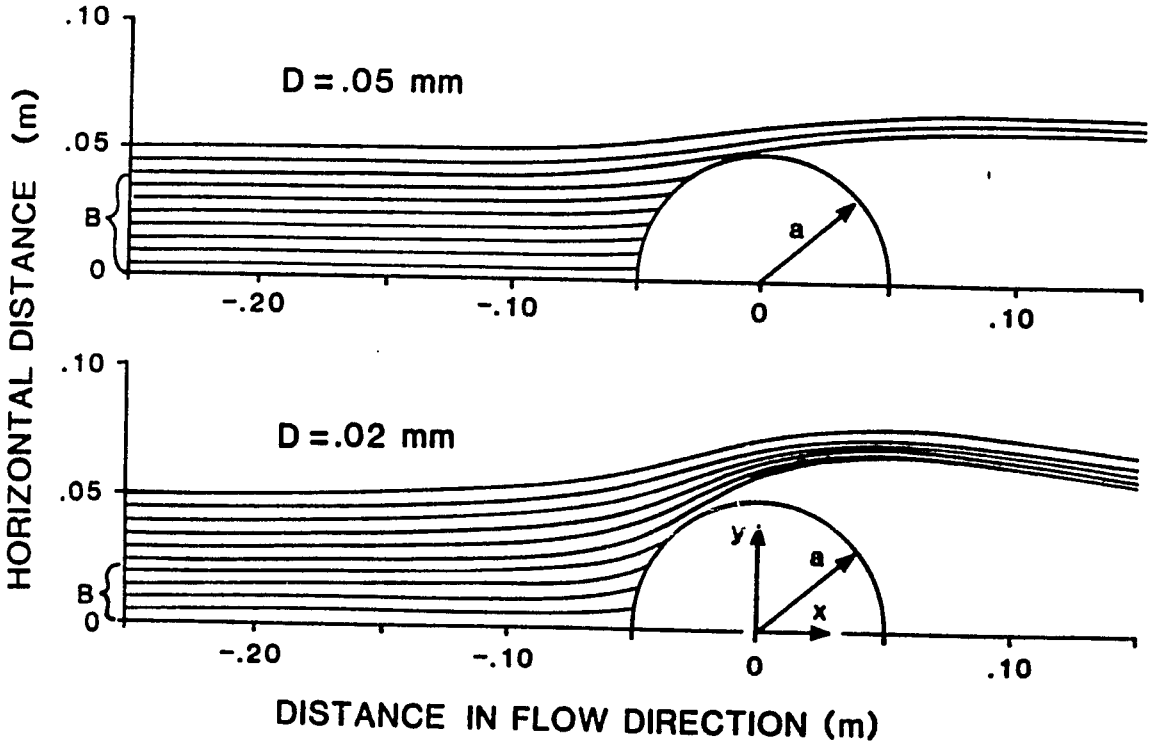

Figure 4.9. View from above of representative paths of two particle sizes around a 0.05m radius vertical cylindrical obstacle, with a 41m/s free stream velocity, representing wind speeds at 1.0m in a wind storm characterized by $u_* = 4.0$m/s (4m anemometer velocity of 200km/hr). Grain density is that of quartz (2650kg/m^3). Collection efficiency is simply the ratio of lengths B and a.

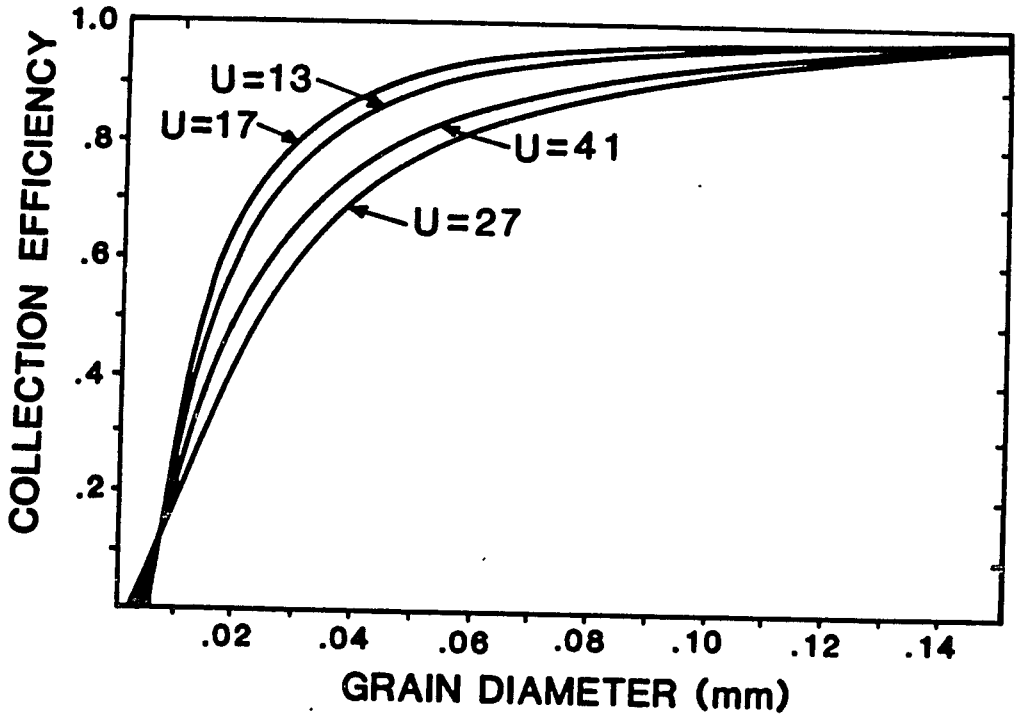

Figure 4.10. Collection efficiency as a function of grain size for 27m/s and 41m/s wind velocities and .05m obstacle radius, corresponding to .25 and 1.0m heights on fenceposts in the San Joaquin dust storm peak winds; and for 13 and 17m/s wind velocities and .015m obstacle radius, corresponding to probable peak winds of the Coachella Valley experiment (Sharp,1980).

Suspension kinetic energy flux profiles, calculated using u_*=4.0m/s, and a grain size distribution as measured by H.Wilshire (personal communication,1985) in 9.3cm auger samples taken near the San Joaquin fenceposts, are shown in figure 4.11, with (solid) and without (dashed) incorporation of collection efficiency . The grain size dependence of the magnitude and height of the maxima is well illustrated. The collection efficiency reduces dramatically the contribution from the finest grain size fraction (D =.031mm) by approximately 50%, whereas it reduces the contribution from the .63mm fraction by roughly 15%; larger fractions are essentially unaffected, in accord with figure 4.10.

4.4 DISCUSSION

It is clear from the analysis of suspension profiles that the structure of the observed erosion profiles, characterized by erosion maxima averaging .2-.3m above the ground, must be dominated by the flux of kinetic energy due to saltating grains. Again using the reported grain size distribution from the auger samples (detailed in the figure 4.11 caption), the sum of the saltation-imposed fluxes of 1,2, and 4mm grains is shown in figure 4.12 (curve A), together with a total flux profile obtained by adding the total suspension profile.

Two difficulties are evident: (1) the calculated erosion maximum, at approximately .1m, is too low for most measured San Joaquin profiles (contrast figures 4.2 and 4.12, curve A); and (2) the profile above the maximum falls off too rapidly, and shows a prominent local minimum not observed in the fencepost profiles. Both of these objections may be resolved if the mean liftoff velocities during saltation were underestimated in the original calculations. It is noted by H.Wilshire (personal communication,1982) that the mean height of truncation of San Joaquin fenceposts immediately downwind of paved roads is significantly higher (.43m; mean of 20 posts) than on those immediately upwind of the same roads (.28m; mean of 29 posts). The expression for the mean liftoff velocity used in our original calculations was based upon wind tunnel experiments in which grain sizes were not greatly dispersed, and

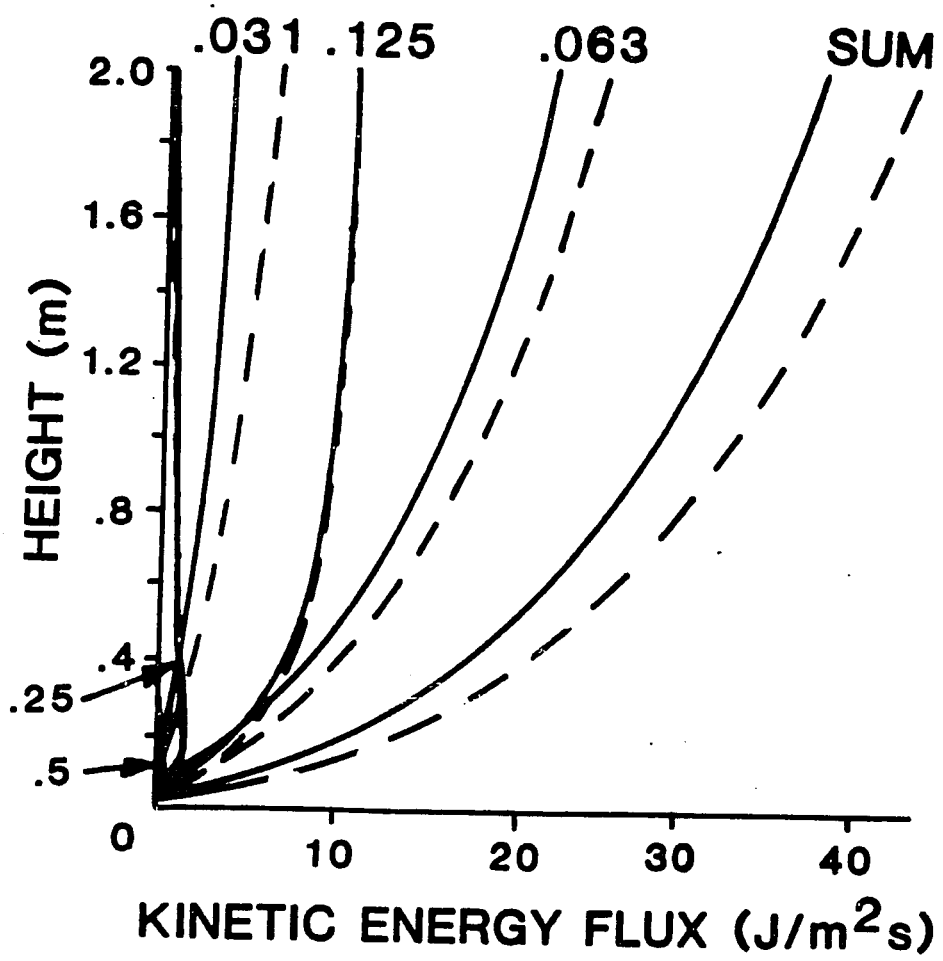

Figure 4.11. Calculated profiles of kinetic energy flux for suspended particles (D <.6mm) during the San Joaquin dust storm, characterized by u_*=4.0m/s, and grain size distribution from 9.3cm auger sample: D=4.0,2.0,1.0,.50,.25,.125,.063,.031 mm composing .26,.28,.19,.12,.08,.05,.015 and .005 percent of the bed, respectively. Curves labelled "SUM" represent the summation of the contributions from all grain size classes in suspension. Dashed curves represent expected fluxes in the absence of collection efficiency corrections; solid curves include collection efficiency.

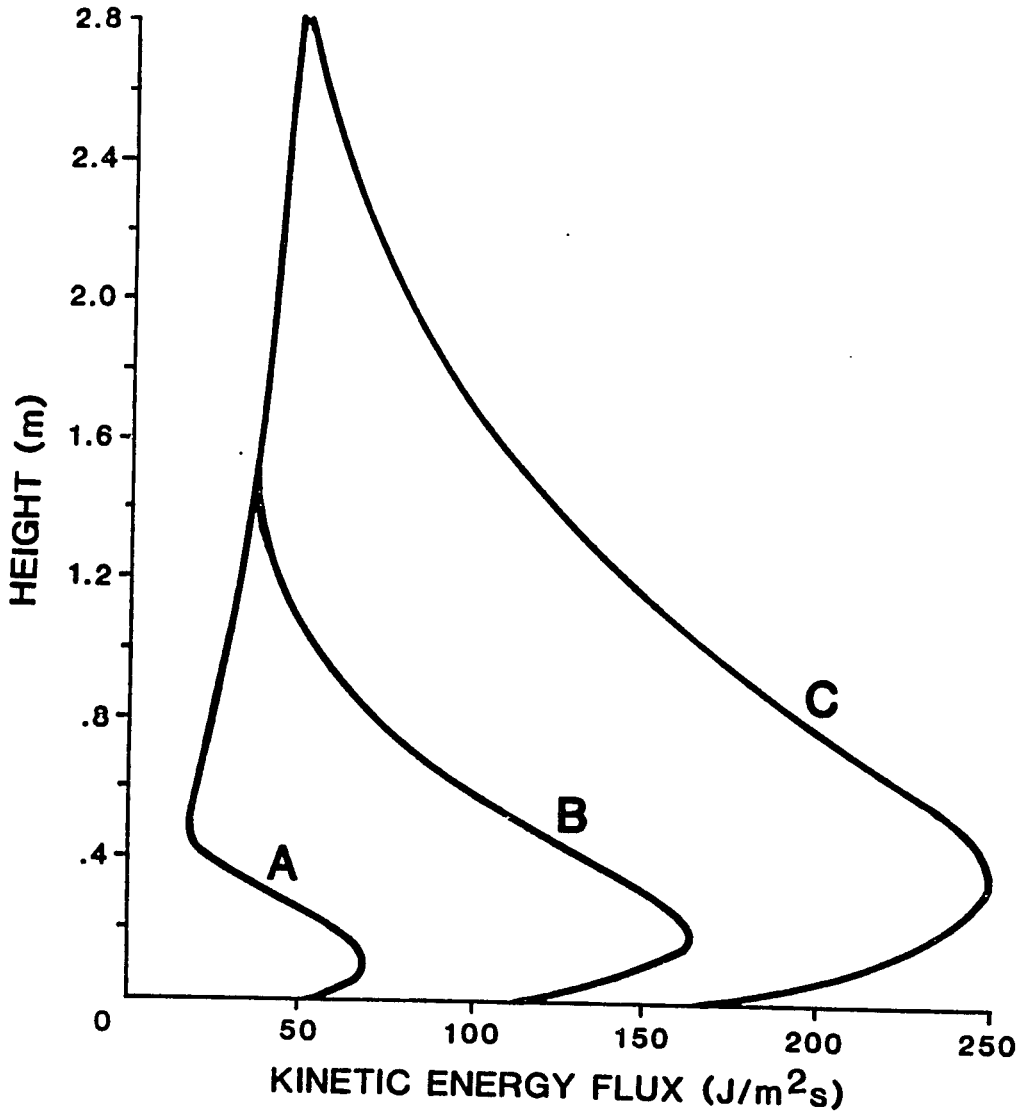

Figure 4.12. Calculated kinetic energy flux profiles for both saltating and suspended particles, for wind velocities and grain size distributions described in figure 4.11. Saltation fluxes are the sum of contributions from largest three fractions; suspension from the five smaller fractions. Curve A: mean saltation liftoff velocities as prescribed in Anderson and Hallet(1986). Note the marked local minimum in the kinetic energy flux above the maximum imposed by saltation. Curves B and C: mean saltation liftoff velocities enhanced two-fold (B) and four-fold (C). Note saltation peaks higher off the ground and the local prominent minimum evident in case A is reduced. In case B the height of the maximum kinetic energy flux and the shape of the profile both compare well with measured fencepost erosion profiles (see figure 4.2).

the entire bed was mobile. For this condition, Anderson and Hallet (1986) have shown numerically that the mean particle ejection velocity must be on the order of 1/4 of the mean impact velocity. If the mean impact is more elastic -- as we might expect from small grains bouncing off very large grains, off relatively well indurated deflationary surfaces, and (in the extreme) off pavement -- the mean liftoff velocity may be enhanced as much as about four-fold. Essentially, this would alter the effective restitution coefficient for grain-bed collisions. Figure 4.12 also shows total kinetic energy flux profiles resulting from incorporation of this effect, with mean liftoff velocities enhanced two- and four-fold.

We advocate the two-fold case as the most realistic for areas upwind of paved surfaces, and the four-fold case for downwind areas. The erosion maxima now correspond better with the observed values, and the shapes now display no prominent mimimum within the 2m profile cut into the fenceposts. The calculated pattern of instantaneous kinetic energy flux now matches remarkably well the pattern of erosion observed in the San Joaquin fence posts [compare figure 4.12 (curves B and C) with figure 4.2].

Suzuki and Takahashi (1981) have also obtained what appear to be reasonable fits to Sharp's lucite rod erosion profiles. Their assumption that all grains travel at approximately the local wind velocity is, however, inappropriate for saltating grains, whose velocity continues to increase throughout the trajectory, and typically obtains only 50-70% of the wind velocity at the top of the hop (Anderson and Hallet,1986). When combined with an assumed exponentially decaying concentration profile, this necessaily gives rise to a maximum of erosion at some height above the bed, as in the suspension analysis presented here. It also requires that the erosion vanish at the bed, where the wind velocity and hence the particle velocity vanish. That saltation plays an important role in cutting at least the lower portion of the erosion profile is evident in that significant erosion occurs very near the bed. This derives ultimately from the large kinetic energy retained by a saltating particle in the last portion of its descent. The present model of erosion due to saltating grains tracks the kinetic energy of the particle through its trajectory, weighs this by the time the particle spends in each height increment of its trajectory to derive the pattern of kinetic energy flux due to that particular trajectory, and then sums over a realistic

distribution of initial trajectory conditions to arrive at an instantaneous profile of kinetic energy flux.

The final erosion profile will reflect the integral over the entire wind record of the kinetic energy flux, but the peak winds will tend to dominate in setting the erosion maximum. The lowering of an obstacle surface, L, expected in a time interval T, will be

$$L = \int_0^T \dot{L} dt = \frac{S_a}{\rho_t} \int_0^T q_{ke}(t) dt \tag{4.20}$$

If the probability density of shear velocities during this interval is represented as $p(u_*)$, this may be rewritten as

$$L = \frac{S_a}{\rho_t} T \int_0^\infty q_{ke}(u_*) p(u_*) du_* \tag{4.21}$$

where S_a is the susceptibility of the obstacle to abrasion, in mass removed per unit kinetic energy supplied, ρ_t is the density of the target material, and $q_{ke}(u_*)$ is the total kinetic energy flux expected from both saltating and suspended grains (with collection efficiency included) for a given grain size distribution and shear velocity. For the case in which the excess shear stress, S, is far greater than unity, but γS is far less than unity (conditions typical of high winds), the reference concentrations scale roughly with the boundary shear stress, or as u_*^2 (see eqn.12), and we may therefore expect the contribution to the kinetic energy flux due to suspension to scale as u_*^5 (see eqn.7). In addition, a series of numerical saltation calculations in which only the shear velocity was allowed to vary indicates the saltation contribution to the kinetic energy flux probably also scales roughly as u_*^5. This implies that erosion profiles will reflect very strongly the instantaneous rate of abrasion occurring during the maximum winds. A wind of one third of the peak shear velocity would have to be maintained for more than 200 times that of the peak wind to produce equivalent erosion. The influence of the peak winds will also vary with height, as the low wind velocities fail to mobilize much material well off the bed. The portion of the abrasion profile above the maximum should therefore fall off relatively smoothly, dominated by the profile cut during the peak winds, whereas that below the maximum will be more strongly influenced by the longer duration and more frequent wind speeds.

4.5 CONCLUSIONS

This analysis of eolian erosion has provided an exacting test of the eolian sediment transport model, and it provides insights into the evolution of ventifact shapes. The saltation model required a more or less ad hoc modification of mean liftoff velocities to accomodate the relatively elastic nature of the bed surface, pointing again to the need to address the grain-bed interaction explicitly (Anderson and Hallet,1986; Ungar and Haff,in press). The sensitivity of the suspension results to the chosen form of the reference level concentrations and to the value of γ is high, though it is encouraging that previous modelling (Anderson and Hallet,1986) gives reasonable relative fluxes of suspended and saltating grains even in these extreme conditions.

As noted by Greeley and Iversen (1985,p.126), "the relative importance of saltating sand versus suspended dust, as agents of erosion, is contentious." The present analysis yields a quantitative assessment of the relative importance of saltation and suspension in performing erosion as a function of wind velocity, height above the bed, grain size distribution of available impactors, and obstacle size.

Although the present analysis has been restricted to instantaneous erosion profiles produced in two-dimensional objects, it also provides a firm basis for making several general statements concerning ventifact formation and morphology. That erosion rates due to both saltation and suspension increase dramatically with wind speed suggests that the net erosion pattern will closely reflect the pattern of instantaneous kinetic energy flux imposed by the highest winds. This reduces greatly the time-dependent nature of the erosion problem, and explains why ventifacted surfaces in any particular locality are so well aligned (e.g. Sharp,1949; Hunter,1979; Lancaster,1984).

Delivery of kinetic energy to small stones ($<$.1-.2m) is due primarily to saltating grains that travel paths essentially unaffected by the presence of the obstacle. In addition, the upper portions of saltation trajectories, representing the greatest flux of kinetic energy (see fig.4a), are well aligned with the direction of the mean wind, independent of the three-dimensional nature of trajectories (Anderson and Haff, in

prep.). The instantaneous rate of erosion of an upwind surface element on a small stone will therefore depend only upon its height above the bed, and the angle α it makes with the mean wind at that height. As the number of impacts per unit area on an upwind surface scales as $\sin(\alpha)$, and the mass removed per impact scales as $(V\sin\alpha)^2$ (eqn.1, with n=2, V_o=0), surfaces normal to the wind will erode much more quickly than oblique surfaces. In the absence of significant spatial variations in susceptibility, S_e, initial surface irregularities should be highly unstable, and the upwind surface of the stone should evolve into a facet normal to the strongest winds. The general upwind dip of this facet, and the common existence of a "ground sill" representing reduced erosion near the bed (Sharp,1964, 1980), in turn reflect the expected decrease in kinetic energy flux in close proximity to the bed.

Erosion of stones or outcrops protruding well above the ground will be increasingly influenced by kinetic energy flux due to suspended grains. Therefore, in addition to imposing a pattern of erosion through the $\sin(\alpha)$ dependence of mass removal, the three-dimensional obstacle geometry affects particle paths and hence impact points. On large stones, the corners separating eroding and non-eroding surfaces will be preferentially attacked by deflected particles. Grooves and flutes (Sharp,1949; Whitney and Dietrich,1973; Whitney,1978,1979; McCauley and others,1979; Lancaster,1984; Greeley and Iversen,1985) occur predominantly around the upwind edges of large obstacles (see figure 4.1), and often occur in divergent sets displaying symmetry about the direction of the peak winds. These reflect the enhanced numbers of impacts of particles small enough to be significantly deflected by the air flow around the obstacle, and to be spun in local vortices. A stability analysis of local surface erosion to small initial irregularities, in combination with numerical modelling of specific test cases, promises to better our understanding of ventifact formation and morphology.

CHAPTER 5

A THEORETICAL MODEL FOR EOLIAN IMPACT RIPPLES

Eolian ripples form some of the most regular and esthetically pleasing patterns in nature, and figure importantly in the interpretation of eolian sandstones (e.g. Hunter, 1977; Koceruk, 1981). Despite their ubiquity in present-day deserts and coastal regions, as well as in the geological record, no general theory exists for the complex interactions of wind and sand responsible for the formation of this smallest class of eolian bedforms.

The study of eolian ripples has been largely guided by Bagnold's seminal work of the 1930's (Bagnold, 1941), wherein he stressed the causal connection between ripple spacing and a "characteristic path length" in saltation. This connection was supported by several subsequent studies (Ellwood and others, 1975; Wilson, 1972). However, it has been challenged, most notably by Sharp (1963), and Warren (1983) emphasized that considerable evidence negates Bagnold's concept of ripple formation. Nonetheless, no general and analytically rigorous model has appeared to aid in assessing the relative importance of the various processes that contribute to the phenomenon. Recent theoretical and experimental work on eolian saltation (Rumple, 1985; Mitha and others, 1985; Anderson and Hallet, 1986; Ungar and Haff, 1986) provides the foundation for such a framework. When combined with recent formalism developed for analyzing the stability of fluvial granular beds (e.g., Kennedy, 1964; Smith, 1970; Smith and McLean, 1977; Engelund and Fredsoe, 1982; Richards, 1984; McLean and Smith, 1986), a simplified model of the saltation process, which includes the essense of the grain-bed interaction, yields a reasonable picture of the initial formation of eolian ripples. Following a brief review of the ripple literature, we present first a qualitative description of the eolian saltation process, emphasizing recent experimental work on grain-bed impacts that motivates clarifying definitions of successive saltation, reptation, and creep. The resulting picture of the grain-bed system is then simplified by making several important assumptions, in order to make the stability analysis tractable. After presentation of the results, implications of these assumptions are briefly discussed, and directions for further research are suggested.

5.1 LITERATURE REVIEW

Bagnold (1941) introduced the image of a rhythmic barrage of grains from one ripple to another, creating alternating zones of high and low impact intensity and, hence, of imposed motion of surface grains. He pointed to a close correspondence between his calculated saltation path lengths and observed ripple wavelengths. This correspondence, based upon very rough calculations of trajectories whose heights were forced to match the height of the observed "kink" in the wind velocity profile, has dominated the literature for four decades. The coupling between saltation impacts and surface grain motion, and the relative importance of these two particle populations in ripple translation were discussed only qualitatively.

Wilson (1972), and Ellwood and others (1975) extended Bagnold's model to treat poorly sorted or bimodal sands. Using an experimentally determined "rebound probability matrix", they proposed that the entire range of observed ripple wavelengths corresponds to the range of mean hop lengths of one size fraction off another. Again, no explicit model of saltation-imposed surface motion of grains was proposed. The image of a rhythmic barrage of saltating grains was retained.

Sharp's (1963) work stands alone in clear dissent. He argued that because ripples begin as small amplitude, short wavelength forms, and grow to their ultimate steady state dimensions, Bagnold's concept is at least suspect. Sharp argued qualitatively, on geometrical grounds, that ripple wavelength should depend on ripple amplitude and on the angle at which saltating grains approach the bed, both of which are controlled by air velocity and particle size. Later experimental work of Seppala and Linde (1978) empirically quantifies Sharp's initial observations of the evolution of ripple dimensions.

Walker's (1981) careful experiments, and his extensive review of the eolian ripple literature pointed to serious difficulties in simply relating ripple wavelength to a "characteristic path length". A well-defined "kink" in the wind velocity profile during saltation, upon which Bagnold based his trajectory calculations, was not observed. A clear empirical relation was demonstrated between flow velocity at a

given height above the bed, grain size, and ripple wavelength, height and index; however, in agreement with Sharp, Walker argued that no recourse need be made to characteristic path lengths.

5.2 THE ROLE OF IMPACTS -- A CONCEPTUAL MODEL OF EOLIAN SALTATION

Stability analyses of perturbed subaqueous granular beds all begin by assuming that the pattern of sediment flux is governed entirely by the pattern of fluid shear stress imposed by the topography of the bed (e.g. Kennedy, 1964; Smith, 1970; Engelund, 1970; Jain and Kennedy, 1974; Smith and McLean, 1977; Engelund and Fredsoe, 1982; Richards, 1984). The view adopted here contrasts with these studies of aqueous ripples, but conforms in general with that of previous eolian studies (Bagnold, 1941; Sharp, 1963): the motion of grains in eolian ripples is viewed as resulting not directly from shear stress imposed by the air, but rather from the impacts of long-trajectory saltating particles that are themselves accelerated by the wind. As air is a low viscosity, low density fluid, its ability to lift grains off the bed is quite poor. For the same reason it does little to reduce the velocities of high density grains about to impact the bed. Although eolian saltation must be initiated by aerodynamic forces, it is the impacts of saltating grains that appear responsible for most of the mass flux in steady state saltation (e.g. Rumple, 1985; Ungar and Haff, 1986).

5.2a IMPACT EXPERIMENTS

In order to quantify the effect of a single impact, and to scale properly their laboratory experiments on impact dynamics, Mitha and coworkers (1985) define an "impact number", N_{ke}, to be the ratio of the kinetic energy of an impacting grain with the energy necessary to raise a similar grain out of its pocket against the force

of gravity. Extending their treatment to allow for differences in diameter between the impacting and bed grain diameters, D_{im}, and D, respectively, the impact number becomes

$$N_{ke} = (\frac{D_{im}}{D})^3 \frac{V_{im}^2}{gD} \tag{5.1}$$

where V_{im} is the speed of the impacting grain. Note the extreme sensitivity of the impact number to diameter of the bed particles. For typical sediment transport conditions ($u_* = .5$m/s, and $D = .25$mm), impact velocities of typical trajectories are of the order 1-5m/s (Anderson and Hallet, 1986), yielding, for $\frac{D_{im}}{D} = 1$, $N_{ke} = 400\text{-}2000$. Clearly, even if only a small fraction of the impact energy is made available for ejection of other grains from the bed, such impacts are a major source of energy for maintaining a large population of small trajectory grains.

Recent physical and numerical experiments help clarify the response of a granular bed to such pointwise inputs of energy. The only major set of measurements of the dynamics of single grain impacts into a granular material composed of similar grains is that produced by Haff and coworkers (Mitha and others, 1985), who used 4mm diameter spherical steel pellets in order to make the grain-bed interactions more visible. Figure 5.1 represents a typical impact of a single pellet into a bed of similar pellets, recorded with a double strobe system (from Mitha and others, 1985, figure 1). A high energy impact characteristically gives rise to two distinct groups of trajectories: (1) a single high-energy trajectory, usually the impacting grain itself, reflected quasi-specularly off the bed, and (2) a set of O(1-10) low energy recoils with ejection speeds an order of magnitude lower than the impacting grain. The high energy recoils represent on average almost 60 percent of the impact energy (Mitha and others, 1985, table 2). The average ejection angle for these high energy grains is significantly greater than the impact angle, meaning that a relatively large fraction of the impact velocity has been redirected upward by the bed collision. The low energy ejecta emerge shortly after the impact from a region roughly 10 grain diameters across centered slightly ahead of the impact site. The average ejection angle for low energy ejecta seems also to be significantly higher than the impact angle, and is typically inclined "downwind". A plot of the distribution of the ejection speeds for a specific

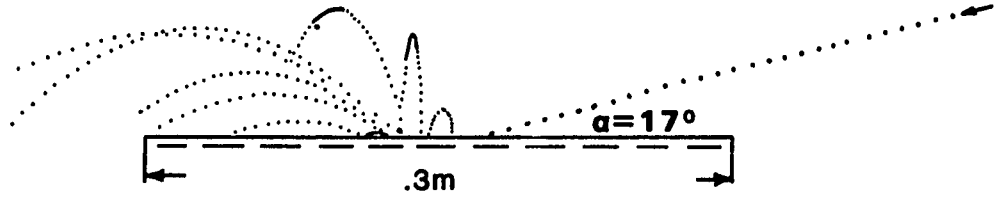

Figure 5.1. High energy impact of a single 4mm diameter steel pellet into a bed of identical pellets (after Mitha and others, 1986, figure 1). Impacting grain travelling from right at 21 m/s, 17 degrees from horizontal is shown at successive instants with high speed strobe. The high energy ejection, probably the same pellet, leaves to the upper left. Nine low energy ejections are shown at successive instants by a lower speed strobe. The edge of the .3m wide tray containing the pellets hides the actual level of the bed (approximated by dashed line).

set of impact conditions is shown in figure 5.2; the mean ejection speed is over an order of magnitude smaller than the impact speed; hence even ten such ejections represent only a few percent of the original kinetic energy. The remaining energy must therefore induce local dilation and subsequent rearrangements of grains in the bed, and must eventually be dissipated as frictional heat.

Mitha and others (1986, p.9) report no significant correlation between the mean ejection speed and either the impact angle or the impact speed over the ranges of angles (17-31 degrees) and speeds (20-25 m/s) measured in the steel pellet experiments. Numerical simulation using the concurrent processor (Werner and Haff, 1985; 1986) sheds further light on the grain impact process. They show (Werner and Haff, 1985, tables 3,4) that the kinetic energy of the ejected low energy recoils increases strongly with impact energy, and that the ejected kinetic energy increases monotonically with increasing angle of incidence.

5.2b MODEL OF EOLIAN SALTATION

The impact experiments described above, and earlier numerical work on eolian saltation (esp. Anderson and Hallet, 1986; Ungar and Haff, 1986), lead to the following conceptual model of eolian saltation, an idealization of which forms the basis for the ripple analysis to follow. Saltation transport is initiated by fluid lift and drag forces, resulting in relatively short trajectories that impact the bed after having been accelerated by the wind to several times their initial velocities. The kinetic energy of each impact can be distributed among (1) rebound of the original grain from the bed, or "successive saltation" [after the usage of Tsuchiya, 1972; Reizes, 1974; and Rumple, 1985], (2) ejection of a number of other grains from the bed, which then comprise the small trajectory, or "reptating" population [after Ungar and Haff, 1986; Mitha and others, 1986], and (3) dissipation by frictional rearrangement of bed grains. We define the resultant of the many small displacements within the bed to be "creep", a term used very loosely in the past. For instance, Greeley and Iversen (1985, p.293) define creep to be " slow, forward motion of grains that are too large to be lifted by

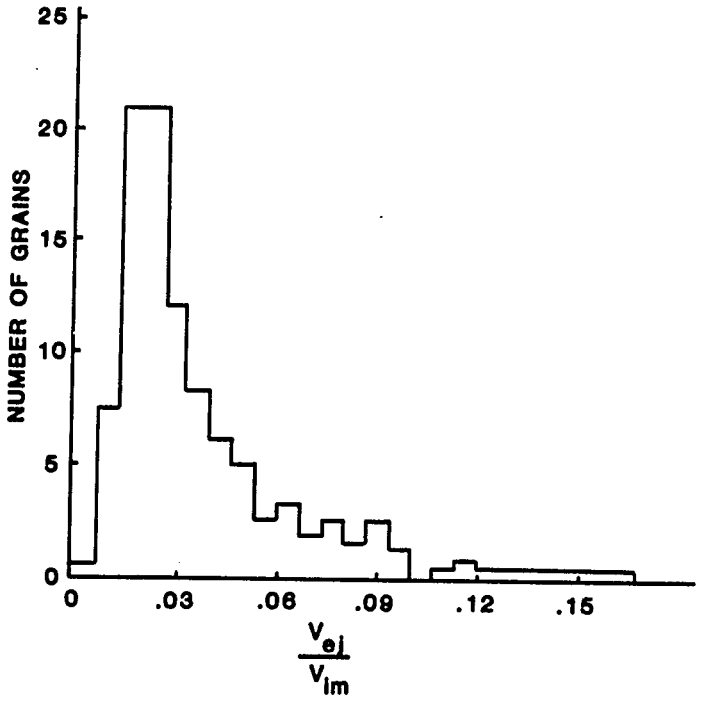

Figure 5.2. Distribution of low energy ejection speeds resulting from many identical impacts, normalized with the impact speed, for 17 degree, 21m/s impacts of 4mm steel pellets with a bed of similar pellets (after Mitha and others, 1986, table 2). Note that the mean ejection speed is on the order of 3 percent of the impact speed.

the wind, whose motion is produced by impact from saltating grains." They do not distinguish between those grains actually induced to hop (our reptation), and those merely rearranged within the bed (our creep).

The result of any individual impact cannot be known exactly, owing to the local microtopography and packing of the bed surface, meaning that the description of the grain-bed interaction can be formulated only statistically. This is the essense of Ungar and Haff's (1986) "splash function", that returns the number of ejections and the probability distribution of their ejection velocities for a given input distribution of impact velocities.

Because the wind accelerates grains to several times their initial velocities, and because higher energy impacting grains both retain a larger fraction of their energy upon impact, and are more efficient at imparting energy to low energy ejecta, the initial, aerodynamically generated set of trajectories leads easily to a chain reaction. Increasing numbers of grains are mobilized in saltation with a broader distribution of ejection velocities through time. The largest fraction of this saltating population will be the low velocity or reptating grains.

The grain-bed-wind system reaches a steady state only when there is no longer change in the number and velocity distribution of the ejected grains. It is presently thought that this is made possible primarily by the reduction of near-bed wind velocities due to the acceleration of saltating grains (negative feedback) [Ungar and Haff, 1986; Anderson, 1986b], reflecting the image of the self-regulatory nature of the saltation process first envisioned by Owen (1964).

The following biological analogy is fruitful in that it provides an appropriate terminology. First generation trajectories, which we here call repatation, can originate by either aerodynamic or ballistic forces. Upon impact many of these first generation trajectories "die": due to the inelasticity of the bed, the relatively low impact velocity, and/or to an unfavorable local microtopography of the bed; they neither reproduce themselves, nor give "birth" to other trajectories. Those few grains that do rebound tend to have higher ejection velocities at each successive saltation -- they "age". After many generations, a stable population is achieved that may best be characterized by the probability distribution of its hop lengths, hop

heights, liftoff or impact velocities, analogous to the age distribution in a biological population. Anderson and Hallet (1986) show that plausible probability distributions of liftoff velocities are exponential, the lowest ejection velocities being the most probable. Such a bottom-heavy distribution is comparable to the age structure in a biological population with high birth rate and low survival rate (e.g., Krebs, 1978). The following generalizations appear justified: (1) high impact velocity trajectories have a low but finite probability of death, and a high "fecundity" at each impact, whereas low impact velocity trajectories have a high probability of death; and (2) low energy grains that make several subsequent rebounds are necessary to replace the small fraction of high velocity grains that do die in any generation, thereby maintaining a stable probability distribution of trajectories. Ungar and Haff's splash function is closely analogous to the transition matrix, or life tables used in the life sciences to calculate the evolution of the age structure within a biological population (Keyfitz, 1970; Krebs, 1978, ch.4-5; Vandermeer, 1981, ch.2). To complete the analogy, the momentum of the wind acts as the "limiting resource" that ultimately controls the size of the steady state saltating population.

In the eolian ripple analysis to follow, we idealize this broad steady-state saltating population as being comprised of its two end-members: the high energy successive saltations, and the low energy reptations. In essense this assumes that the successive saltation population has *zero* probability of death (it reproduces itself perfectly), whereas the reptations have exactly *unit* probability of death upon impact. Note that true creep is ignored in the present model.

Further assumptions may be made to simplify the analysis. Earlier modelling of eolian saltation (Anderson and Hallet, 1986) has shown that the saltation impact velocity at a constant wind speed rises monotonically with increasing ejection velocity, and that the impact angle of all but the shortest trajectories is essentially constant. This implies that high impact velocity trajectories, comprising a relatively small portion of the population, supply most of the energy available for ejecting surface grains in a narrow angular band. A set of saltation trajectory calculations for a single combination of shear velocity and grain size was performed to demonstrate these relationships. The product of the impact kinetic energy with the probability density of each trajectory is presented in figure 5.3. Ignoring any dependence of the

number of ejections or of their velocities on the impact energy, this product reflects the importance of each trajectory class in ejecting grains from the bed. There exists a distinct maximum in this product, representing the trajectories most effective in delivering energy to the bed, and hence in driving reptation. Figure 5.3 also demonstrates that these high energy trajectories represent a broad distribution of hop lengths, which tend to be considerably longer (many decimeters) than the .05 m wavelengths characteristic of the existing ripple field. Moreover, the associated range of impact angles is very narrow. These considerations motivate the simplifying assumptions that (1) all saltating grains descend at an identical angle, and that (2) the spatial distribution of their impacts on a horizontal surface would be uniform. No "rhythmic barrage" of saltating grains is inferred.

The low numbers of high energy grains, and the low probability that they are incorporated into the ripple surface, allows us to ignore their *direct* contribution to ripple transport. Rather, their role in ripple formation and translation is here idealized as merely an energy supply for initiating and maintaining reptation. Because the angle of descent of these high-energy trajectories is so well collimated, the spatial variations in energy available for initiating creep are imposed solely by the local surface topography, the steeper the inclination toward the "beam" of impacting grains, the greater the number of impacts per unit area of bed.

5.3 RIPPLE MODEL

We assume a two-dimensional flow of air over a granular bed. From continuity of material in the bed, the relation between the change of height of bed elevation and the divergence of sediment flux, otherwise called the "erosion equation", is

$$\frac{\partial z}{\partial t} = -\frac{1}{\rho_b}\left(\frac{\partial Q}{\partial x} + \frac{\rho_p \partial V_s}{\partial t}\right) \tag{5.2}$$

where z is the local elevation of the bed, referenced to some arbitrary datum, x is the horizontal coordinate parallel to the wind direction, Q is the local horizontal flux of sediment per unit width of flow, ρ_b is the bulk density of the sediment in the bed

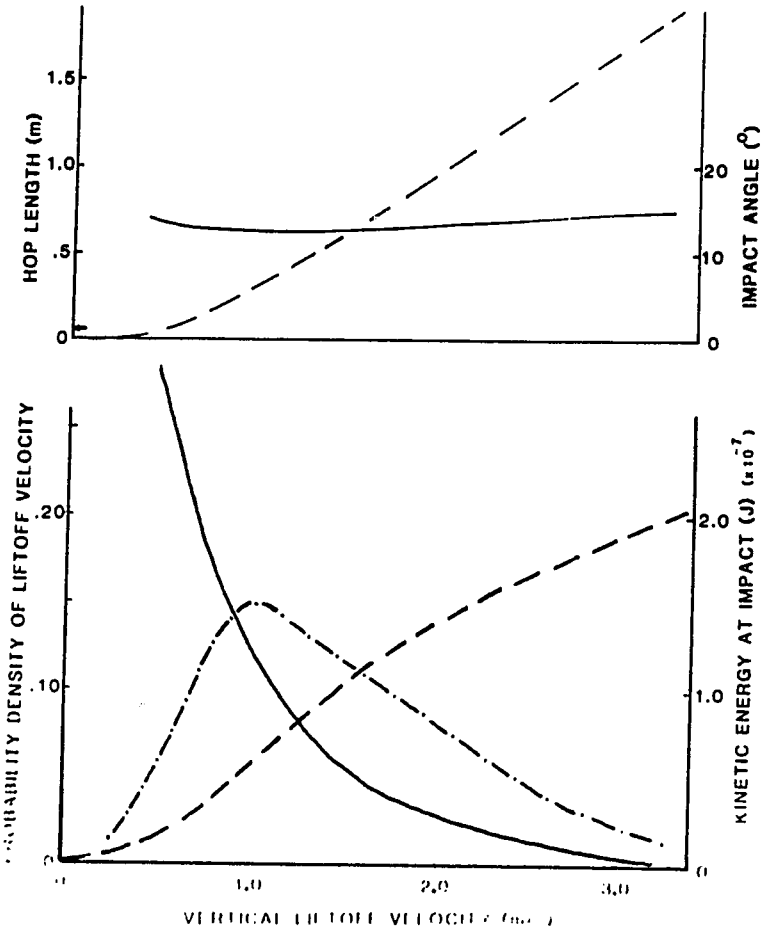

Figure 5.3. Probability distribution of vertical liftoff velocity (solid line, lower figure), kinetic energy of impact (dashed line, lower figure), impact angle (solid line, upper figure), and hop length (dashed line, upper figure) as functions of vertical liftoff velocity for $u_* = .42$m/s, $D = .25$mm (Walker, 1981, run number 47). The product of impact kinetic energy with probability density of each trajectory is plotted on the lower figure (dash-dot line). The most-effective trajectories in delivering kinetic energy to the bed (at the peak of the dash-dot line) correspond to hop lengths of $\approx .3$m, much longer than the mean ripple length reported by Walker for this run ($\approx .05$m, marked with arrow).

(for air, the air density is so small that $\rho_b \approx \rho_p(1-\eta)$, with ρ_p the particle density, and η the porosity of the bed, generally taken to be 0.35), and V_s is the total volume of sediment in transport per unit area of bed. In the following we will ignore time rate of change in sediment transport conditions; neither net deposition nor net erosion of the bed through time is permitted. The fastest rise in the bed elevation will be associated with the greatest downwind decline in sediment flux; conversely, the greatest rate of erosion will coincide with the greatest downwind rate of increase of sediment flux.

We assume a translating sinusoidal perturbation on an otherwise flat granular bed (see figure 5.4):

$$z = z_o e^{ik(x-ct)} \tag{5.3}$$

where z_o is the initial amplitude of the bedform (half the height from the trough to the crest of the form). Taking the phase speed, c, to be complex, $c = c_r + ic_i$, yields the following equation for the bed elevation, with the growth or decay in amplitude now made explicit:

$$z = z_o e^{kc_i t} e^{ik(x-c_r t)} \tag{5.4}$$

Note that $c_r > 0$ now indicates forward translation of the bedform, while the imaginary part of the phase speed determines the growth or decay of the amplitude: $c_i > 0$ implies growth; $c_i < 0$ implies decay; only if $c_i = 0$ is the form unchanging under translation. The results of the stability analysis will be in the form of expressions for the rates of growth and translation speeds as functions of wavenumber.

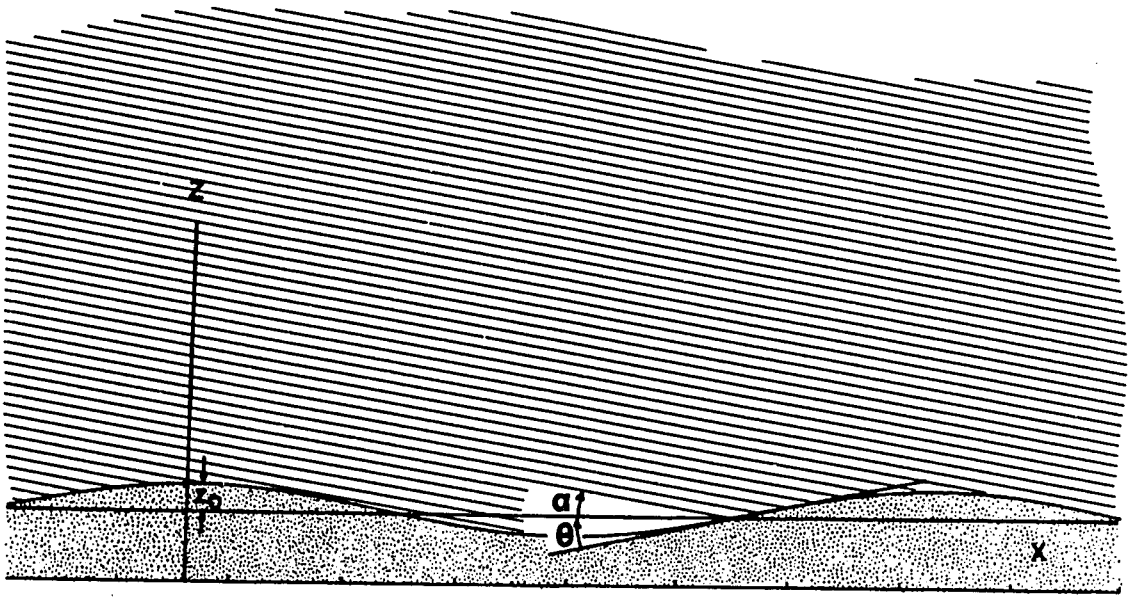

Figure 5.4. Schematic diagram for the bed topography and impacting saltating curtain. The angle α between the descending saltation "beam" and the horizontal is taken positive. The angle θ between the bed slope and the horizontal is positive on the stoss sides of bed perturbations, and negative in the lee.

5.4 IMPACT DRIVEN SEDIMENT TRANSPORT RELATION

In this section we seek an expression for the local mass transport of sediment per unit width of flow, and its dependence on position on the waveform. As the simplest possible case, each grain ejected from the bed is assumed to hop a length, a, with unit probability. Assuming steady sediment transport conditions, the mass flux per unit width across the plane perpendicular to the flow is then (see figure 5.5):

$$Q(x) = \int_{x-a}^{x} m_p N_{ej}(x)dx + Q_s \tag{5.5}$$

where m_p is the particle mass, N_{ej} is the number of particles ejected per unit area of bed per unit time (the "ejection rate"), evaluated at a specific position on the bed, and Q_s is the saltation flux due to the long-trajectory grains, assumed independent of position. The ejection rate is taken to be directly proportional to the impact rate of high energy grains. In this simplest case, each impacting grain is assumed to produce n_1 low energy trajectories; implicitly, this assumes that the ejection efficiency of an impact is independent of impact angle. We may then rewrite the flux relation as

$$Q(x) = m_p n_1 \int_{x-a}^{x} N_{im}(x)dx + Q_s \tag{5.6}$$

where m_p is the mass of an individual grain, and N_{im} is the local areal density of impacts on the bed, or the "impact rate". As stated previously, the impact rate is a function of position because the bedslope determines the effective cross section of the descending particle "beam" that will be intercepted. Simple geometric considerations lead to the relation

$$\frac{N_{im}}{(N_{im})_o} = [1+\frac{\tan\theta}{\tan\alpha}]\cos\theta \tag{5.7}$$

where θ is the angle the bed makes with the horizontal (defined such that $\theta>0$ where the bed dips upwind) and α is the incident angle of the impacting grains (defined such that $\alpha>0$ when the descent is inclined downwind, in the +x direction) [see figure 5.4], and $(N_{im})_o$ is the impact rate on a flat ($\theta=0$) surface. For small bed slopes, $\cos\theta\approx1$, and we may write

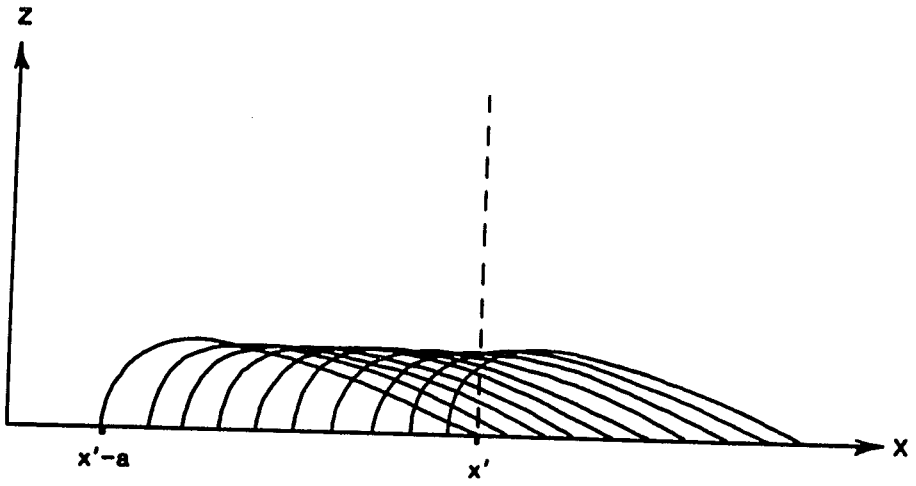

Figure 5.5. Two-dimensional schematic diagram of reptation flux. High energy saltating grains are not shown, but give rise to these low energy ejections, here assumed to follow identical reptation trajectories. Horizontal flux across a plane perpendicular to the wind direction is seen to be dependent upon the ejection rate per unit area of bed, and the hop length, a. In this simple case, no contribution to the flux occurs from portions of the bed beyond a distance a upwind of the plane perpendicular to the flow at x'. The reptation length in turn reflects the ejection speed and the wind velocity profile.

$$N_{im}(x) = (N_{im})_o \ [1+cot\,\alpha\frac{\partial z}{\partial x}] \tag{5.8}$$

The expression in brackets is identical to Bagnold's (1941, p.147-148) "surface component of impact intensity". Equations 5.7 and 5.8 are plotted in figure 5.6 for a typical wind ripple geometry, and for different impact angles. As expected, the impact intensity peaks where the perturbed bed slopes most steeply upwind. For the lower impact angles illustrated, the impact rate vanishes over a significant portion of the lee slope, representing Sharp's (1963) notion of total "shadowing" of the bed. Combining this relation for the impact rate with the previous expression for mass flux allows the sediment flux relation to be written as the sum of a spatially varying quantity, and two mean rates, one associated with reptation, the other with saltation:

$$Q(x) = m_p\, n_1 (N_{im})_o\, cot\,\alpha \int_{x-a}^{x} \frac{\partial z}{\partial x} dx \ + m_p\, n_1 (N_{im})_o\, a \ + Q_s \tag{5.9}$$

Performing the integration, approximating the resulting difference $[z(x) - z(x-a)]$ as a Taylor series, and dropping all terms second order in a and higher, we may write for our final expression for the mass flux

$$Q(x) = Q_o \ + q_{im}\, cot\,\alpha[a\frac{\partial z(x-a)}{\partial x}] \tag{5.10}$$

where

$$Q_o = Q_s + q_{im}\, a$$

and

$$q_{im} = m_p\, n_1 (N_{im})_o$$

is the "mass ejection rate" from a flat bed. Q_o is the total mass flux expected over a flat bed, whereas the integral term in equation 5.9 represents the spatially varying flux involved in transport of ripples. In accord with our simplification of the coupling between saltation and reptation, i.e. that all the saltating grains effectively reproduce themselves by quasi-specular reflection off the bed, and that all reptations land with insufficient energy either to rebound or to eject other grains, an expression similar to that for the flat bed reptation flux, $(=q_{im}\, a)$, may be developed for the saltation flux:

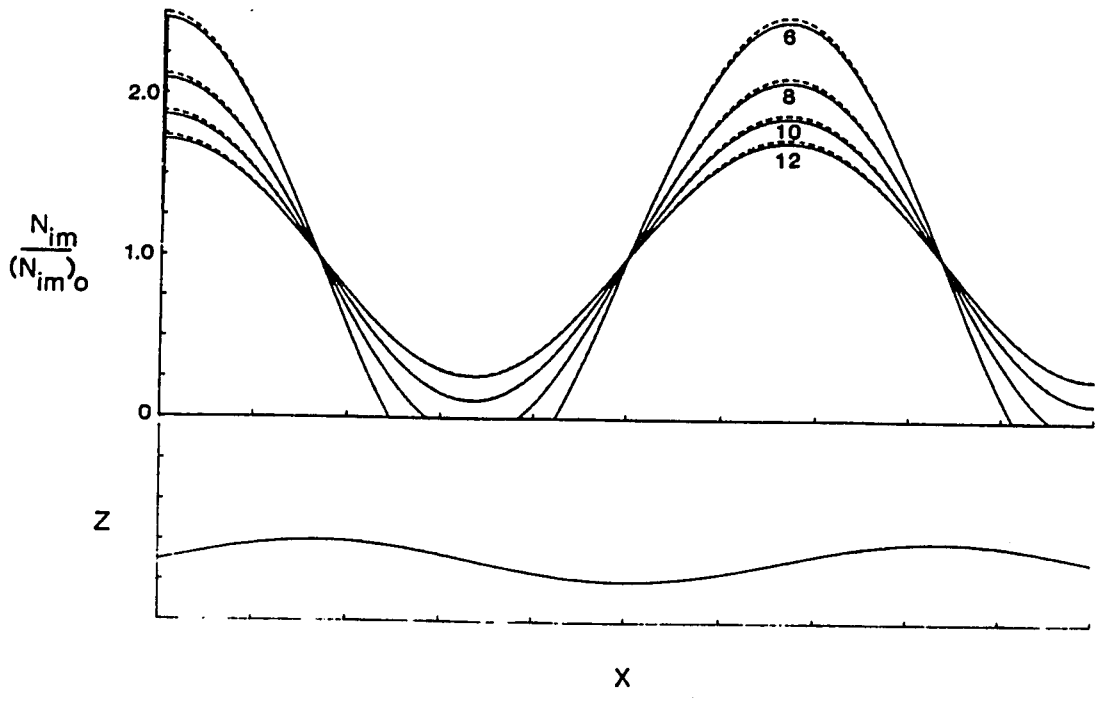

Figure 5.6. Impact intensity, normalized with the impact intensity over a flat bed, shown as a function of position on a typical eolian ripple of 5mm amplitude, .15m wavelength. Cases for four impact angles, α, (labelled) are shown.

$$Q_s = m_p \; n_1 \, (N_{im})_o \; \overline{a_s} \tag{5.11}$$

where n_1=1 represents the perfect self-replication of the successive saltation population, and $\overline{a_s}$ is the mean saltation trajectory length.

5.5 DISPERSION RELATION FOR THE CONSTANT a CASE

Given the physical assumptions and their mathematical expressions above, we now seek expressions for the growth rate and the translation speeds of bed perturbations of various wavelengths. These arise straight-forwardly from inserting the expressions for sediment flux (5.10) and bed elevation (5.3) into the sediment continuity equation (5.2). The complex phase speed, c, becomes:

$$c = \beta \, ka \; [i \; exp \, (-ika)] \tag{5.12}$$

where $\beta = \dfrac{q_{im} \cot \alpha}{\rho_b}$ has the dimensions of a velocity. The real and imaginary parts of the phase speed, corresponding to the translation speed (or "celerity"), and the amplification rate, respectively, are

$$c_r = \beta \, ka \; sin \, (ka) \tag{5.13a}$$

$$c_i = \beta \, ka \; cos \, (ka) \tag{5.13b}$$

These are plotted in nondimensional form in figures 5.7a and 5.7b, as dashed and solid lines, respectively. Two scales are shown to illustrate both the details of the first (longest wavelength) maximum, and the apparent harmonic behavior at higher frequencies. A maximum in the growth rate corresponds to the combination of ripple wavelength, $\lambda \, (=2\pi/k)$, and hop length, a, that produces, simultaneously, the strongest decline of mass flux over the crest of the ripple, and the strongest increase in mass flux over the trough. The wavelength associated with the first peak in the growth rate, at $ka \approx .9$, corresponds to ripples approximately 7 creep lengths long. However, faster growing forms can be found associated with every successive ka multiple of 2π. These correspond to bedforms growing in response to hops that originated on the stoss sides of bedforms one, two and more wavelengths upwind (see figure 5.8). This unrealistic, pathological behavior arises from the strict assumption that all

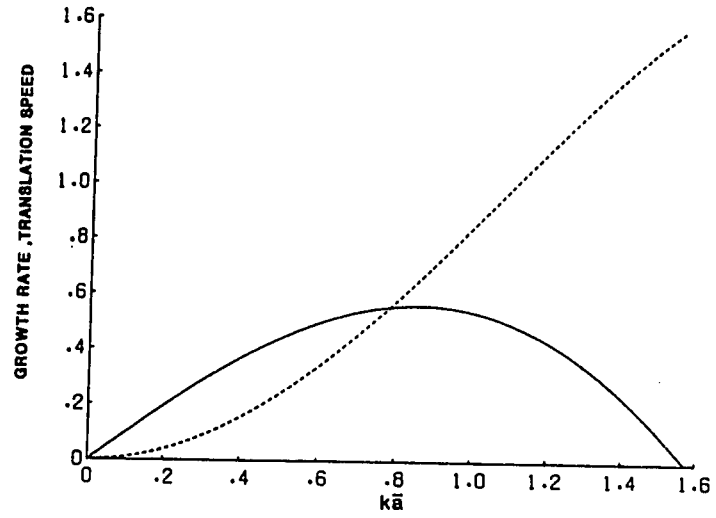

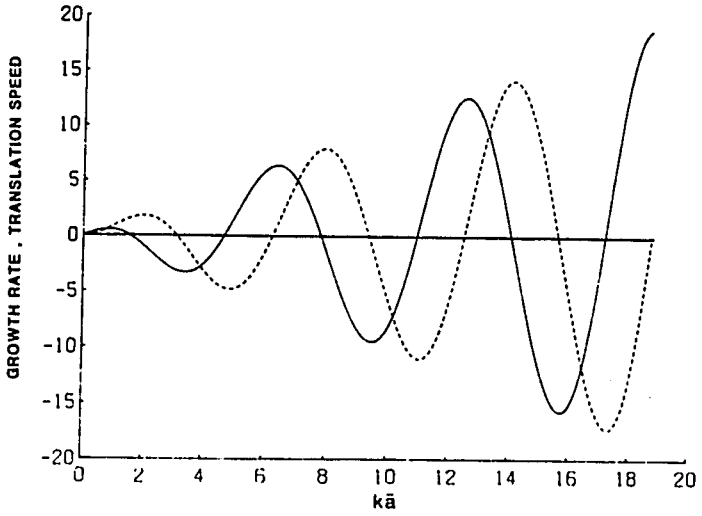

Figure 5.7. (a) Normalized growth rate (solid line) and translation speed (dashed line) for the constant reptation length case, plotted against the product of the wave number $k = 2\pi/\lambda$ with the reptation length, a. The peak in growth rate -- the fastest growing wave -- at $ka \approx .9$ corresponds to wavelengths approximately 7 times greater than the reptation length.
(b) Same as (a) except for expanded ka scale, showing many faster growing high frequency harmonics. See text for explanation.

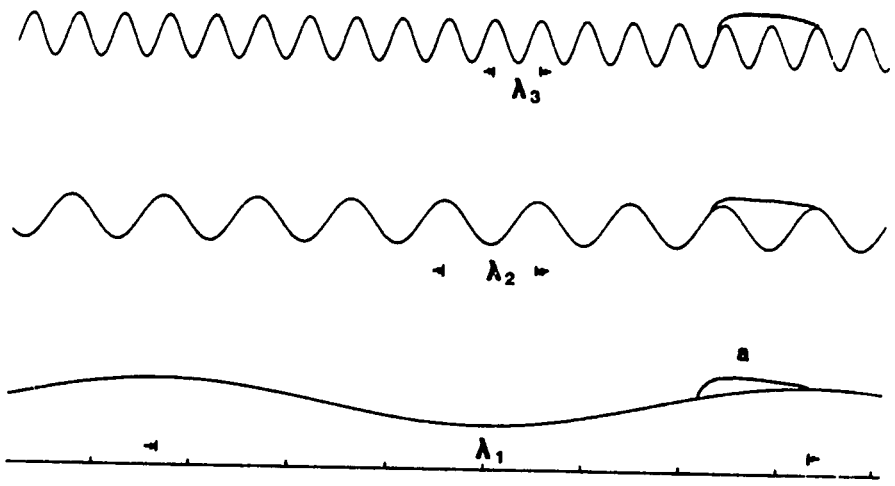

Figure 5.8. Schematic diagram illustrating the origin of the higher frequency peaks in the growth rate arising from the constant reptation length analysis.

hops are identical in length. Any breadth in the distribution of a, which arises from the stochastic nature of the grain-bed impact process, or from small alterations of saltation trajectories due to turbulent fluctuations of the wind (e.g. Nalpanis, 1986; Anderson, 1986c) is expected to damp out the growth of such fortuitous harmonics by landing with essentially equal probability on the lee and stoss slopes.

Ripple translation velocities predicted from the constant hop analysis show a monotonic, almost linear increase with increase in wavenumber throughout the region of the first maximum (see figure 7a). The shorter forms travel faster than the longer forms. Negative ripple velocities shown in figure 5.7b represent upwind translating forms. These correspond to undulations for which the maximum rate of increase of mass flux occurs on the upwind slope of the form, allowing this portion of the form to increase in height while the lee side of the form deflates. Such behavior has not been reported in natural eolian systems.

5.6 THE EFFECTS OF A DISTRIBUTION IN REPTATION LENGTH

In order to assess the effects of a realistic distribution in the trajectory lengths resulting from grain impacts, the foregoing analysis is extended to include a probability density of hop lengths, $p(a)da$. We see that the first case then corresponds to a delta function for this probability density, or $p(a)da = \delta(a-\bar{a})da$, where δ is the kronecker delta, and $\bar{a}$ refers hereafter to the mean hop length. The simple picture illustrated in figure 5.5 breaks down, as trajectories originating at all positions upwind that cross the plane of concern must be counted in the local rate of sediment flux. The flux at a position x therefore becomes a convolution of the slope evaluated a distance a upwind, with the fractional number of hops of that length, expressed as $a\ p(a)da$:

$$Q(x) = Q_s + \beta \int_0^\infty \frac{\partial z(x-a)}{\partial x}\ a\ p(a)da \tag{5.14}$$

An analysis parallel to that presented above then yields for the phase speed

$$c = i\beta k \int_0^\infty a\ p(a) e^{-iak}\, da = i\beta k\ \overline{ap(a)} \tag{5.15}$$

where the overbar denotes the Fourier transform of the expression.

Two cases were addressed, corresponding to exponential and gamma function probability densities, both of which may be expressed as

$$p(a) = Aa^b \exp(-da) \qquad a > 0 \tag{5.16}$$

$$p(a) = 0 \qquad a < 0$$

with b, d real, >0. The most probable hops correspond to $a = b/d$, and the mean is $\bar{a} = (b+1)/d$. Setting $b = 0$ results in an exponential distribution, while $b = 1$ yields a gamma function with a broadly peaked maximum in the probability density. Performing the Fourier transform (Kaplan, 1981, p.222), the phase speed becomes

$$c = i\beta k\ \frac{(b+1)!}{b!} d^{b+1} \frac{1}{(ik+d)^{b+2}} \tag{5.17}$$

The real and imaginary components of the phase speed become, for the exponential distribution ($b = 0$):

$$\frac{c_r}{\beta} = \frac{2(k\bar{a})^2}{(1+(k\bar{a})^2)^2} \tag{5.18a}$$

$$\frac{c_i}{\beta} = \frac{k\bar{a}(1-k\bar{a})^2}{(1+(k\bar{a})^2)^2} \tag{5.18b}$$

and for the gamma distribution ($b = 1$):

$$\frac{c_r}{\beta} = \frac{\frac{1}{2}(k\bar{a})^2(3-\frac{1}{4}(k\bar{a})^2)}{(1-\frac{3}{4}(k\bar{a})^2)^2 + (\frac{3}{2}k\bar{a} - \frac{1}{8}(k\bar{a})^3)^2} \tag{5.19a}$$

$$\frac{c_i}{\beta} = \frac{k\bar{a}(1-\frac{3}{4}(k\bar{a})^2)}{(1-\frac{3}{4}(k\bar{a})^2)^2 + (\frac{3}{2}k\bar{a} - \frac{1}{8}(k\bar{a})^3)^2} \tag{5.19b}$$

The results are plotted in figures 5.9a and 5.9b.

The most striking alteration of the pattern of ripple growth resulting from the introduction of a probability distribution of ejection velocities is the disappearance of

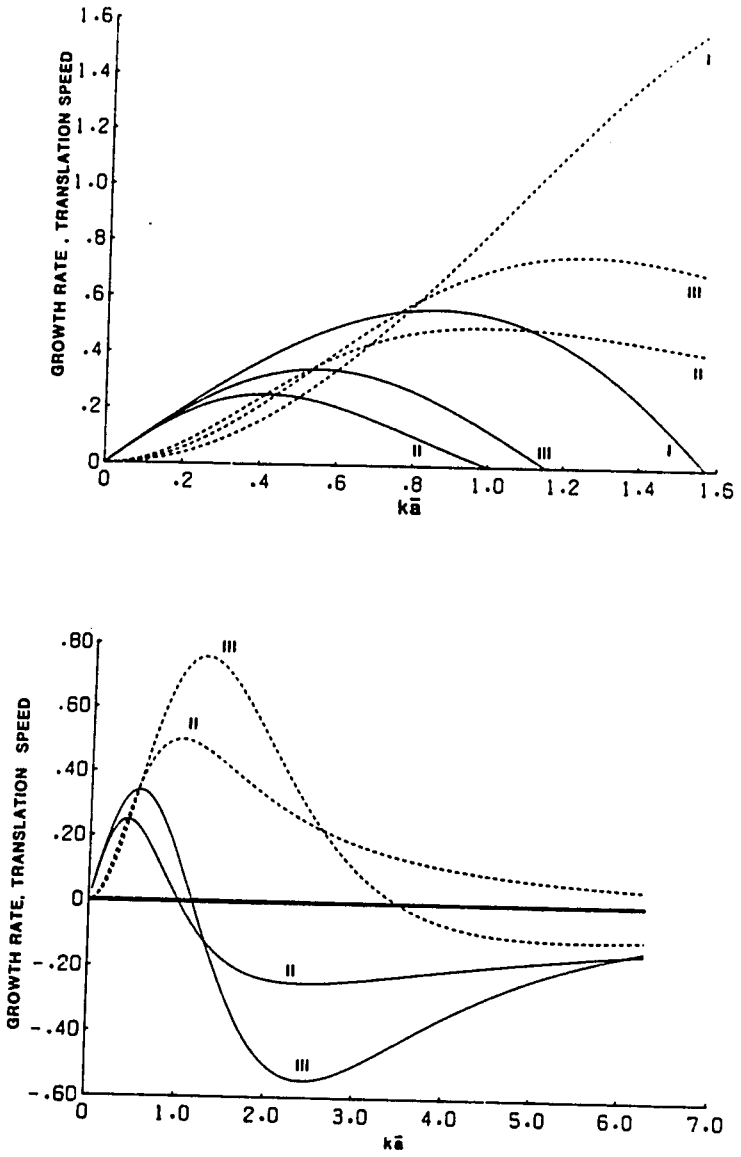

Figure 5.9. (a) Normalized growth rate (solid lines) and translation speed (dashed lines) for exponential distribution of reptation lengths (case II), and gamma distribution of reptation lengths (case III), shown together with the results from the constant reptation length analysis (case I).
(b) Same as (a) except for expanded $k\bar{a}$ scale. Case I is not shown. In contrast with the patterns in figure 5.7b, there exists a single peak in the growth rate and translation speed, corresponding roughly to the first maximum in the constant reptation length analysis.

the high-frequency fast-growing harmonics. There exists a single fastest-growing wavenumber corresponding to wavelengths on the order of 15 and 12 times the mean reptation length, for the exponential and gamma distributions, respectively. The translation speeds of the fastest growing waves are reduced from those predicted using the identical reptation-length model, and in both cases all growing waves travel downwind.

5.7 DISCUSSION

The only previous attempt to incorporate impacts in an analysis of the stability of eolian ripples (Walker,1981) neglected the finite hop lengths resulting from saltation impacts. The short downwind lag between impact intensity and sediment flux was therefore not incorporated, leading to the unsatisfying result (corresponding to $a=0$ in our constant-hop-length case) that all wavelengths grow ($c_i>0$), and that none translates ($c_r=0$).

It remains to be shown that a fastest growing wavelength on the order of 12-15 reptation lengths is physically reasonable. Assuming that the saltation trajectories most effective in driving reptation transportcorrespond to liftoff velocities of roughly twice the shear velocity (see figure 5.3); that saltation impact velocities are roughly 3-4 times the liftoff velocities (Anderson and Hallet, 1986, figure 7); and that the mean liftoff velocity for reptations is on the order of 3 percent of the saltation impact velocity (see figure 5.2), the mean liftoff velocity for the repations ought to be a small fraction of the shear velocity. Calculations of associated reptation hop lengths are on the order of a large fraction of a centimeter. The corresponding initially fastest-growing wavelengths of 5-10 centimeters are in rough accord with the wavelengths of initial surface undulations measured in wind tunnel experiments (Seppala and Linde, 1981), and in field experiments (Sharp, 1963). We conclude by reiterating the assumptions made in the present analysis, and by discussing the implied restrictions on the generality of the model.

(1) The granular bed is composed of identical grains. As most eolian sands are well

sorted, this should not impose undue constraint on the applicability of the model. Truly bimodal sands, however, would require a more complete analysis of the divergent rates of transport of the various grain sizes. "Grain jams" of larger particles near the crests of ripples may be expected; not only does the efficiency of impacts of the finer, successively saltating grain population drop as the cube of the bed particle diameter, but the effective size of the pocket from which the bed particle must exit increases with the size of the neighboring grains, giving rise to the D^{-4} dependence of the impact number in equation 5.1.

(2) There is no spread in the impact angle of high-energy trajectories. Our calculations demonstrate that this angle should be quite constant; however, the angle varies slightly with grain size, implying that in natural eolian systems the assumption will break down somewhat.

(3) The reptation transport is a function of the impact rate only. The probability distribution of the ejection velocities (which leads to a distribution in the creep lengths), and the number of grains ejected per impact, n_1, are both assumed to be independent of the angle the impacting grain makes with the local surface [i.e. of the sum $(\alpha+\theta)$]. This assumption is based upon results of Mitha and coworkers (1986), but the range of impact angles they tested (17-34 degrees) was restricted by the experimental setup. Numerical work of Werner and Haff (1985, table 4) indeed indicates a dependence of the ratio of the mean ejection velocity to the impact velocity on impact angle, though the difference is only approximately 10 percent between the 15 and 25 degree cases run. Further experiments, both physical and numerical at the more important low-incident angles are encouraged. It is anticipated that the character of the granular splash may become strongly dependent on incident angle at low angles. Such a functional dependence would complicate the present analysis, but we suspect the results will not be materially altered. We anticipate that there is a monotonic decrease in both the number of ejections and in their mean velocities with decreasing impact angle. This would merely serve to accentuate the pattern of ejection intensity derived in the present analysis; superposed on the pattern imposed by impact intensity, a systematic increase in ejection rate on stoss slopes, and decrease on lee slopes, would arise, yielding an asymmetry to the essentially sinusoidal pattern derived in the present analysis (See figure 5.6.).

(4) Perhaps most importantly, the present analysis is strictly applicable to *infinitesmal* perturbations of the bed, and to the *initial* growth rates and translation speeds of incipient ripples. Once the amplitudes become large enough to introduce other physical effects, a more complicated finite amplitude analysis may be required. Coalescence of rippleforms due to the dispersion of ripple translation speeds should be expected. All three analyses imply that the shortest wavelength forms should travel faster than longer waveforms. This leads to a coalescence of ripples, as the short forms cannot travel as fast in the low impact-intensity zones in the lee of the larger forms, and should thus be captured by them (P.K.Haff, personal communication, 1985). The result should be the disappearance of the higher frequency forms through times, as is indeed reported from both wind tunnel (Seppala and Linde, 1978) and natural experiments (Sharp, 1963).

Besides the "grain jams" resulting from a diversity of grain sizes in the bed, the only other "finite amplitude effect" would be the increased aerodynamic shear over ripple crests as they grow in amplitude, and the associated pattern in ejection of bed grains due to aerodynamic lift and drag. The role of fluid shear stresses in ejecting grains from the bed has been ignored entirely in the present analysis. First order "inviscid" solutions for flow over a sinusoidally perturbed bed display shear stress maxima over the crests and minima over the troughs (e.g., Kennedy, 1964). A more detailed fluid mechanical model of the flow field over a perturbed subaqueous bed (Smith, 1970) demonstrates that the shear stress maximum is shifted a small fraction of a wavelength upstream of the topographic crest when "real fluid" effects such as viscosity and inertia are introduced. Smith argues that only when the downstream transport distance associated with saltation -- the "sediment inertia effect" -- is sufficient to compensate for this upstream advance in the fluid stress maximum will a stable ripple field exist. The stable wavelength is found to be approximately an order of magnitude greater than the saltation hop length (Smith,1970).

The pattern of fluid shear stresses due to turbulent air flow over a low amplitude, low slope sinusoidal bump in the bed might be expected to be similar to that in water. Relevant detailed flow experiments in air are rare. The results of wind tunnel experiments over a wooden sinusoidal bed (Motzfeld, 1937) display patterns very similar to the inviscid solution, with a basal shear stress maximum very close to the

crest of the form.

Further theoretical and experimental work of a detailed fluid mechanical nature are suggested. The implication of available information, however, is that the pattern of ejection rate due to fluid shear stresses should be roughly in phase with the topography, and should increase in amplitude with the height of the bedform.

5.8 CONCLUSIONS

Stability analysis using a simplified model of eolian saltation that retains the essense of the grain-bed impact process shows that a range of sizes of infinitesimal initial bed undulations grows; the analysis also yields the wavenumber of the fastest-growing form. The associated wavelength is indeed scaled by a grain transport distance, as initially proposed by Bagnold (1941). The relevant length is not, however, the mean saltation distance (one interpretation of his "characteristic path length"), but is rather the mean reptation length. Nor is the relation a simple equivalence between transport distance and ripple length. The relevant physics is not a rhythmic barrage of trajectories; it is a pattern of divergence and convergence of mass flux dominated by reptating grains with a probability distribution of hop lengths. The pattern of ejection intensity for the reptating population is set by a pattern in impact intensity that in turn reflects both the local bed slope, and the angle of impact of the high energy saltations effectively driving the reptation. The resulting fastest-growing ripple wavelength corresponds to 12-15 times the mean reptation distance, corresponding well with the observed 5-10 cm wavelengths of initial disturbances in laboratory and field settings.

Though the present analysis is restricted by several important assumptions, we believe the essence of the initial ripple growth is captured. We close by suggesting further theoretical, numerical, and physical experiments. The present analysis can be extended by (1) incorporation of different grain sizes, which may require numerical, rather than analytical treatment; (2) addressing the evolution of an initial spectrum of bed disturbances, an analysis that would resemble that of Jain and Kennedy

(1974) for aqueous systems; (3) further experimental and theoretical work on wind velocity profiles over a rippled bed, in order to determine more precisely the pattern of fluid shear stresses to be expected [an analysis complicated by the alteration of the wind velocity field by the presence of saltating grains (see Chapter 3)]; (4) further numerical and physical experiments of single impacts into granular beds, especially at the low angles relevant to the saltation problem; and (5) field experiments using simple ripple measuring devices (Werner and others, 1985) to obtain detailed information about the evolution of ripple spectra through time, the changes in single ripple geometries through time (e.g. their asymmetry), and the importance of coalescence in the growth of ultimate ripple forms.

BIBLIOGRAPHY

Abbott, J.E. and Francis, J.R.D., 1977, Saltation and suspension trajectories of solid grains in a water stream: Philosophical Transaction of the Royal Society of London, Series A, v.284, p.225-254.

Akerman, H.J., 1980, Studies on periglacial geomorphology in west Spitzbergen: Royal Univ. of Lund, Sweden, Department of Geography publication number 89. 297 p.

Anderson, R.S., 1986, Erosion profiles due to sediment entrained by wind: Application of an eolian sediment transport model: Geological Society of America Bulletin (in press).

Anderson, R.S., 1986b, Eolian sediment transport as a stochastic process: Effects of a fluctuating wind on particle trajectories (Chapter 2).

Anderson, R.S., 1986c, Modification of wind velocity profiles by saltating grains (Chapter 3).

Anderson, R.S. and Haff, P.K., 1986, Dispersion of saltating grains over a rough, immobile surface: in preparation.

Anderson, R.S., and Hallet, B., 1986, Sediment transport by wind: Toward a general model: Geological Society of America Bulletin, v.97, p.523-535.

Arya, S.P.S., 1975, A drag partition theory for determining large-scale roughness parameters and wind stress on Arctic pack ice: Journal of Geophysical Research, v.80, p.3447-3454.

Bagnold, R.A., 1936, The movement of desert sand: Proceedings of the Royal Society

of London, v.A157, 594-620.

_____ 1941, *The Physics of Blown Sand and Desert Dunes*: London, Methuen and Co., 265p.

_____ 1966, An approach to the general sediment transport problem from general physics: United States Geological Survey Professional Paper 422I, p.1-37.

Belly, P.Y., 1964, Sand movement by wind: TM No.1, U.S.Army Coastal Engineering Research Center, 80p.

Berg, N., 1983, Field evaluation of some sand transport models. Earth Surface Processes and Landforms, v.8, p.101-114.

Blackwelder, E., 1934, Yardangs: Geological Society of America Bulletin, v.45, p.159-166.

Blank, M., Leinen, M., and Prospero, J.M., 1985, Major Asian eolian inputs indicated by the mineralogy of aerosols and sediments in the western North Pacific: Nature, v.314, p.84-86.

Bridge, J.S., and Dominic, D.F., 1984, Bed load grain velocities and sediment transport rates: Water Resources Research, v.20, p.476-490.

Brookfield, M.E., 1977, The origin of bounding surfaces in ancient aeolian sandstones: Sedimentology, v.24, p.303-332.

Budd, W.F., 1966, The drifting of non-uniform snow particles, *in*, Rubin, M., ed., Studies in Antarctic Meteorology: American Geophysical Union Antarctic Reseasrch Series, v.9, p.59-70.

Budd, W.F., Dingle, R., and Radok, U., 1966, The Byrd snow drift project: outline and basic results, *in* Rubin, M., ed., Studies in Antarctic Meteorology: American Geophysical Union Antarctic Research Series, v.9, p.71-134.

Burtt, E.H.Jr., 1981, The adaptiveness of animal colors: Bioscience, v.31, p.723-729.

Chamberlain, A.C., 1983, Roughness length of sea, sand, and snow: Boundary Layer Meteorology, v. 25, p.405-409.

Chepil, W.S., 1945, Dynamics of wind erosion. I. Nature of movement of soil by wind: Soil Science, v.60, p.305-320.

_____, 1945b, Dynamics of wind erosion. II. Initiation of soil movement: Soil Science, v.60, p.397-410.

_____, 1945c, Dynamics of wind erosion. III. The transport capacity of the wind: Soil Science, v.60, p.475-480.

_____, 1958, The use of evenly spaced hemispheres to evaluate aerodynamic forces on a soil surface: Transactions of the American Geophysical Union, v.39, p.397-403.

Chepil, W.S., and Woodruff, N.P., 1963, The physics of wind erosion and its control: Advances in Agronomy, v.15, p.211-302.

Decker, R., and Brown, R.L., 1983, A turbulent mixture theory for the atmospheric mixture of snow and air: Annals of Glaciology, v.4, p.37-41.

Dietrich, W.E., 1982, Settling velocity of natural particles: Water Resources Research, v.18, p.1615-1626.

van Dop, H., Nieuwstadt, F.T.M., and Hunt, J.C.R., 1985, Random walk models for

particle displacements in inhomogeneous unsteady turbulent flows: Physics of Fluids, v.28, p.1639-1653.

Drew, D.A., 1975, Turbulent sediment transport over a flat bottom using momentum balance: Journal of Applied Mechanics, v.42, p.38-44.

Einstein, H.A., and Chien, N., 1955, Effects of heavy sediment concentration near the bed on velocity and sediment distribution: University of California Institute for Engineering Research, v.8.

Ellwood, J.M., Evans, P.D., and Wilson, I.G., 1975, Small scale aeolian bedforms: Journal of Sedimentary Petrology, v.45, p.554-561.

Emlet, R.B. and Strathman, R.R., 1985, Gravity, drag and feeding currents of small zooplankton: Science, v.228, p.1016-1017.

Engelund, F., 1970, Instability of erodible beds: Journal of Fluid mechanics, v.42, p.225-244.

Engelund, F., and Fredsoe, J., 1982, Sediment ripples and dunes: Annual Review of Fluid Mechanics, v.14, p.13-37.

Fredsoe, J., 1982, Shape and dimensions of stationary dunes in rivers: Journal of the Hydraulics Division, ASCE, v.108, p.932-947.

Gerety, K., 1986, Problems with determination of U_* from wind-velocity profiles measured in experiments with saltation: *in* Proceedings of the International workshop on the physics of blown sand, Department of Theoretical Statistics Memoir 8, Aarhus University, Aarhus, Denmark.

Gerety, K.M., and Slingerland, R., 1983, Nature of the saltating population in wind tunnel experiments with heterogeneous size-density sands, *in* Brookfield, M.E.,

and Ahlbrandt, T.S., eds., Eolian Sediments and Processes: Amsterdam, Elsevier Press, p.115-131.

Gierasch, P.J., 1974, Martian dust storms: Reviews of Geophysics and Space Physics, v.12, p.730-734.

Gillette, D.A., 1981, Production of dust that may be carried great distances, *in* Pewe, T.L., ed., Desert Dust: Origin, Characteristics, and Effect on Man: Geological Society of America Special Paper 186, p.11-26.

Gillette, D.A., Blifford, D.A., and Fenster, C.R., 1972, Measurements of aerosol size distributions and vertical fluxes of aerosols on land subject to wind erosion: Journal of Applied Meteorology, v.11, p.977-987.

Gillette, D.A., Blifford, D.A., and Fryrear, D.W., 1974, The influence of wind velocity on the size distributions of aerosols generated by the wind erosion of soils: Journal of Geophysical Research, v.79, p.4068-4075.

Gillette, D.A., and Goodwin, P.A., 1974, Microscale transport of sand sized soil aggregates eroded by wind: Journal of Geophysical Research, v. 79, p.4080-4084.

Gillette, D.A., and Walker, T.L., 1977, Characteristics of airborne particles produced by wind erosion of sandy soil, high plains of west Texas: Soil Science, v.123, p.97-110.

Goudie, A.S., 1983, Dust storms in space and time: Progress in Physical Geography, v.7, p.502-529.

Greeley, R., and Iversen, J.D., 1985, *Wind as a geological process:* Cambridge, Cambridge Press, 333p.

Greeley, R., Williams, S., White, B.R., Pollack, J., Marshall, J., and Krinsley, D., 1984, Abrasion by eolian particles: Earth and Mars: NASA Contractor Report 3788.

Greeley, R., Williams, S.H., and Marshall, J.R., 1983, Velocities of windblown particles in saltation: preliminary laboratory and field measurements, *in* Brookfield, M.E., and Ahlbrandt, T.S., eds., Eolian Sediments and Processes: Amsterdam, Elsevier Press, p.133-148.

Greeley, R., and others, 1982, Rate of wind abrasion on Mars: Journal of Geophysical Research, v.87, p.10009-10024.

Greeley, R., and others, 1984, Windblown sand on Venus: preliminary results of laboratory simulations: Icarus, v.57, p.112-124.

Greeley, R., and Marshall, J.R., 1985, Transport of Venusian rolling stones by wind?: Nature, v.313, p.771-773.

Guelphenbaum, G., and Smith, J.D., 1985, Experimental evaluation of a generalized theory of suspended transport, *in* Shelf Sands and Sandstones Symposium Memoir: Canadian Society of Petroleum Engineers, (in press).

Hanna, S.R., 1982, Applications in air pollution modeling: *in* F.T.M. Nieuwstadt and H.van Dop (eds.) *Atmospheric turbulence and air pollution modelling*: Dordrecht, Holland, Reidel, p.275-310.

Hassan, M.H.A., 1984, Sand transport and desertification in arid lands, *in* Wickramasinghi, ed., Fundamental Studies and the Future of Science: Cardiff, University College of Cardiff Press, p.353-360.

Hinze, J.O., 1972, Turbulent fluid and particle interaction: *in* Hetsroni, G., et al. (eds.) *Progress in Heat and Mass Transfer, v.6*, New York, Pergamon, p.433-

452.

_____, 1975, *Turbulence*, 2nd. ed., New York, McGraw-Hill, 790p.

Hunt, J.C.R., 1982, Diffusion in the stable boundary layer: *in* F.T.M. Nieuwstadt and H. van Dop (eds.) *Atmospheric turbulence and air pollution modelling*: Dordrecht, Holland, D. Reidel Publishing Company, p.231-272.

Hunt, J.C.R., and Weber, A.H., 1979, A lagrangian statistical model analysis of diffusion from a ground-level source in a turbulent boundary layer: Quarterly Journal of the Royal Meteorological Society, v.105, p.423-443.

Hunt, J.C.R., and Nalpanis, P., 1986, Saltating and suspended particles over flat and sloping surfaces I. Modelling concepts: *in* Proceedings of International Workshop on the Physics of Blown Sand, Department of Theoretical Statistics, Aarhus University, 1985.

Hunter, W.A., 1979, Ventifacts on Garnet Hill: unpublished senior thesis, Department of Earth Sciences, California State Polytechnic University, Pomona, California, 223 p.

Hunter, R.E., 1977, Basic types of stratification in small eolian dunes: Sedimentology, v.24, p.361-387.

Iversen, J.D., and others, 1976, Saltation threshold on Mars: the effect of interparticle force, surface roughness, and low atmospheric density: Icarus, v.29, p.381-393.

Jain, S.C., and Kennedy, J.F., 1974, The spectral evolution of sedimentary bed forms: Journal of Fluid Mechanics, v.63, p.301-314.

Jensen, J.L., and Sorenson, M., 1986, Estimation of some aeolian saltation transport parameters: a reanalysis of Williams' data: Submitted to Sedimentology.

Jonas, P.R., and Bartlett, J.T., 1972, The numerical simulation of particle motion in a homogeneous field of turbulence: Journal of Computational Physics, v.9, p.290-302.

Kaplan, W., 1981, *Advanced Mathematics for Engineers*: Reading, Massachusetts, Addison-Wesley, 929p.

Kawamura, R., 1951, Study of sand movement by wind (in Japanese): Technical Research Institute of Tokyo University, Tokyo, Japan, Reports, v.5.p.95-112.

Kennedy, J.F., 1964, The formation of sediment ripples in closed rectangular conduits and in the desert: Journal of Geophysical Research, v.69, p.1517-1524.

Keyfitz, N., 1970, Finding probabilities from random rates, or how to make a life table: American Statistics, v.24, p.28-33.

Kikuchi, T., 1981, A wind tunnel study of the aerodynamic roughness associated with drifting snow: Cold Regions Science and Technology Reports, v.5, p.107-118.

Kind, R.J., 1980, A critical examination of the requirements for model simulation of wind-induced erosion/deposition phenomena such as snow drifting: Atmospheric Environment, v.10, p.219-227.

Kobayashi, D., 1972, Studies of snow transport in low level drifting snow: Contributions from the Institute of Low Temperature Studies, v.A(24), p.1-58.

Koceruk, G., 1981, Significance of interdune deposits and bounding surfaces in aeolian dune sands: Sedimentology, v.28, p.753-780.

Koceruk, G., and Dott, R.H., Jr., 1981, Distinctions and uses of stratification types in the interpretation of eolian sandstones: Journal of Sedimentary Petrology, v.51, p. 579-595.

Krebs, C.J., 1978, *Ecology: The experimental analysis of distributions and abundances, 2nd edition*: New York, Harper and Row, 678p.

Lancaster, N., 1984, Characteristics and occurrence of wind erosion features in the Namib desert: Earth Surface Processes and Landforms, v. 9, p.469-478.

Langmuir, I., and Blodgett, K.B., 1946, A mathematical investigation of water droplet trajectories: Army Air Force Technical Report 5418.

Leeder, M.R., 1983, On the dynamics of sediment suspension by residual Reynolds stresses -- confirmation of Bagnold's theory: Sedimentology, v.30, p.485-491.

Long, C.E., 1981, A simple model for time-dependent stably stratified turbulent boundary layers(Ph.D. dissertation): Seattle, Washington, University of Washington, 173p.

Lumley, 1957, Some problems associated with the motion of small particles in turbulent fluid: Ph.D. thesis, Johns Hopkins University.

McCauley, J.F., Breed, C.S., Farouk El-Baz, Whitney, M.I., Grolier, M.J., and Ward, A.W., 1979, Pitted and fluted rocks in the western desert of Egypt: Viking comparisions: Journal of Geophsical Research, v.84, p.8222-8232.

McCauley, J.F., Grolier, M.J., and Breed, C.S., 1977, Yardangs of Peru and other desert regions.U.S.Geological Society, Interagency Report: Astrogeology 81.

McLean, S.R., and Smith, J.D., 1986, a model for flow over two-dimensional bed forms: Journal of Hydraulic Engineering, v.112, p.300-317.

McTigue, D.F., 1983, Mixture theory for turbulent diffusion of heavy particles, *in* Meyer, R.E., ed., Theory of Multiphase Flow: New York, Academic Press, p.227-250.

Makkonen, L., 1984, Atmospheric icing on sea structures: Cold Regions Research and Engineering Laboratories, Monograph 84-2. U.S. Army Corps of Engineers, Hanover, New Hampshire.

Male, D.H., 1980, The seasonal snow cover, *in* Colbeck, S., ed., Dynamics of Snow and Ice Masses: New York, Academic Press, p.305-395.

Mellor, M., 1965, Blowing snow, Cold Regions Research and Engineering Laboratory Monographs: Hanover, N.H., U.S. Army Cold Regions Research and Engineering Laboratory, pt.3, sec.A3c, 79p.

Mellor, M., and Radok, U., 1960, Some properties of drifting snow, *in* Antarctic Meteorology: Oxford, Pergamon Press, p.333-346.

Minsk, L.D., 1980, Icing on structures: Cold Regions Research and Engineering Laboratories, Report 80-31. U.S. Army Corps of Engineers, Hanover, New Hampshire.

Mitha, S., Tran, M.Q., Werner, B.T., and Haff, P.K., 1986, The grain-bed impact process in aeolian saltation: submitted to Acta Mechanica.

Morales, C., ed., 1979, Saharan Dust: New York, John Wiley and Sons, 297p.

Morsi, S.A., and Alexander, A.J., 1972, An investigation of particle trajectories in two phase flow systems. Journal of Fluid Mechanics, v. 55, p.193-208.

Motzfeld, H., 1937, Die turbulente Stromung an welligen Wanden: Zeitschrift fur angewandte mathematik und mechanik, v.17, p.193-212.

Nalpanis, P., 1986, Saltating and suspended particles over flat and sloping surfaces II. Experimental and numerical simulations: *in* Proceedings of International Workshop on the Physics of Blown Sand, Department of Theoretical Physics,

Aarhus University, 1985.

Nickling, W.G., 1978, Eolian sediment transport during dust storms: Slims River Valley, Yukon Territory: Canadian Journal of Earth Science, v.15, p.1069-1084.

Nickling, W.G., 1983, Grain-size characteristics of sediment transported during dust storms: Journal of Sedimentary Petrology, v.53, p.1011-1024.

Niklas, K.J., 1981, Simulated wind pollination and airflow around ovules of some early seed plants: Science, v.211, p.275-277.

_____, 1985, Wind pollination -- a study in controlled chaos: American Scientist, v.73, p.462-470.

Oura, H., 1967, Studies on blowing snow, *in* Oura, H., ed., Physics of Snow and Ice, v.l, pt.2, 1085-1097.

Owen, P.R., 1964, Saltation of uniform grains in air: Journal of Fluid Mechanics, v. 20, p.225-242.

Paola, C., 1983, Flow and skin friction over rough natural beds: [PhD. Dissertation] Cambridge, Massachusetts, Massachusetts Institute of Technology Department of Earth and Planetary Sciences, 347p.

Pasquill, F., 1974, *Atmospheric Diffusion* (2nd edition): New York, John Wiley and Sons.

Peskin, 1959, Some effects of particle-particle and particle-fluid interactions in two-phase flow systems: Ph.D. thesis, Princeton University, Princeton, New Jersey.

Pewe, T.L., ed., 1981, Desert dust: origin, characteristics, and effect on man: Geological Society of America Special Paper 186, 303p.

Radok, U., 1968, Deposition and erosion of snow by the wind, Cold Regions Research and Engineering Reports: Hanover, New Hampshire, U.S. Army Cold Regions Research and Engineering Laboratory, v.230, 23pp.

Rasmussen, K.R., Sorenson, M., and Willetts, B.B., 1986, Measurement of saltation and wind strength on beaches: *in* Proceedings of the international conference on the physics of blown sand, Department of Theoretical Statistics Memoir 8, Aarhus, University, Denmark.

Rea, D.K., Leinen, M., Janecek, T.R., 1985, Geologic approach to the long-term history of atmospheric circulation: Science, v.227, p.721-725.

Reizes, J.A., 1978, Numerical study of continuous saltation: American Society of Civil Engineers Journal of the Hydrology Division, v. 104, p.1305-1321.

Richards, K.J., 1980, The formation of ripples and dunes on an erodible bed: Journal of Fluid Mechanics, v.99, p.597-618.

Rouse, H., 1937, Modern conceptions of the mechanics of fluid turbulence. Transactions of the American Society of Civil Engineers, v.102, p.463-543.

Routbort, J.L., Scattergood, R.O., and Kay, E.W., 1980, Erosion of silicon single crystals: Journal of the American Ceramic Society, v.63, p.635-640.

Rubin, D.M., and Hunter, R.E., 1982, Bedform climbing in theory and nature: Sedimentology, v.29, p.121-138.

Rubinow, S., and Keller, J., 1961, The transverse force on a spinning sphere in a viscous fluid: Journal of Fluid Mechanics, v.11, p.447-459.

Rumple, D.A., 1985, Successive aeolian saltation: studies of idealized collisions: Sedimentology, v.32, p.267-275.

Sakomoto-Arnold, C.E., 1981, Eolian features produced by the December 1977 windstrom, southern San Joaquin Valley, California: Journal of Geology, v.89, p.129-137.

Scattergood, R.O., and Routbort, J.L., 1983, Velocity exponent in solid-particle erosion: Journal of the American Ceramic Society, v.66, p.C184-C186.

Schmidt, R.A., 1977, A system that measures blowing snow. U.S.Forest Service Rocky Mountain Forest and Range Experiment Station Research Paper RM-194, 80p.

_____, 1980, Threshold speeds and elastic impact in snow transport: Journal of Glaciology, v.26, p.453-467.

_____, 1982a, Properties of blowing snow: Reviews of Geophysics and Space Physics, v.20, p.39-44.

_____, 1982b, Vertical profiles of wind speed, snow concentration, and humidity in blowing snow: Boundary Layer Meteorology, v.23, p.223-246.

_____, 1984, Transport rate of drifting snow and the mean wind speed profile(in preparation).

Schutz, L., 1980, Long range transport of desert dust with special emphasis on the Sahara: Annals of the New York Academy of Science, v.338, p.515-532.

Seppala, M., and Linde, K., 1978, Wind tunnel studies of ripple formation: Geografiska Annaler, v.60, p.29-60.

Sharp, R.P., 1949, Pleistocene ventifacts east of the Bighorn Mountains, Wyoming: Journal of Geology, v.57, p.175-195.

_____, 1963, Wind ripples: Journal of Geology, v.71, p.617-636.

_____, 1964, Wind-driven sand in the Coachella Valley, California: Geological Society of America Bullletin, v.75, p.785-804.

_____, 1980, Wind-driven sand in the Coachella Valley, California: further data: Geological Society of America Bulletin, v.91, p.724.

Sharp, R.P., and Malin, M.C., 1984, Surface geology from Viking landers on Mars: a second look: Geological Society of America Bulletin, v.95, p.1138-1412.

Shiotani, M., and Arai, H., 1967, On the vertical distribution of blowing snow, *in* Oura, H., ed., Physics of Snow and Ice, v.1, pt.2, p.1075-1083.

Smith, J.D., 1970, Stability of a sand wave subjected to a shear flow of low Froude number, Journal of Geophysical Research, v.75, p.5928-5940.

Smith, J.D., 1977, Modelling of sediment transport on continental shelves, *in* Goldberg, E.B., ed., The Sea: New York, John Wiley and Sons, p.539-577.

Smith, J.D., and McLean, S.R., 1977, Spatially averaged flow over wavy boundaries: Journal of Geophysical Research, v.82, p.1735-1746.

Snyder, W.H., and Lumley, J.L., 1971, Journal of Fluid Mechanics, v.48, p.41-71.

Soo, S.L., 1967, *Fluid Dynamics of Multiphase Systems*: Waltham, Massachusetts, Blaisdell Publishing Company, 524p.

Sorensen, M., 1986, Estimation of some aeolian saltation transport parameters from transport rate profiles: Submitted to Acta Mechanica.

Stallabrass, J.R., and Hearty, P.F., 1967, The icing of cylinders in conditions of

simulated freezing sea spray: Natural Resources Council, Ottawa, Canada, Mechanical Engineering Report MD-51.

Strickler, J.R., 1982, Calanoid copepods, feeding currents, and the role of gravity: Science, v.218, p.158-160.

Sumer, B.M., and Oguz, B., 1978, Particle motions near the bottom in turbulent flow in an open channel: Journal of Fluid Mechanics, v.86, p.109-127.

Sumer, B.M., and Diegaard, 1981, Particle motions near the bottom in turbulent flow in an open channel. Part 2: Journal of Fluid Mechanics, v. 109, p.311-337.

Sumer, B.M., 1984, Lift forces on moving particles near boundaries: Journal of Hydraulic Engineering, v.110, p.1272-1278.

Suzuki, T., and Takahashi, K., 1981, An experimental study of wind abrasion: Journal of Geology, v.89, p.23-36.

Tabler, R.D., 1980, Self-similarity of wind profiles in blowing snow allows outdoor modeling: Journal of Glaciology, v.26, p.421-431.

Takeuchi, M., 1980, Vertical profile and horizontal increase of drift-snow transport: Journal of Glaciology, v.26, p.481-492.

Tennekes, H., 1982, Similarity relations, scaling laws, and spectral dynamics: *in* Nieustadt, F.T.M., and van Dop, H., editors, *Atmospheric turbulence and air pollution modelling*, Dordrecht, Holland, D.Reidel Publishing Company, p.37-64.

Tsuchiya, Y., 1969a, Mechanics of successive saltation of sand particles on a granular bed in a turbulent stream: Bulletin of the Disaster Prevention Research Institute, Kyoto University, v.19, p.31-44.

_____, 1969b, On the mechanics of saltation of a spherical sand particle in a turbulent stream: Bulletin of the Disaster Prevention Research Institute, Kyoto University, v. 19, p.52-57.

Uhlenbeck, G.E. and Ornstein, L.S., 1930, On the theory of brownian motion: Physical Review, v.36, p.823-841.

Ungar, J.E., and Haff, P.K., 1985, Steady state saltation in air: Sedimentology, in press.

Vandermeer, J., H., 1981, *Elementary Mathematical Ecology*: New York, John Wiley and Sons, 294p.

Vanoni, V.A., 1946, Transportation of suspended sediment by water: Transactions of the American Society of Civil Engineers, v.111, p.67-133.

Veverka, J., and others, 1974, Variable features on Mars, III: comparison of Mariner 1969 and Mariner 1977 photographs, Icarus, v.21, p.317-368.

Walker, J.D., 1981, An experimental study of wind ripples: [M.Sc. thesis] Cambridge, Massachusetts, Massachusetts Institute of Technology Department of Earth and Planetary Sciences, 145p.

Walker, G.P.L., Wilson, L., and Bowell, E.L.G., 1971, Explosive volcanic eruptions -- I. The rate of fall of pyroclasts: Geophysical Journal of the Royal Astronomical Society, v.22, p.377-383.

Ward, A.W. and Greeley, R., 1984, Evolution of yardangs at Rogers Lake, California: Geological Society of America Bulletin, v.95, p.829-837.

Ward, A.W., and others, 1985, Global map of eolian features on Mars: Journal of Geophysical Research, v.90, p.2038-2056.

Warren, A., 1983, Progress report on arid geomorphology: Progress in Physical Geography, v.7, p.397-403.

Werner, B.T., and Haff, P.K., 1985, A simulation study of the low energy ejecta resulting from single impacts in eolian saltation: Submitted to Minneanapolis ASCE Conference Proceedings.

_____, 1986, Dynamical simulations of granular materials using concurrent processing computers: Submitted to Geotechnique.

Werner, B.T., Haff, P.K., Livi, R.P., and Anderson, R.S., 1985, The measurement of eolian ripple cross-sectional shapes: Submitted to Geology.

White, B.R., and Schulz, J.C., 1977, Magnus effect in saltation: Journal of Fluid Mechanics, v.81, p.497-512.

White, B.R., 1979, Soil transport by wind on Mars: Jourournal of Geophysical Research, v.84, p. 4643-4651.

_____, 1982, Two phase measurements of saltating turbulent boundary layer flow: International Journal of Multiphase Flow, v.8, p.459-473.

Whitney, M.I., 1978, The role of vorticity in developing lineation by wind erosion: Geological Society of America Bulletin, v.89, p.1-18.

_____, 1979, Electron miscroscopy of mineral surfaces subjected to wind-blast erosion: Geological Society of America Bulletin, v.90, p.917-934.

_____, 1983, Eolian features shaped by aerodynamic and vorticity processes, *in* Brookfield, M.E., and Ahlbrandt, T.S., eds., Eolian Sediments and Processes: Amsterdam, Elsevier Press, p.223-246.

Whitney, M.I., and Dietrich, R.V., 1973, Ventifact sculpture by windblown dust: Geological Society of America Bulletin, v.84, p.2561- 2582.

Wiberg, P., and Smith, J.D., 1985, A theoretical model for saltating grains in water: Journal of Geophysical Research, v.90, p.7341-7354.

Willetts, B., 1983, Transport by wind of granular materials of different grain shapes and densities: Sedimentology, v.30, p.669-679.

Willetts, B. and Rice, A., 1986, *in* Proceedings of the international conference on the physics of blown sand, Department of Theoretical Statistics Memoir 8, Aarhus University, Aarhus, Denmark.

Williams, G.P., 1964, Some aspects of the eolian saltation load: Sedimentology, v.9, p.89-104.

Wilson, I.G., 1972, Aeolian bedforms -- their development and origins: Sedimentology, v.19, p.173-210.

Wilshire, H.G., Nakata, J.K., and Hallet, B., 1981, Field observations of the December 1977 wind storm, San Joaquin Valley, California: Geological Society of America Special Paper 186, p.233-251.

Yalin, M.S., 1972, Mechanics of Sediment Transport: Oxford, Pergamon, 290p.

Zingg, A.W., 1953, Wind tunnel studies of the movement of sedimentary material: Proceedings of the 5th Hydraulics Conference, University of Iowa Studies in Engineering, v.24, p.111-135.

BIOGRAPHICAL NOTE

Robert Stewart Anderson was born November 17, 1952 in Denver, Colorado, the son of John David and Florence Atwater Van Dyke Anderson. He was educated in the Denver area, receiving his high school diploma from Golden High School. His collegiate education includes:

B.A. in geology, Williams College, Williamstown, Massachusetts, June 1974.
Honors thesis: Petrology and emplacement of the Lake George intrusive complex, Colorado.

M.S. in geology, Stanford University, Stanford, California, August 1977
Thesis: A biography of Clarence Edward Dutton (1841-1912): 19th century geologist and geographer.

Ph.D. in geology, University of Washington, Seattle, Washington, August 1986
Dissertation: Sediment transport by wind: Saltation, suspension, erosion, and ripples.